



SELECTIVE THERAPY
WITH MINOR GROOVE BINDERS

by

CLAIRE BOURDIN

A report submitted to the Department of Pure and Applied Chemistry,
University of Strathclyde, Glasgow, in part fulfilment of the regulations
for the degree of Master of Philosophy in Chemistry.

February 2010

This thesis is the result of the author's original research. It has been composed by the author and has not been previously submitted for examination which has lead to the award of a degree.

The copyright of this thesis belongs to the author under the terms of the United Kingdom Copyright Acts as qualified by University of Strathclyde Regulation 3.50. Due acknowledgement must always be made of the use of any material contained in, or derived from, this thesis.

Signed:

Date:

MASTER RESEARCH AT STRATHCLYDE UNIVERSITY

Duration: October 1st 2008 to September 30th 2009

Location : University of Strathclyde

Department of Pure and Applied Chemistry

Thomas Graham Building lab 416

295 Cathedral Street

Glasgow

G1 1XL

Tel: +44 (0)141 548 2282

Fax: +44 (0)141 548 4822

Supervisors: Prof. Colin J. Suckling and Prof. Colin L. Gibson

This report was written after a 12 month laboratory work, which took place at the University of Strathclyde in Glasgow, Scotland, UK, under the supervision of Prof. Colin J. Suckling and Prof. Colin L. Gibson.

This report was typed during August 2009, in Glasgow, Scotland.

ACKNOWLEDGMENT

I would like to thank Prof. C.J. Suckling and Prof. C. Gibson who accepted my application for a Master, who supervised and mentored my work, for their attention and advice, which were both useful and appreciated, and also for all the time they awarded to me.

I would like to take this opportunity to thank Dr. Adedawn I. Khalaf, Dr. David Breen who helped me to get acquainted with the equipment and for their patience and the time they spent explaining how to run specific experiments and their good advice.

Thank you to Donna MacMillan, Craig McInnes, Niaz McGuire and all the students in the chemistry lab 416 during the year 2009 who made the lab an enjoyable place and who were always ready to help me and discuss problems encountered.

Thank you to Dr. Elizabeth Ellis, who supervised the biological testing and gave me the opportunity to broaden my knowledge in biology, and the students in the SIPBS lab R421 who explained to me for running biological experiments previously unknown to me.

I would like to thank Dr. Nahoum G. Anthony for his help on molecular dynamics.

Finally, I would like to thank my mentor Mrs. Adyna Ryckebush, for her precious advice without which I would not have gained the rewards brought by a one year exchange program in my career development.

ABBREVIATIONS

<u>Abbreviations</u>	<u>NMR data</u>
A Adenine	s : singlet
Ac Acetyl	d : doublet
Boc <i>t</i> -Butoxycarbonyl	t : triplet
C Cytosine	
DAPI 4',6'-diamidino-2-phenylindole	q : quartet
DCM Dichloromethane	
DIEA N,N-Diisopropylethylamine	Q : quintet
DMF <i>N,N</i> -Dimethylformamide	S : septet
DNA Deoxyribonucleic acid	o : octet
Et Ethyl	m : multiplet
EtOAc Ethyl acetate	
EtOH Ethanol	
G Guanine	
HBTU <i>O</i> -Benzotriazole- <i>N,N,N',N'</i> -tetramethyluroniumhexafluorophosphate	
NaOH Sodium hydroxide	
Me Methyl	
MeOH Methanol	
MGB Minor groove binder	
Pd/C (10%) Palladium over activated carbon	
Py <i>N</i> -Methylpyrrole	
T Thymine	
TFA Trifluoroacetic acid	
THF Tetrahydrofuran	
TLC Thin layer chromatography	
T ₃ P Propane phosphonic acid anhydride	

ABSTRACT

Over the past five years, the University of Strathclyde has developed extremely potent anti-bacterial molecules known as minor groove binding agents (MGB) which intrinsic helicity allows binding to the minor groove of DNA. These molecules were effective *in vivo*, non-toxic and showed activity and selectivity against Gram positive bacteria. Whilst such selectivity is an advantage, an extension of activity of such agents towards Gram negative organisms and eventually targeting cancer cells would be valuable. Since the biological properties of such minor groove binders are related to the chemical feature, this aim could be achieved by modifying the structure of the tail group only.

The MPhil project involved the synthesis of a small number of selected minor groove binders differing in their tail groups (Boc protected, OAc protected, guanidine, cyano alkene, nitro alkene) but bearing the same fluorescent head group ((*E*)-4-(3-methoxystyryl)benzyl). The yield of the coupling reaction between the head group and the pyrrole-pyrrole core linked with a protected tail group (Boc or OAc) was improved up to two- to five- fold, using propane phosphonic acid anhydride as a mild reagent.

These MGBs were then evaluated for anti-bacterial and anti-cancer drug activity in screens available at the Strathclyde Institute of Pharmaceutical and Biological Sciences (SIPBS). They were tested against Gram negative *E. coli*, against Gram positive *Staph. aureus* and against the fibroblast hamster cell line V79, in order to evaluate respectively their anti-bacterial activity and their toxicity.

The penetration of these synthesized molecules into bacteria and cells was observed under microscopy in order to assess the structural features that could lead to a potential anti-bacterial and/or anti-cancer molecule if nuclear permeation occurs.

Almost all MGBs tested permeate into Gram positive bacteria, but not all of them showed an anti-bacterial activity. These results were consistent with earlier experiments. However permeation in Gram negative bacteria was observed for the first time in these kind of MGB, but only one molecule appeared to be toxic towards this family of Gram negative bacteria above 20µg/mL. Furthermore, tested MGBs showed permeation into V79 mammalian cells with or without reaching the nucleus, and only one molecule developed significant toxicity towards the V79 cell line, thus giving an idea of which molecule could potentially bind to DNA and become a potential anti-cancer drug.

KEYWORDS: Minor Groove Binders (MGBs), Deoxyribonucleic Acid (DNA), fluorescence, V79 fibroblast hamster cell line, Gram positive bacteria, Gram negative bacteria.

TABLE OF CONTENTS

A. INTRODUCTION.....	11
I. DEOXYRIBOSE NUCLEIC ACID (DNA)	11
1. <i>Structure and discovery</i>	11
2. <i>DNA grooves</i>	12
II. MINOR GROOVE BINDERS (MGBS)	13
1. <i>Introduction</i>	13
2. <i>Minor groove recognition</i>	16
a) Interactions between MGB-DNA	16
b) Non-covalent minor groove recognition	16
3. <i>Structure of binding and interactions with DNA</i>	21
a) DNA curvature	22
b) Width of the minor groove	22
c) Hydrophobicity	23
d) Selectivity and biological results	24
III. AIMS OF THIS STUDY	29
B. SYNTHESIS OF MGBS.....	30
I. CHOICE AND SYNTHESIS OF THE HEAD GROUP.....	30
1. <i>UV and fluorescence measurements</i>	30
2. <i>Synthesis of (E)-4-(3-methoxystyryl)benzoic acid I.3</i>	31
II. CHOICE OF DIFFERENT TAIL GROUPS.....	32
III. SYNTHESIS OF MGBS	34
1. <i>Preparation of 1-methyl-4-nitro-1H-pyrrole-2-carbonyl chloride III.1.5</i>	35
a) Aromatic substitutions: Friedel and Crafts followed by nitration	35
b) Preparation of the 1-methyl-4-nitro-1H-pyrrole-2-carboxylic acid 8 and 1-methyl-4-nitro-1H-pyrrole-2-carbonyl chloride III.1.5	37
2. <i>Preparation of N-methylpyrroles with functionalized tail groups</i>	38
3. <i>Coupling with a second N-methylpyrrole</i>	40
4. <i>Coupling of the pyrrole dimer to the head group</i>	40
5. <i>Elaboration of tail groups from (E)-t-Butyl 2-(4-(4-(4-(3-methoxystyryl)benzamido)-1-methyl-1H-pyrrole-2-carboxamido)-1-methyl-1H-pyrrole-2-carboxamido)ethylcarbamate III.4.3 and (E)- 2-(4-(4-(4-(3-methoxystyryl)benzamido)-1-methyl-1H-pyrrole-2-carboxamido)-1-methyl-1H-pyrrole-2-carboxamido)ethylacetate III.4.4</i>	43
a) Tail group variation from (E)-t-butyl 2-(4-(4-(4-(3-methoxystyryl)benzamido)-1-methyl-1H-pyrrole-2-carboxamido)-1-methyl-1H-pyrrole-2-carboxamido)ethylcarbamate III.4.3	44
b) Tail group variation from (E)- 2-(4-(4-(4-(3-methoxystyryl)benzamido)-1-methyl-1H-pyrrole-2-carboxamido)-1-methyl-1H-pyrrole-2-carboxamido)ethylacetate III.4.4	46
6. <i>Other variations of the tail group</i>	49
IV. CONCLUSION	51
C. BIOLOGICAL TESTING.....	53
I. INTRODUCTION.....	53
1. <i>Gram bacteria</i>	53
2. <i>Mammalian cells</i>	54

II.	KILLING CURVES OF GRAM POSITIVE AND GRAM NEGATIVE BACTERIA.....	54
1.	<i>Growth curves of bacteria</i>	54
2.	<i>Killing curves of bacteria</i>	55
a)	Gram positive bacteria: <i>Staphylococcus aureus</i> RN4220	56
b)	Gram negative bacteria: <i>Escherischia coli</i> NM522	68
c)	Discussion	79
III.	CYTOTOXICITY ASSAY USING V79 CHINESE HAMSTER CELLS	80
1.	<i>MTT assay : Experimental</i>	81
2.	<i>Results</i>	81
a)	Tertiary alkyl amine tail group series	81
b)	Morpholine tail group series	82
c)	Intermediate MGBs and (E)-N-(2-guanidinoethyl)-1-methyl-4-(1-methyl-4-(4-(2-(quinolin-3-yl)vinyl)benzamido)-1H-pyrrole-2-carboxamido)-1H-pyrrole-2-carboxamide IV.1 series	83
d)	New MGBs series	83
e)	Discussion	83
IV.	FLUORESCENT MICROSCOPY	84
1.	<i>Bacteria</i>	85
a)	Tertiary alkyl amine tail group series	86
b)	Morpholine tail group series	88
c)	Intermediate MGBs and (E)-N-(2-guanidinoethyl)-1-methyl-4-(1-methyl-4-(4-(2-(quinolin-3-yl)vinyl)benzamido)-1H-pyrrole-2-carboxamido)-1H-pyrrole-2-carboxamide IV.1 series	90
d)	New MGBs series	92
e)	Conclusion	93
2.	<i>Mammalian cells</i>	94
a)	Tertiary alkyl amine tail group series	94
b)	Morpholine tail group series	95
c)	Intermediates and new MGBs	97
3.	<i>Conclusion</i>	98
D.	DISCUSSION	100
E.	CONCLUSION AND FUTURE WORK	105
F.	EXPERIMENTAL	106
I.	CHEMISTRY PROCEDURES.....	106
1.	<i>Preparation of (E)-4-(3-methoxystyryl)benzoic acid</i>	106
a)	First step: formation of methyl 4-[(diethoxyphosphoryl)methyl]benzoate I.2.2	106
b)	Second step: formation of (E)-4-(3-methoxystyryl)benzoic acid I.3	106
2.	<i>Preparation of the 2-trichloroacetyl-N-methylpyrrole</i> III.1.2	107
3.	<i>Preparation of the 2,2,2-trichloro-1-(1-methyl-4-nitro-1H-pyrrol-2-yl)ethanone</i> III.1.3	108
4.	<i>Preparation of 1-methyl-4-nitro-1H-pyrrole-2-carboxylic acid</i> III.1.4	108
5.	<i>Preparation of 1-methyl-4-nitro-1H-pyrrole-2-carbonyl chloride</i> III.1.5	109
6.	<i>Preparation of t-butyl 2{[(1-methyl-4-nitro-1H-pyrrol-2-yl)carbonyl]amine} ethylcarbamate</i> III.2.1	110
7.	<i>Preparation of N-(2-hydroxyethyl)-1-methyl-4-nitro-1H-pyrrole-2-carboxamide</i> III.2.2	110
8.	<i>Preparation of 2{[(1-methyl-4-nitro-1H-pyrrol-2-yl)carbonyl]amino}ethyl acetate</i> III.2.3	111

9. Preparation of <i>t</i> -Butyl 2{[(1-methyl-4-[(1-methyl-4-nitro-1 <i>H</i> -pyrrol-2-yl)carbonyl]amine)-1 <i>H</i> -pyrrol-2-yl]carbonyl]amino}ethylcarbamate III.3.3	112
10. Preparation of 2{[(1-methyl-4-[(1-methyl-4-nitro-1 <i>H</i> -pyrrol-2-yl)carbonyl]]-1 <i>H</i> -pyrrol-2-yl)carbonyl]amino}ethyl acetate III.3.4	113
11. (<i>E</i>)- <i>t</i> -Butyl 2-(4-(4-(4-(3-methoxystyryl)benzamido)-1-methyl-1 <i>H</i> -pyrrole-2-carboxamido)-1-methyl-1 <i>H</i> -pyrrole-2-carboxamido)ethylcarbamate III.4.3	114
12. Preparation of (<i>E</i>)-2-(4-(4-(4-(3-methoxystyryl)benzamido)-1-methyl-1 <i>H</i> -pyrrole-2-carboxamido)-1-methyl-1 <i>H</i> -pyrrole-2-carboxamido)ethyl acetate III.4.4	115
13. Preparation of III.5.3 , III.5.4 and III.5.5	116
a) Preparation of (<i>E</i>)- <i>N</i> -(2-aminoethyl)-4-(4-(4-(3-methoxystyryl)benzamido)-1-methyl-1 <i>H</i> -pyrrole-2-carboxamido)-1-methyl-1 <i>H</i> -pyrrole-2-carboxamide III.5.1	116
b) Preparation of <i>N</i> -((<i>Z</i>)-4-cyano-3-(methylamino)but-3-en-1-yl)-4-(4-(4-(<i>E</i>)-3-methoxystyryl)benzamido)-1-methyl-1 <i>H</i> -pyrrole-2-carboxamido)-1-methyl-1 <i>H</i> -pyrrole-2-carboxamide III.5.3	117
c) Preparation of (<i>E</i>)-amino((2-(4-(4-(4-(3-methoxystyryl)benzamido)-1-methyl-1 <i>H</i> -pyrrole-2-carboxamido)-1-methyl-1 <i>H</i> -pyrrole-2-carboxamido)ethyl)amino)methaniminium III.5.4	118
d) Preparation of 4-(4-(<i>E</i>)-3-methoxystyryl)benzamido)-1-methyl- <i>N</i> -(1-methyl-5-((2-((<i>E</i>)-1-(methylamino)-2-nitrovinyl)amino)ethyl)carbamoyl)-1 <i>H</i> -pyrrol-3-yl)-1 <i>H</i> -pyrrole-2-carboxamide III.5.5	119
14. Preparation of (<i>E</i>)- <i>N</i> -(2-hydroxyethyl)-4-(4-(4-(3-methoxystyryl)benzamido)-1-methyl-1 <i>H</i> -pyrrole-2-carboxamido)-1-methyl-1 <i>H</i> -pyrrole-2-carboxamide III.5.6	120
15. Preparation of (<i>E</i>)-4-(4-(3-methoxystyryl)benzamido)-1-methyl- <i>N</i> -(1-methyl-5-(2-(pyrrolidin-1-yl)ethylcarbamoyl)-1 <i>H</i> -pyrrol-3-yl)-1 <i>H</i> -pyrrole-2-carboxamide III.5.9	121
a) Preparation of 2-chloro-1,3-dimethyl-1,3,2-diazaphospholidine III.5.7	121
b) Preparation of (<i>E</i>)- <i>N</i> -(2-(1,3-dimethyl-1,3,2-diazaphospholidin-2-yloxy)ethyl)-4-(4-(4-(3-methoxystyryl)benzamido)-1-methyl-1 <i>H</i> -pyrrole-2-carboxamido)-1-methyl-1 <i>H</i> -pyrrole-2-carboxamide III.5.8	121
c) Preparation of (<i>E</i>)-4-(4-(3-methoxystyryl)benzamido)-1-methyl- <i>N</i> -(1-methyl-5-(2-(pyrrolidin-1-yl)ethylcarbamoyl)-1 <i>H</i> -pyrrol-3-yl)-1 <i>H</i> -pyrrole-2-carboxamide III.5.9	122
II. BIOLOGY ASSAYS	123
1. Anti-bacterial assays	123
2. Cytotoxicity assays	123
3. Microscopy assays	124
REFERENCES	125
APPENDIX	129

A. INTRODUCTION

I. Deoxyribonucleic acid (DNA)

1. Structure and discovery

Deoxyribonucleic acid (DNA) is a polyanionic polymer consisting of two polynucleotide chains running in opposite directions. It contains the genetic instructions for the synthesis of proteins in all known living organisms and some viruses. It was discovered as a major chemical within the nucleus in the 19th century ^[1] and acts as a carrier of genetic information in all living species. DNA is made up of nucleotides, which contain three components: a phosphate group and a nitrogenous base attached to a five membered ring sugar called pentose ^[2]. Two families of nitrogenous bases can be found in DNA: the purine family, consisting of adenine (A) and guanine (G), and the pyrimidine family which includes the cytosine (C) and thymine (T). Within the DNA helix, A:T base pairs form 2 hydrogen bonds, whereas G:C base pairs form 3 hydrogen bonds, and all ring atoms lie in the same plane (Figure 1).

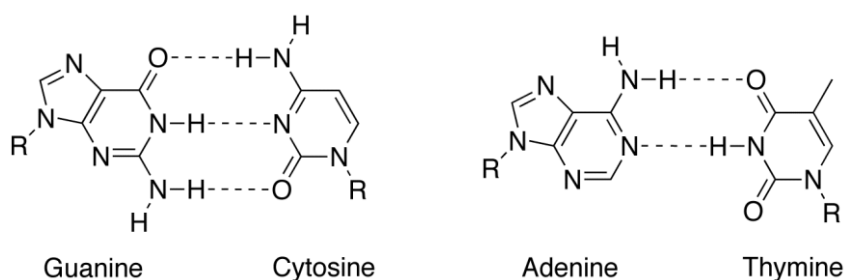


Figure 1. Hydrogen bonding in base pairs.

These bases are attached to a pentose sugar forming the deoxyribonucleoside. The deoxyribonucleosides are joined at both the 3'-hydroxyl and 5'-hydroxyl groups to phosphate groups in ester links, also known as "phosphodiester" bonds. These structures are called deoxyribonucleotides. The right handed spiral formed by the double helix of DNA has two grooves: the width of the major groove (22 Å) allows the edges of the bases to be more accessible compared to the minor groove whose width is half of the major (Figure 2).

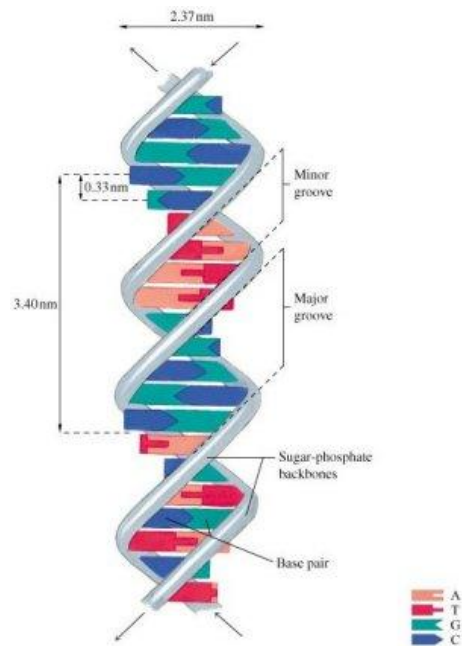


Figure 2. DNA: structure of double helix ^[3].

The structure of the DNA double helix, stabilized by hydrogen bonds, was determined in 1953 by James Watson, Francis Crick, Maurice Wilkins and Rosalind Franklin for which all received the Nobel Prize in 1962, except Rosalind Franklin who died in 1958. To test their ideas on the possible structure of DNA - the molecule responsible for heredity - Rosalind Franklin and Maurice Wilkins used X-ray diffraction. This method provided the evidence of the helical structure of the DNA, formed by alternating deoxyribose and phosphate molecules ^[4]. The major breakthrough came later with X-ray crystallography proving that the number of A:T and C:G base pairs were equal ^[5]. Later Watson and Crick proposed that one strand of the DNA helix serves as a template for recreating the other half during DNA replication. This hypothesis was proved in 1958 by two pieces of evidence: first, the enzyme that catalyses the synthesis of DNA - DNA polymerase - was discovered and second, using nitrogen isotopes to follow the construction of new DNA, it was observed that each daughter cell contains one strand of the mother cell's DNA. This strand acts then as a template for DNA polymerase to synthesize the complementary strand, thus completing a new DNA molecule ^[4].

2. DNA grooves ^[6]

Among the different families of DNA polymorphs, B-DNA is the most physiologically relevant; it has base pairs approximately orthogonal to the double helix axis and displaced only by a small distance from this axis. The attachment of the phosphodiester backbone to

the base pairs shows two distinct indentations, forming the major (width: 11.6 Å, depth: 8.5 Å) and minor (width: 6.0 Å, depth: 8.2 Å) grooves. The walls of these grooves are formed by the sugar-phosphate backbone whereas the edges of the bases form the floor and are responsible for the convex surface of the grooves and provide hydrogen bond sites (Figure 3).

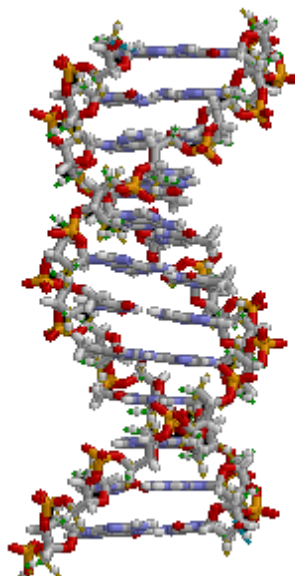


Figure 3. Structure of the DNA groove.
(yellow and orange: phosphate backbone, blue: H bond sites, the bases lie horizontally)

Since the bases are involved in the formation of the grooves, the width of the groove varies depending on the base sequence. The minor groove at A:T base regions tends to be narrower than at G:C base pair regions due to the exocyclic 2-amino group of the guanine, which widens the minor groove. For this reason A:T base pair regions can accommodate only a single layer of water molecules in the minor groove.

II. Minor Groove Binders (MGBs)

1. Introduction

MGBs include several families of structures (Figure 4) such as heterocyclic polyamides (**II.1.1**), amidino arylfurans (**II.1.2**), benzofurans (**II.1.3**), pyrrolobenzodiazepines (**II.1.4**) and aryl benzimidazoles (**II.1.5**)^[7]. Their major interest is their action as potential therapeutic agents in a variety of diseases depending on their binding with DNA and some MGBs have already entered clinical trials^[8]. While the polyamide MGBs are anti-tumor alkylating agents binding to polyanionic DNA, structures related to anthramycin bind

covalently to DNA but target limited sequences since their complex fused heterocyclic structure is less flexible than polyamide MGBs [6][7]. The aryl benzimidazoles demonstrate minor groove binding properties with especially stronger association with A:T regions than G:C, whereas amidino arylfuran - studied as antitrypanocidal agents - showed hydrogen bonding between the amidine group and A:T base pairs [7]. Pyrrolobenzodiazepines bear a chiral carbon which S-configuration allows the molecule to twist and get the right shape to interact with DNA. Nevertheless they show poor selectivity in binding specific DNA sequences.

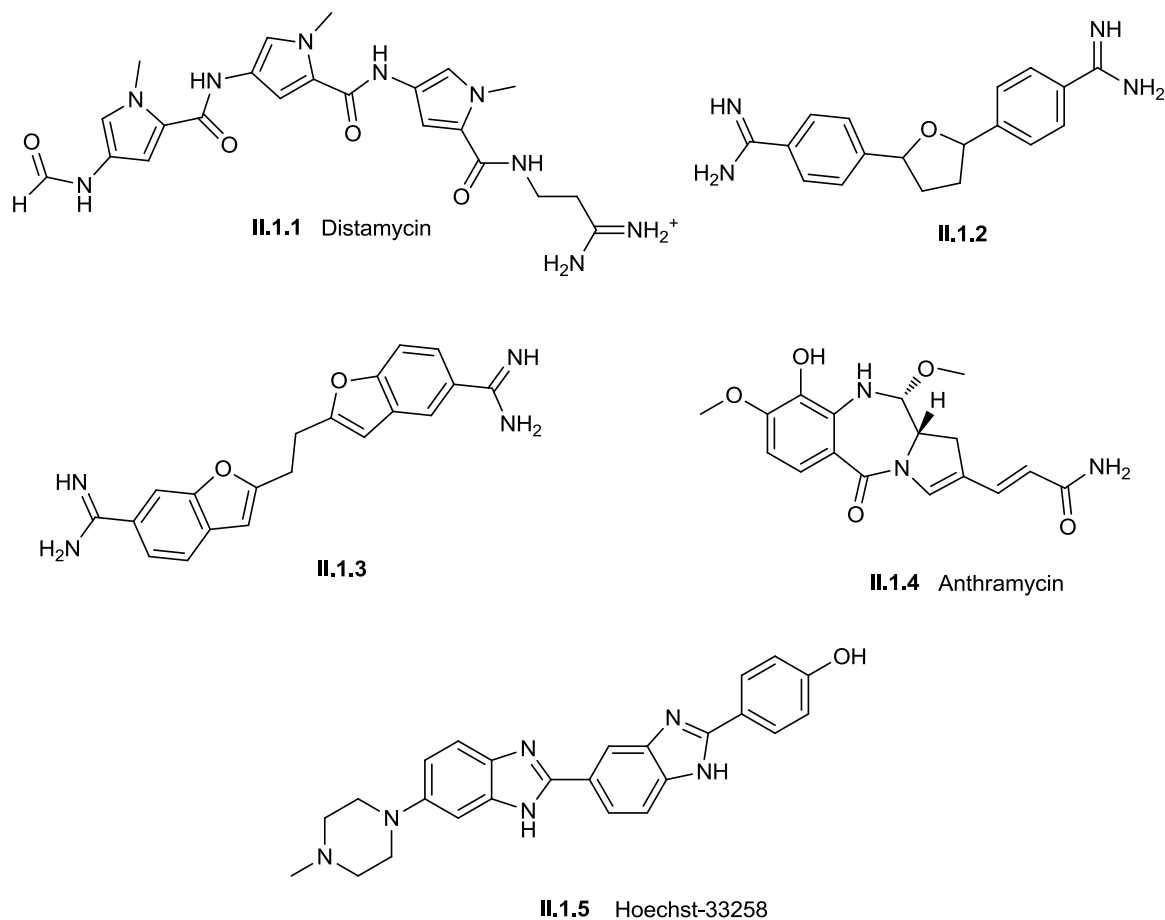


Figure 4. Structures of different classes of MGBs.

Being subject of this work, the polyamide MGBs are known to be small molecules binding non-covalently the minor groove of the B-DNA through interactions with a specific sequence of amino acids [1][2][9]. A series of heteroaromatic rings linked by peptide bonds designs the core of such MGBs, while a tail group and a head group complete the structure (Figure 5). Each part of such a molecule plays a specific role: the head group enables hydrophobic interaction with the DNA, while the aromatic or heterocyclic rings improve the hydrophobic link thanks to π -stacking with the DNA bases, and finally the tail group

promotes the transfer of the MGB into the cell and forms bonds to polyanionic DNA through ionic interactions between the phosphate groups of DNA and the positively charged tail group of the MGB [7]. The formation of hydrogen bonds between MGB and DNA bases is responsible for the non-covalent interaction of the molecule with the core of the minor groove of DNA.

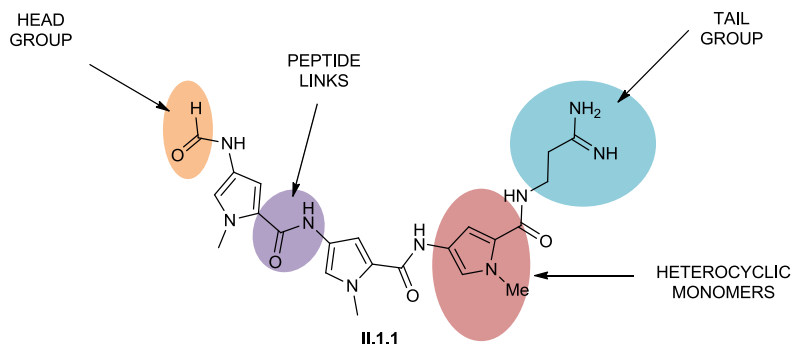


Figure 5. Structure of a minor groove binder molecule.

During the last decade many MGBs have been reported, including analogues and conjugates of naturally occurring polyamide minor groove binding agents, such as netropsin (II.1.6, Figure 6) from *Streptomyces netropsis*, and distamycin (II.1.1, Figure 6) from *Streptomyces distallicus* [10].

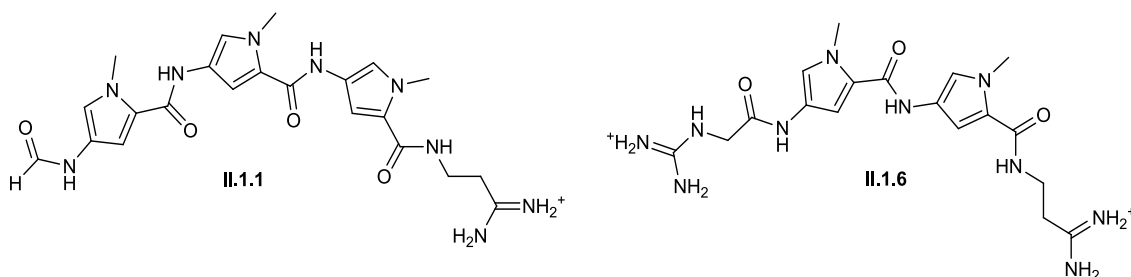


Figure 6. Structures of netropsin and distamycin [11].

Distamycin and netropsin showed significant biological activities, despite high toxicity, and bind selectively and with high affinity to A:T base pairs of the DNA [12]. The development of polyamide MGBs has required the understanding of the pairing rules for minor groove sequence recognition [1] [6] [10] [12] [16], which are based on hydrogen bonding and steric interactions between the MGB and DNA.

2. *Minor groove recognition*

Different factors are involved in selectivity in minor groove recognition by MGBs ^{[6][10]}.

a) *Interactions between MGB-DNA:*

The electrostatic distribution along the DNA sequence is unequal; A:T base pairs have the greater negative potential whereas G:C pairs have the greater positive potential. Hence the cationic charge carried by most MGBs complements A:T regions ^[6]. The sequence specific binding is due to the combination of structural and electronic interactions. However earlier studies suggested that van der Waals and hydrophobic interactions, which increase contacts with the minor groove wall, play a more important role than electrostatic interactions ^[6]: the introduction of several charged groups in the molecule did not affect the binding with DNA, whereas, the binding affinity was significantly improved when increasing the contacts between MGB and the minor groove walls.

b) *Non-covalent minor groove recognition:*

Because of the DNA structure, MGBs must be curved to match the helical curve of the minor groove of the B-DNA ^[2]. As explained in section I.2, the groove width depends on the base sequence. The first X-ray structure of a 1:1 complex of netropsin and DNA was obtained by Richard Dickerson. It emphasized the importance of shape-selectivity recognition by a pyrrole-pyrrole (Py-Py) bond linked with the A:T bases forming the wall of the narrow minor groove. Netropsin binds non-covalently to four consecutive A:T or T:A base pairs ^[10] ^[12] (Figure 7).

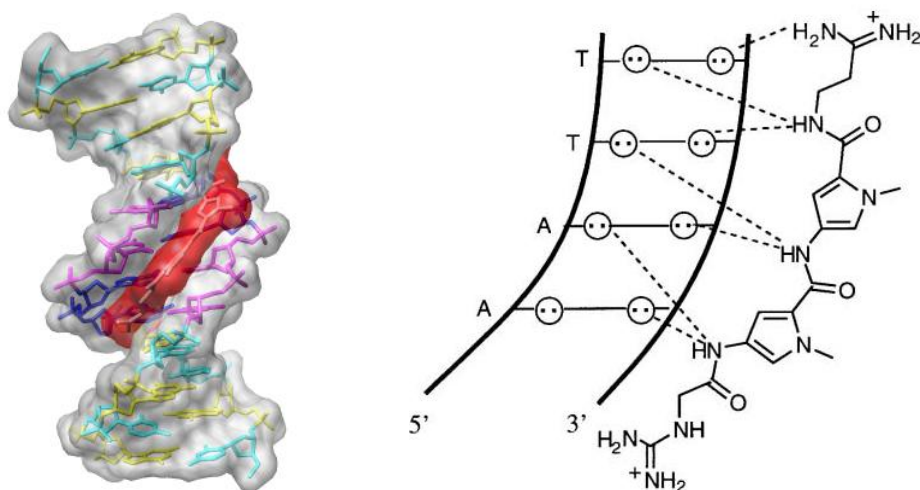


Figure 7. DNA helix with bound netropsin ^{[10][14]}.

This selectivity can be explained by the series of hydrogen bonds formed by the carboxamide NH and the terminal amidinium groups in netropsin that point down into the groove and interact with the base pair edges. The binding with G:C sequences is hindered by their wider groove and by a steric clash with the 2-amino group of the exocyclic *N*-2 of guanine with the proton located on *C*-3 of the pyrrole rings, thus preventing hydrogen bonds from being formed^{[6][15]}. To target G:C base pairs, Kopka et al. proposed a replacement of one pyrrole (Py) ring by imidazole (Im). This arrangement preferred G:C over A:T, both because of the reduced bulk of the imidazole ring and the possibility of an additional H-bond (Figure 8). This netropsin analogue was named lexitropsin^[16].

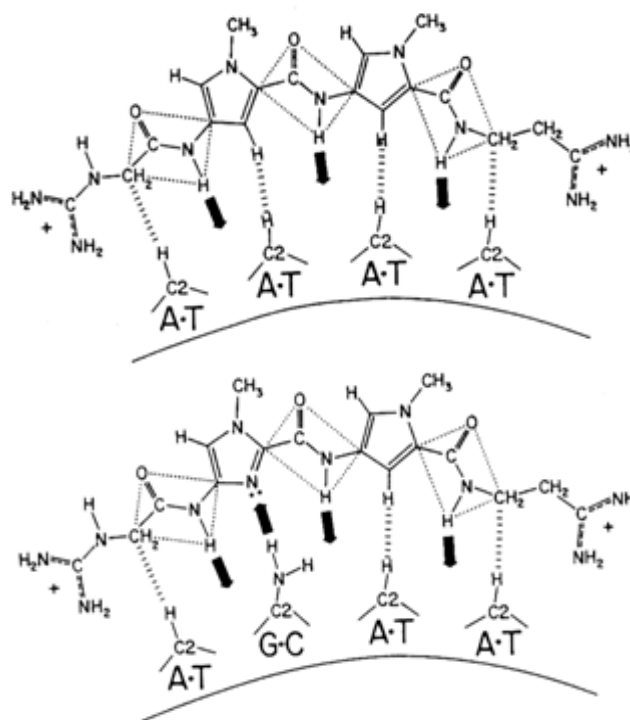


Figure 8.

Comparison of bases sequence binding between netropsin/DNA complex and a lexitropsin/DNA^[16].

In 1989, Wemmer and Pelton demonstrated the formation of a distamycin(Py-Py-Py)/DNA complex in 2 to 1 proportions; as long as the cationic tails of the two distamycins were widely separated allowing the molecules to sit side-by-side as an antiparallel complex within the AT sequences located in minor groove^[16]. Further studies carried out by Dervan showed that an antiparallel dimer Im-Py-Py could also bind to DNA (Figure 9).

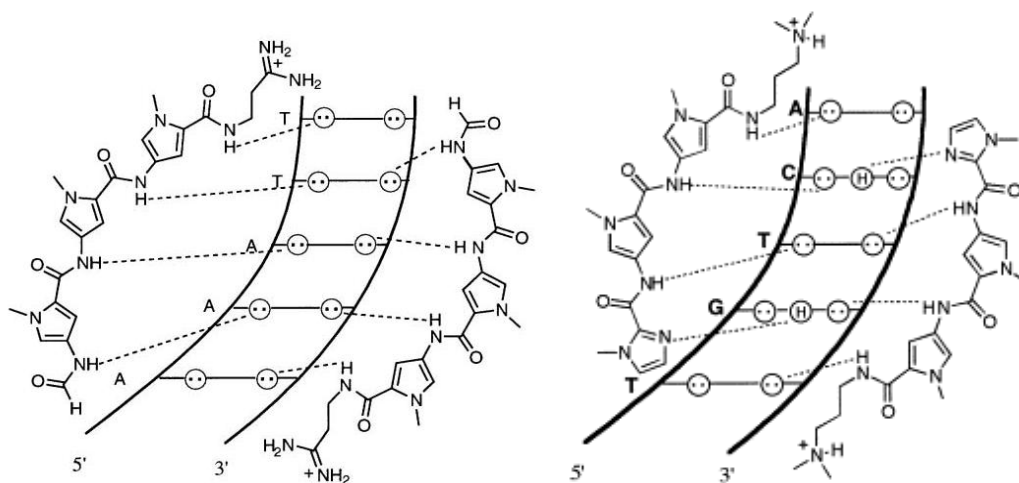


Figure 9. Distamicin/DNA (2:1) complex (right) and Im-Py-Py/DNA (2:1) complex (left) ^[10].

This discovery generated a recognition code regarding the sequence targeted according to heterocycles used in MGBs: Pyr-Pyr targets both A:T and T:A pairs without discrimination, Im-Pyr reads G:C pairs and finally Pyr-Im targets C:G base pairs ^[16].

In the middle of the 1990s, Dervan's group completed the recognition code by distinguishing T:A and A:T base pairs. In order to favour binding to T over A, a hydroxyl group was introduced at C-3 of the pyrrole ring to generate a hydroxypyrrole (Hp) ring. This hydroxyl group destabilizes interactions with adenine on steric grounds but the possibility exists of a new hydrogen bond with the O-2 of thymine ^[10] (Figure 10).

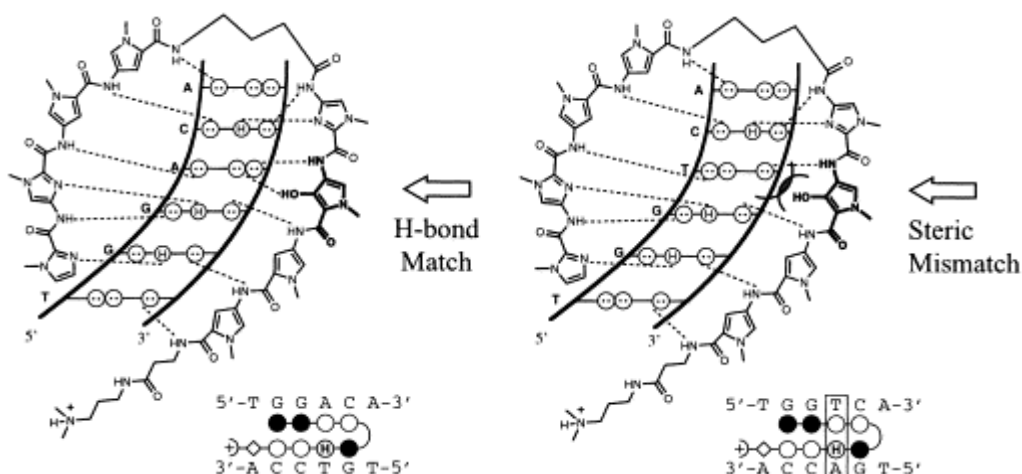


Figure 10. Match and mismatches of Hp-Py/DNA complex ^[10].

Pyr-Hp reads A:T whereas Hp-Py targets T:A base pairs, and Im-Pyr reads G:C whereas Pyr-Im targets C:G base pairs. In this way it became possible to differentiate AT from TA,

and G:C from C:G, by choosing the proper rings to interact with each base pair. The conclusions are the following depending in the succession of aromatic or heterocyclic rings chosen: Pyr-Hp reads A:T whereas Hp-Py targets T:A base pairs, and Im-Pyr reads G:C whereas Pyr-Im targets C:G base pairs ^[10]. Nevertheless, as Walker *and al.* showed, the position of a recognition unit within the minor groove by the binding molecule remains a more critical factor to sequence specificity than its inherent ability to read the sequence ^[6], since the sequence specificity would be lower for a polyamide bearing entirely base-specific rings than for a two or three-ring polyamide composed of one ring that would bind to any of the four bases and of one or two base-specific rings ^[17].

After the discovery of these pairing rules for sequence specificity, the use of MGBs was extended to gene regulation ^[17]. Dervan showed the inhibition of the NF- κ B transcription factor through interactions of the DNA binding site of NF- κ B with a sequence-selective MGB ^[19]. NF- κ B has been related to inflammatory diseases as well as in HIV ^{[20][21]}. In the cytosol, the phosphorylation of the complex NF- κ B with inhibitor protein I κ B - inactive form of NF- κ B - releases the active form of the NF- κ B complex, which then permeates the nucleus and binds to specific regions of DNA, resulting in significant responses in gene expression ^[22]. The NF- κ B's DNA binding site (5'-GGGACTTTCC-3') is quite long in terms of MGB binding. Supporting his theory on the pairing rules, Dervan designed polyamide hairpin MGBs capable of selectively binding portions of this binding site: 5'-GGACT-3' on one hand, and 5'-ACTTTCC-3' on the other hand. The results showed that the binding of DNA with NF- κ B transcription factor was inhibited when MGBs were bound to the 5'-GGACT-3' site only. For example, the 5'-GGAC-3' sequence was targeted by the designed Im-Im-Pyr-Pyr, while the complementary sequence 5'-CCTG-3' was targeted by Pyr-spacer-Pyr-Im (molecule **II.2.1**, Figure 11).

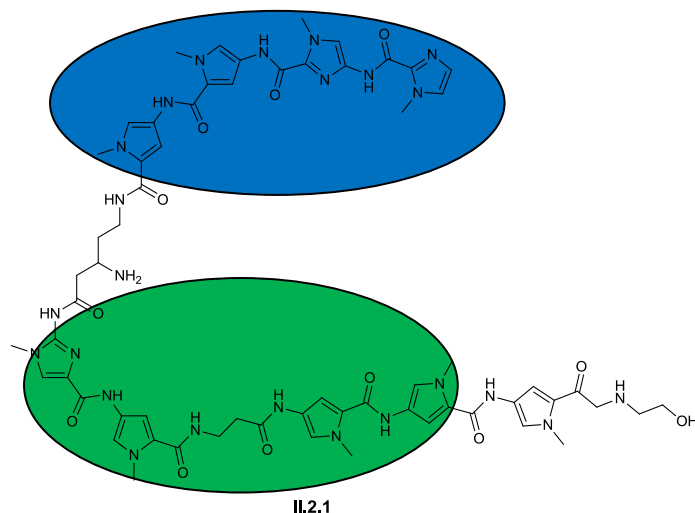


Figure 11. Hairpin linked MGB (targets: 5'-GGAC-3' in blue and 5'-CCTG-3' in green).

Recently various hairpin linked MGBs have been explored as artificial regulators. For example, HOX (homeobox) proteins are transcription regulators^[23] which form a triple helical helix with DNA^[24]. These proteins play a vital role in embryo development^[25]. This role has been explored in *Drosophila melanogaster* where mutations in the Hox ultrabithorax (Ubx) gene led to the transformation of halteres or balancing organs into a set of wings^{[26][27]}. In order to bind strongly with DNA, Hox proteins must interact with a three amino acid loop extension (TALE) and hence bind DNA as a dimer. This dimer interaction, occurring via a short peptide sequence, provides DNA sequence selectivity and high affinity with DNA^[28]. Crystal studies suggested an interaction between Ubx and the drosophile TALE protein extradenticle (Exd) via a docking peptide^{[29][30]}. Dervan decided to synthesize polyamide MGBs that could mimic the action of Ubx thanks to an appropriate peptide side chain, and then could act as an artificial developmental regulator. From this work, the three hairpin MGBs shown Figure 12 were synthesized. Electrophoretic mobility shift assays (EMSA) were carried out to assess the ability of these molecules to enhance the Exd binding with DNA. Only molecule **II.2.3**, bearing the functional hexapeptide, enhanced the binding between Exd and DNA by improving the affinity of Exd to its binding site by at least 200-fold^[31]. On the other hand, molecules **II.2.2** and **II.2.4** did not associate successfully with Exd.

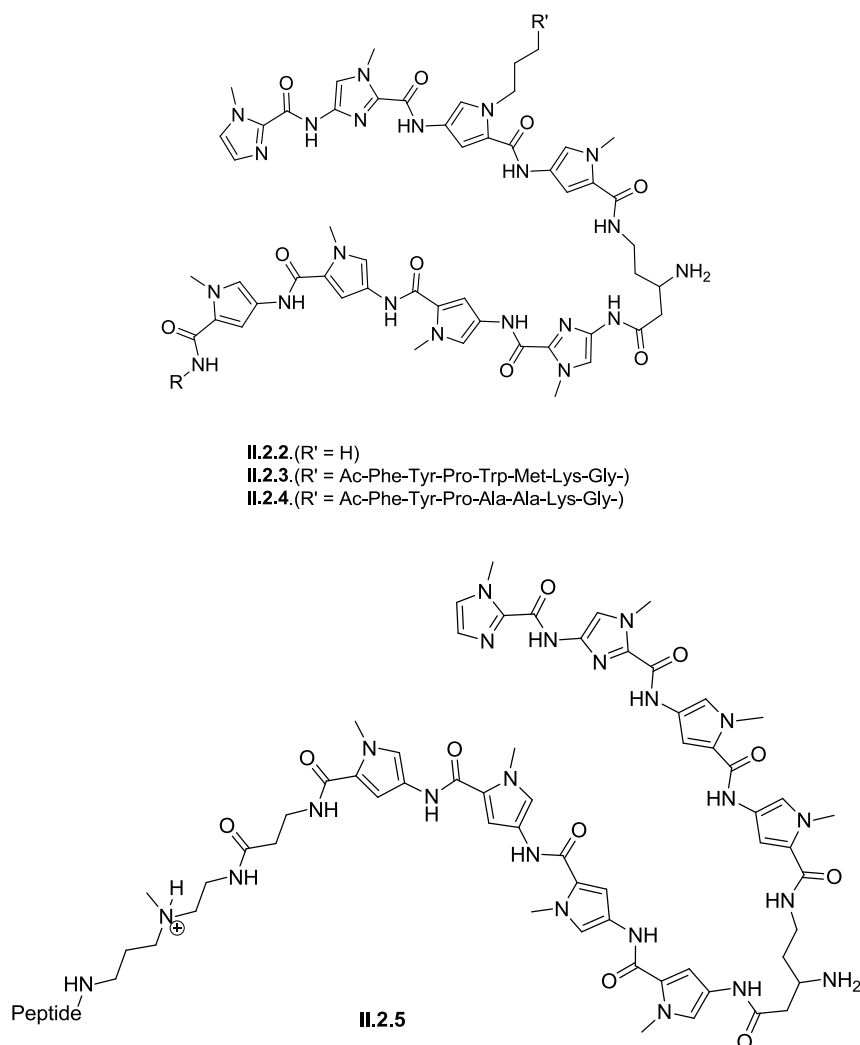


Figure 12. Branched and linear hairpin MGBs mimicking Ubx.

Later, Dervan *et al.* prepared a series of linear polyamide-peptide MGBs^[32] (structure **II.2.5**, Figure 12) to assess the optimum peptide length used, but also to find the optimum location of the MGB into the groove. Studies showed that the hexapeptide could be replaced by a tripeptide without affecting the activity, and Exd binding could be enhanced even at a distance up to 6 base pairs away from the binding site in the Exd major groove.

3. Structure of binding and interactions with DNA

Knowing that gene regulation is controlled by interactions between protein and DNA, it has been estimated that a sequence of 16 to 18 bases in a DNA genome should form the binding site in order to have the ability to target a single gene out of the total human genome, that is to have a unique binding site^[6]. Two approaches have been used to design and synthesize molecules able to discriminate one particular gene and down regulate its expression or to

stop the release of viral proteins ^[6]. The first method uses oligonucleotides to target the major groove of DNA, and form a triple helical structure; this is known as the ‘anti-gene’ approach. The second method uses molecules such as lexitropsins that interact non-covalently with the DNA minor groove ^[6]. The latter approach is the one used in our case. Since the discovery of netropsin and distamycin, strategies have been described to design more selective MGBs which take advantage of hydrophobic interactions as well as hydrogen bonding with the minor groove of DNA ^[2].

a) DNA curvature

Helix bending is a factor of protein/DNA recognition. As stated earlier, the minor groove of B-DNA is convex; hence the bound molecules must possess a curvature to match the helical curve ^[2].

b) Width of the minor groove

Theoretical analysis suggested that the motion of the flexible phosphate backbone and base pairs contribute predominantly to the groove width variations ^[6]. Drug-DNA crystal structures were used for molecular dynamic simulations to analyse the flexibility of the sugar-phosphate backbone in DNA and also to understand the relationship between the base-steps staking, composition or sequences, and sugar-phosphate backbone motion. The introduction of a ligand showed different responses from the sugar-phosphate backbone and the bases. Due to the covalent binding with the backbone, the motion of the bases influences the conformation of the sugar-phosphate backbone, and consequently the width of the minor groove. However, the flexibility of the sugar-phosphate backbone can change the width of the groove without any change in the base-stacking ^[33].

The binding of MGB molecules with DNA is also affected by the sequence-dependent width of the minor groove. As stated earlier, the floor of G:C sequence areas shows discontinuities arising from the hindrance of the exocyclic 2-aminogroup of the guanine, which broadens the minor groove and prevents some binding molecules attaining close contacts with the floor ^[6]. To enable the insertion of a ligand (e.g. MGB) into the minor groove, a deformation of DNA is necessary. First, the energetically demanding movement of the bases occurs by changing the DNA shape, and therefore the width of the groove. This motion optimizes the hydrogen bonding and reduces the major steric clashes between the DNA floor and the ligand. Second, the independent movement of the sugar-phosphate backbone allows induced fit conformation of the ligand in the minor groove and optimizes the complementarity between the bases and the corresponding heterocyclic rings of the ligand ^[33].

c) Hydrophobicity

Nucleobase recognition depends on the shape and specific bonding interactions between DNA and MGBs. The lipophilicity and ionic state of the molecules are also important and must be taken into account. Although the hydrophobic effect, ie. displacement of water molecules in the minor groove during the binding of drug molecules to the DNA, has not been explored as a necessary feature for minor groove recognition, the change of entropy is favorable^[6] and it has been argued to be the main driver for binding the MGB to the minor groove. However, some of our MGBs do not have a favorable entropy of binding, but still show good binding due to their hydrophobic central part having a capacity to form hydrogen bond to the bottom of the groove. Thus to show high affinity, ligands should have large non polar regions. The major concern for such ligands largely composed of non polar subunits, is the possible low solubility in water and, if this is overcome by the use of one basic tail group, the effect on the ability of the molecule to penetrate lipid membranes by passive diffusion^[34].

To increase the hydrophobicity, groups larger than methyl, such as *N*-alkyl or *C*-alkyl groups, were introduced into MGBs. These groups sit on the outside of the helix and prevent side-by-side binding, thus increasing the length of DNA that can be covered. For instance, when the two thiazotropsin A molecules (Figure 13) sit head-tail in the minor groove, the isopropyl substituent and the sulfur atom, located towards the tail group, prevent the overlap of the three heterocyclic rings and thus extend the base-pair coverage^[12].

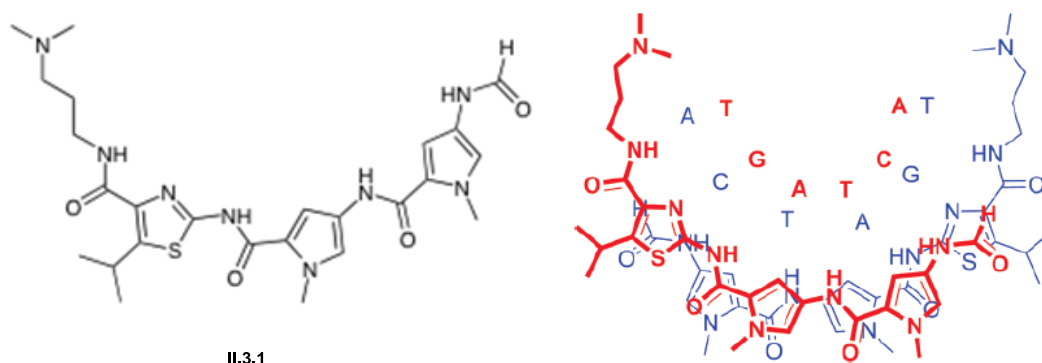


Figure 13. Structure of thiazotropsin A (**III.3.1**) and head-tail overlap of two thiazotropsin A.

The introduction of either a hydrophilic head group or an alkene-linked head group did not improve the binding with DNA.

d) Selectivity and biological results

The selectivity and affinity of binding will depend on the ability of the ligand to make hydrogen bonds to the bottom of the minor groove, where the bases offer a sequence-dependent pattern of H-bond donors and acceptors^[35].

Molecules binding to the minor groove of DNA have a greater chance of reading the information provided by the base-pair sequence as part of the usual process of transcription. To read more than 4 base pairs, an extension of the length of MGBs is necessary to achieve binding with a more specific base pairs sequence^[34], using the base pairing code from Dervan's discovery discussed earlier^[10].

Several groups have prepared antibacterial minor groove binders^[7]. Genesoft's work led to MGBs containing *N*-alkyl substituted pyrroles and variations of the dichloroisothiazole head group, such as molecule **II.3.2** (Figure 14). These extended netropsin analogues showed a minimal inhibitory concentration in the 50 ng/mL range against bacteria^[36]. Genelabs studied extensively netropsin analogues, such as molecule **II.3.3** (Figure 14), which includes a dimer of heterocyclic amides linked head to head by a rigid linker. This structure and the corresponding monomer showed antibacterial and antifungal activity. However the most active antibacterial compounds bear either an *N*-cyclopropylmethyl or *N*-2-methylbutyl pyrrole, with the latter substituent being less toxic^[7]. MGBs containing indoyl amides showed antifungal activity. From these studies, features leading to antimicrobial activity remained unclear. However, the antibacterial activity appeared to be related to planar aromatic head group containing amides, cycloalkyl *C*-, branched alkyl and *N*-alkyl group on the heterocycle. Nevertheless no structure-activity relationship emerged from these studies, even when the binding to DNA was shown.

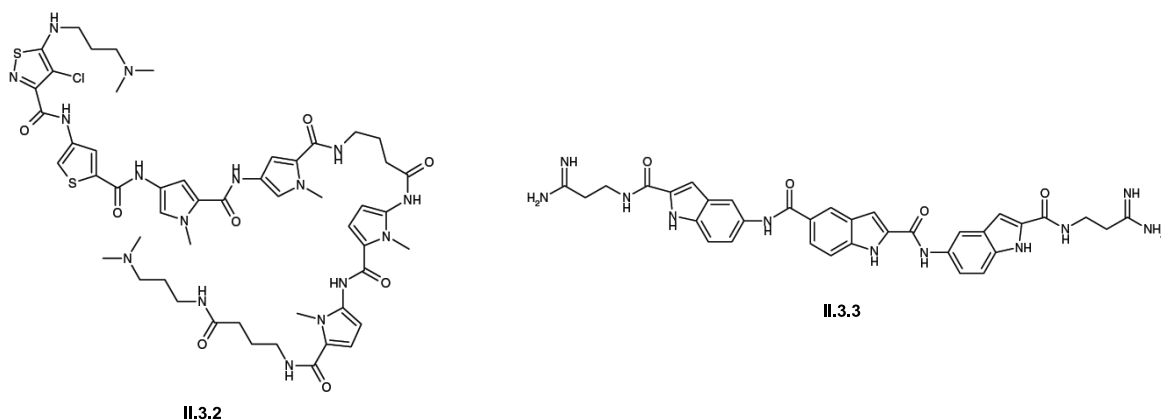


Figure 14. Antibacterial molecules from Genesoft and Genelabs^{[7][36]}.

After Dervan's work, other groups thought that the length of MGB was important for biological activity at a gene level since telomeres contain A:T rich regions. The University of Geneva decided to introduce flexible amphipathic linkers which would not bind strongly to the minor grooves but would allow the MGB to find the favoured binding site^{[7][37]}.

Distamycin derivatives bearing alkylating functional head groups were synthesized and showed potential anti-cancer activity; the most potent was tallimustine (IC₅₀ = 68.5 nM), molecule **II.3.4** (Figure 15), containing a dialkyl head group^[7]. Later monofunctional alkylating agents, such as the clinical candidate brostacillin (**II.3.5**, Figure 15), were found to be more than 10 fold more potent^[38].

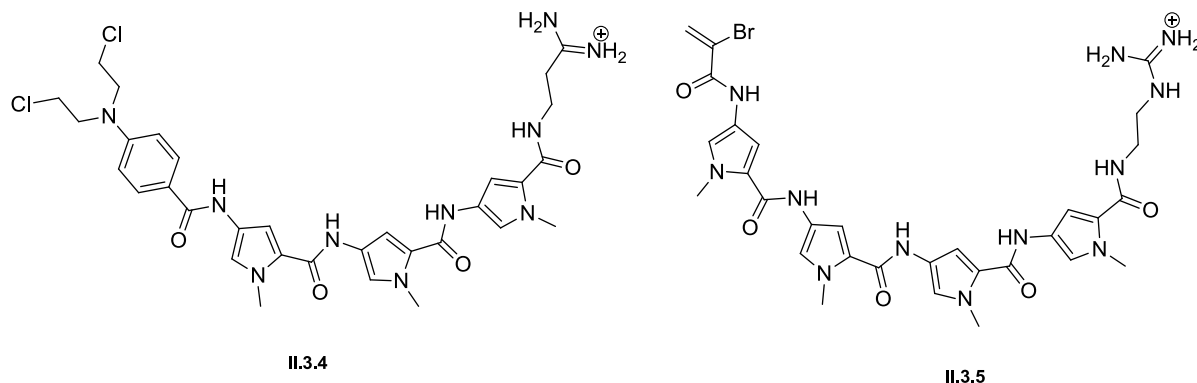


Figure 15. Tallimustine (**II.3.4**) and Brostacillin (**II.3.5**)^{[7][38]}.

Other minor groove binders, based upon a spirocyclopropylquinone structure, showed very high potency despite the high toxicity of the natural products. In this family, cyano CBI-derivatives^{[7][39]} (**II.3.6** and **II.3.7**, Figure 16) were active in the picomolar range. This activity is due to the cyano electron-withdrawing group that enhances the alkylating activity and results in strong binding with DNA. These derivatives also showed high toxicity against mouse lymphatic leukemia cells.

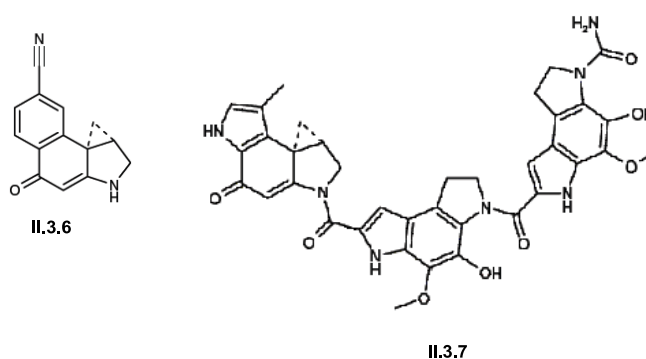


Figure 16. CCBI (**II.3.6**) and a derivative molecule^{[7][39]}.

Taiho Pharmaceutical Company developed benzene fused MGBs, such as molecule **II.3.8** (Figure 17), with a chloromethyl substituent in order to improve the alkylating activity. The

most effective compounds were active against melanomas and breast, ovarian and lung tumor cells but totally inactive against leukemia cells^[40]. The discovery of anthramycin, an antitumour antibiotic, led to pyrrolobenzodiazepines being developed by Spirogen Ltd. These structures still contained a substituted benzene ring and the unsaturated 5-membered ring^{[41][42]} (**II.3.9**, Figure 17), which features are necessary for retaining activity. The S-configuration gives the helical shape necessary to bind to the minor groove. This work led to structure **II.3.10** (Figure 17) which is an ether-linked dimer showing an activity 100-fold higher than the corresponding monomer^[43].

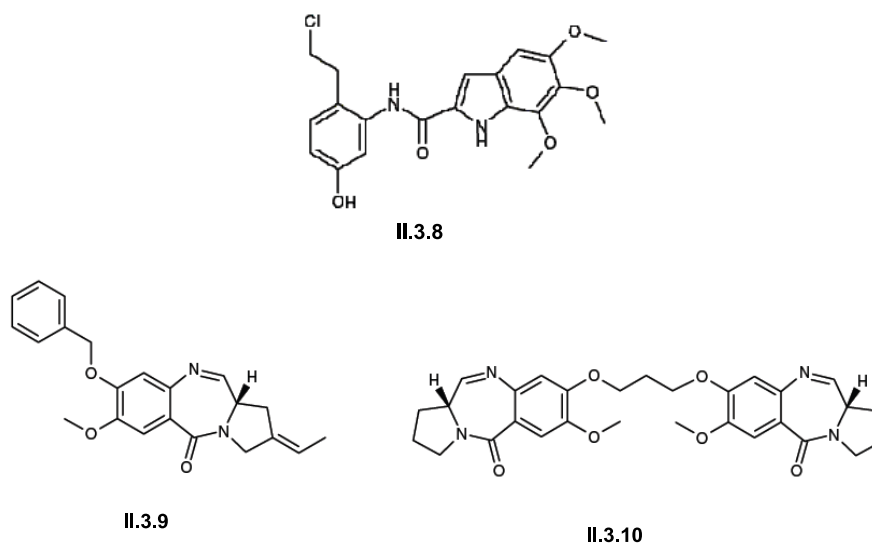


Figure 17. Minor groove binders from Taiho Ltd and Spirogen Ltd^{[7][40][41][42][43]}.

Benzimidazoles were investigated as building blocks for MGBs after the discovery of the bonding between Hoechst-33258 and DNA. They were first coupled to features such as alkylating agents and *N*-methylpyrroles to give molecules such as a trifunctional alkylating MGB which was 150 fold more active than distamycin^[7]. Symmetrical bis-benzimidazoles bearing alkylating or neutral or basic hydrogen bonding head groups, were shown to be 3- to 10- fold more cytotoxic towards ovarian cells than Hoechst-33258^[44]. One compound of this family was found to inhibit DNA transcription (molecule **II.3.11**, Figure 18). Structure **II.3.12** (Figure 18)^[45], which contains benzoxazole amino acid and a bulky tert-butyl head group, showed nanomolar activity towards mouse lymphatic leukemia cells. The University of North Carolina discovered the necessity of two amidine groups in bisbenzofurans and bisbenzothiophenes for biological activity, since the hydrogen bond between the NH of the amidine and DNA is important. Molecule **II.3.13** (Figure 18), a bisbenzothiophene bis-amidine, was found to be active against *Pneumocystis carinii*^[46].

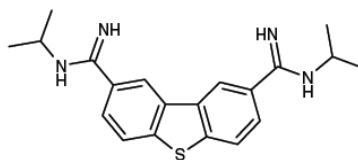
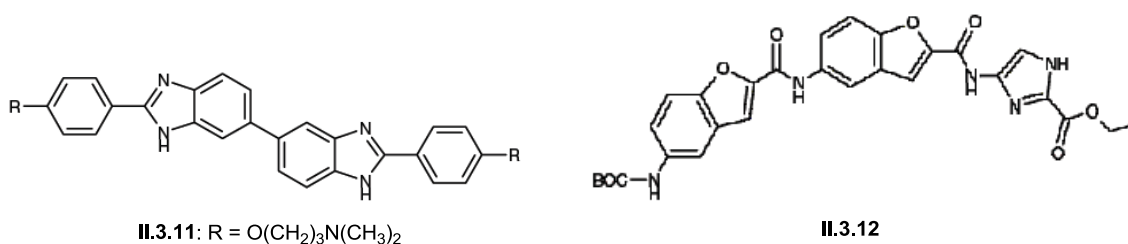


Figure 18. Structures of symmetrical bis-benzimidazole (**II.3.11**), benzofuran polyamide (**II.3.12**) and bisbenzothiophene bis-amidine (**II.3.13**).

Finally, analogues of pentamidine have been studied as potential antibacterial drugs, and alkyl substituents seemed to improve the binding with DNA through van der Waals interactions with ribose in the backbone. Molecules such as **II.3.14** (Figure 19), target essentially A:T regions and the measurement of melting temperature demonstrated the importance of *N*-substitution for greater affinity. Acyl derivatives of amidines were active *in vivo* ^{[47][48]}.

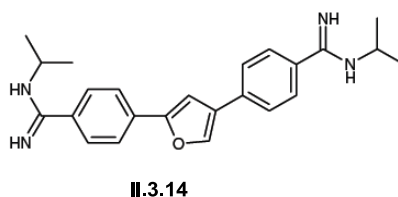


Figure 19. A bisaryl dialkylamidine.

Earlier studies have also demonstrated that molecules showing the most significant antibacterial activity contain alkene links in the *E*-configuration and a source of a hydrogen bonding in the head group ^{[49][2]} (see Table 1 and Figure 20).

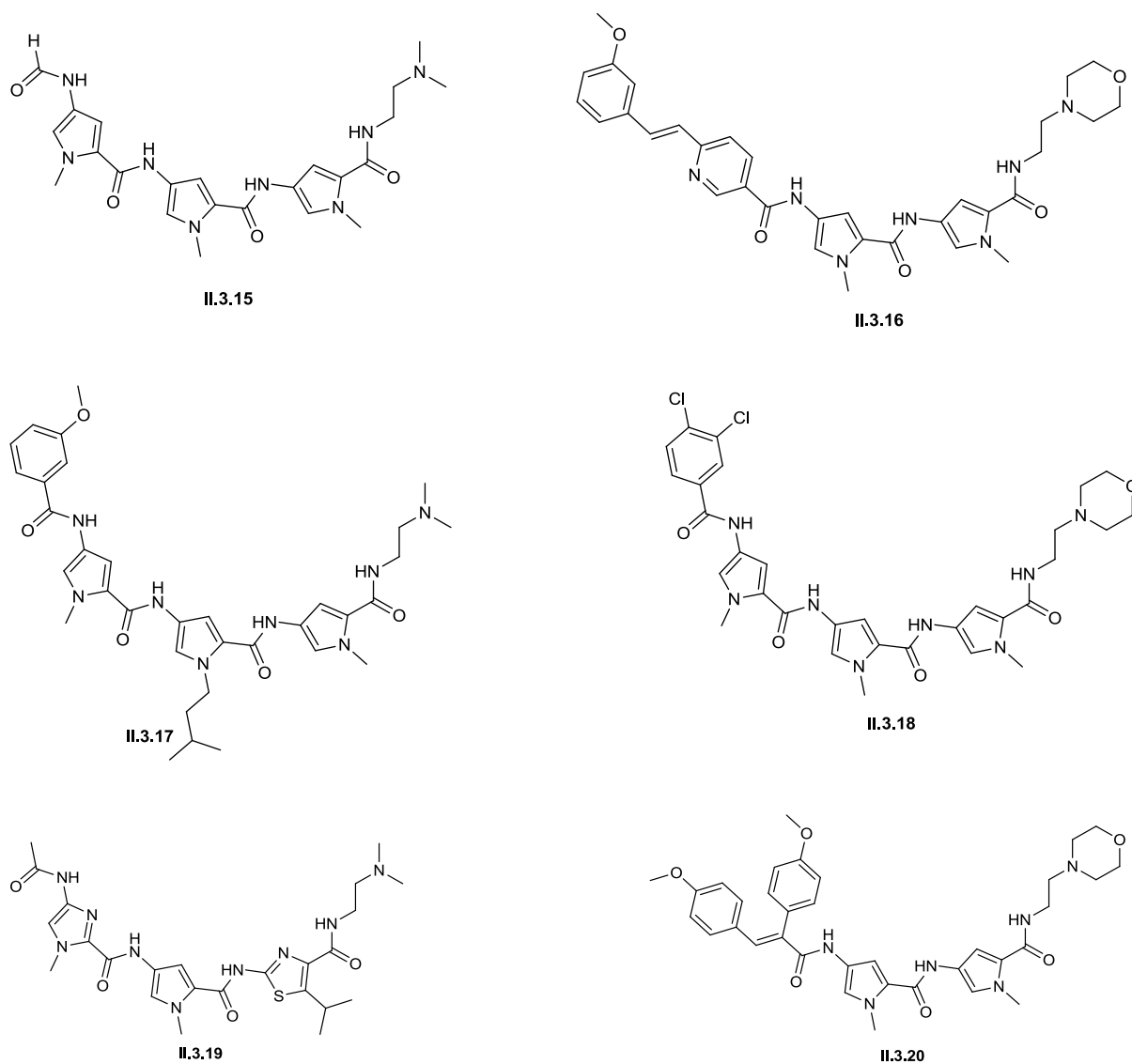


Figure 20. Structures of molecules tested.

Compound	Tail	<i>pK_a</i> tail group	Structural feature	Biological activity
II.3.15	<i>t</i> -amine	9.99	no lipophilic groups	weak antibacterial
II.3.16	morpholine	7.41	H bond head and <i>E</i> -alkene	selective antibacterial
II.3.17	<i>t</i> -amine	9.99	H bond head and <i>N</i> -pentyl	selective antibacterial
II.3.18	morpholine	7.41	2,3-dichlorobenzoyl head	inactive antibacterial
II.3.19	<i>t</i> -amine	9.99	imidazole and <i>C</i> -alkylthiazole	inactive antibacterial
II.3.20	morpholine	7.41	H bond head and <i>Z</i> -alkene	antibacterial
II.1.1	amidine	12.4	amidine	toxic

Table 1. Antibacterial activity of MGBs as a function of the *pK_a* of the tail group ^[2].

These data demonstrate the importance of a head group containing an alkene for antibacterial activity. Furthermore the *E*-configuration is important for selectivity. Head groups containing a strong electron withdrawing substituent, such as chlorine (molecule **II.3.18**), are inactive towards bacteria. In order to improve the antibacterial activity of polyamide MGBs, Prof. Suckling's group, University of Strathclyde, thought of increasing the lipophilicity of MGB molecules, by replacing an amide with an isosteric alkene that is geometrically similar to the amide. The inclusion of the alkene should not change the curvature of the MGB. However, a potential hydrogen bond with DNA is lost and can result in a steric clash between the CH of the alkene and DNA ^[2]. Alkene head groups also give fluorescence properties to the molecule, enabling further investigation regarding their transport into both mammalian and bacterial cells by fluorescence microscopy.

Previous work has shown that the selectivity for the target base sequence by the target molecule can be modified by simply changing the tail group ^[2]. Table 1 shows that a morpholine and *t*-amine, which are both basic tail group, seem to enhance the antibacterial activity compared to the amidine - hence the importance of the protonation state of the tail group. The lack of toxicity of MGBs seems to depend mainly on their basic tail group structure, the pK_a of which has been suggested to have a major influence on access to bacterial and mammalian cells ^[2]. The conclusions of several studies emphasize that molecules possessing the least basic tail group show the best antibacterial activity ^{[2][50][51]}.

III. Aims of this study

Taking into consideration the earlier results defining the structure and properties required for antibacterial activity, we proposed to synthesize new MGBs differing principally in the tail group to evaluate their activity, potency and selectivity towards different cells, such as Gram positive or Gram negative bacteria and mammalian cells, and also to understand better the transport mechanism. The first part of the work in this thesis consists of the total synthesis of small molecule analogues of distamycin as potential antibacterial agents. As the tail group is significant for both the cell membrane permeation and the binding with DNA, the importance of pK_a of the tail group will be then investigated by preparing analogues containing the same head group but different tail groups. The second aim is to run the biological assays with the different molecules synthesized to finally investigate the influence of the tail group on antibacterial activity and selectivity between bacterial and mammalian cells.

B. SYNTHESIS OF MGBs

1. Choice and synthesis of the head group

Earlier studies have demonstrated that molecules showing the most significant antibacterial activity against Gram positive bacteria ^[52] containing a head group with an alkene in the *E*-configuration. This alkene promotes identical but stronger binding with DNA than amide linked analogues ^{[49][12]}, and increases the hydrophobicity of the molecule.

The choice of the head group was made between three head groups containing an alkene function (**I.1**, **I.2**, and **I.3**, Figure 21). The head group was chosen on the basis of two important properties:

- a) satisfactory fluorescence, which enables one to see permeation through the cell membrane to reach the nucleus, and
- b) good solubility.

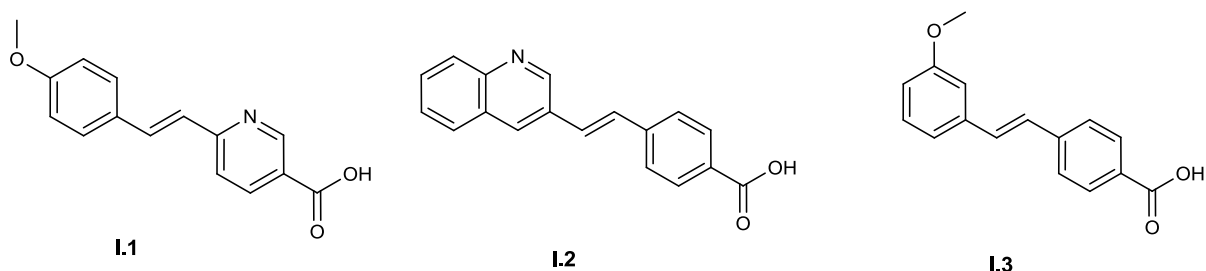
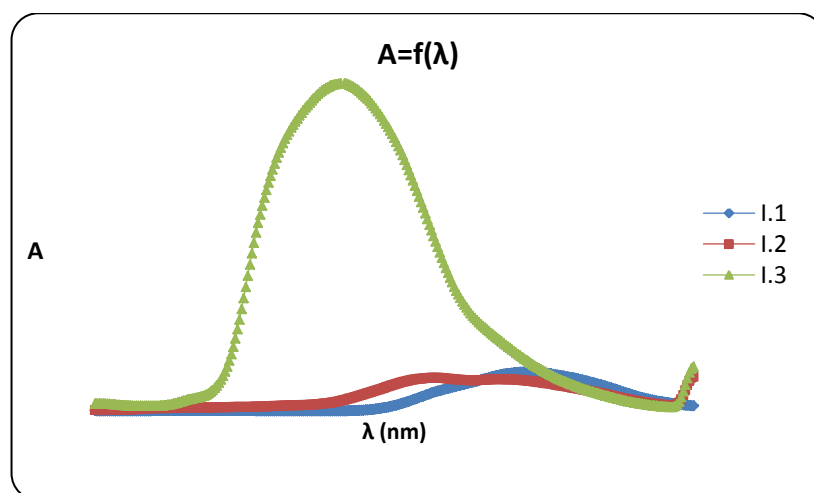


Figure 21. Head groups.

1. UV and fluorescence measurements

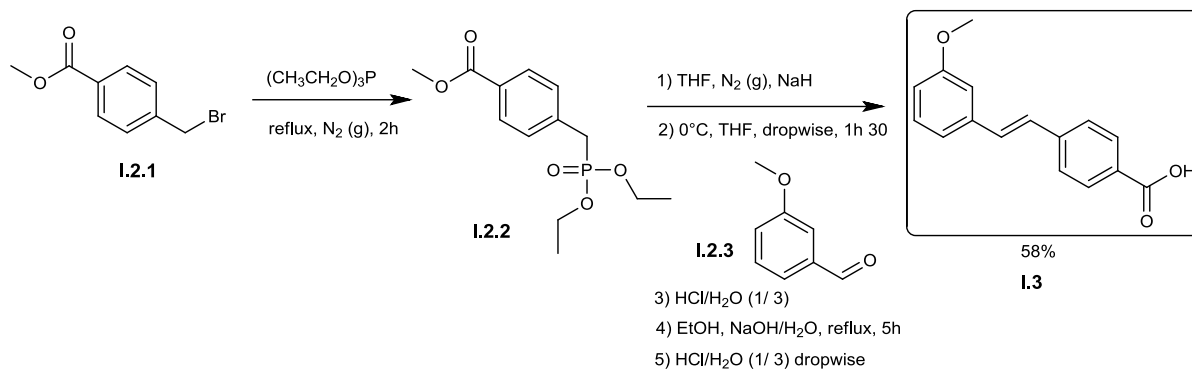
UV measurements gave the average wavelength (between 315 nm and 325 nm) at which the three head groups showed good absorption. Then fluorescence measurements were taken, dissolving **I.1**, **I.2**, and **I.3** in water to get a concentration of 3.1 mmol.L⁻¹. The solutions were excited at 300 nm and gave the spectra (Graph 1), which showed that **I.3** has the greatest fluorescence and would therefore give the highest chance to see our molecules within the cells.



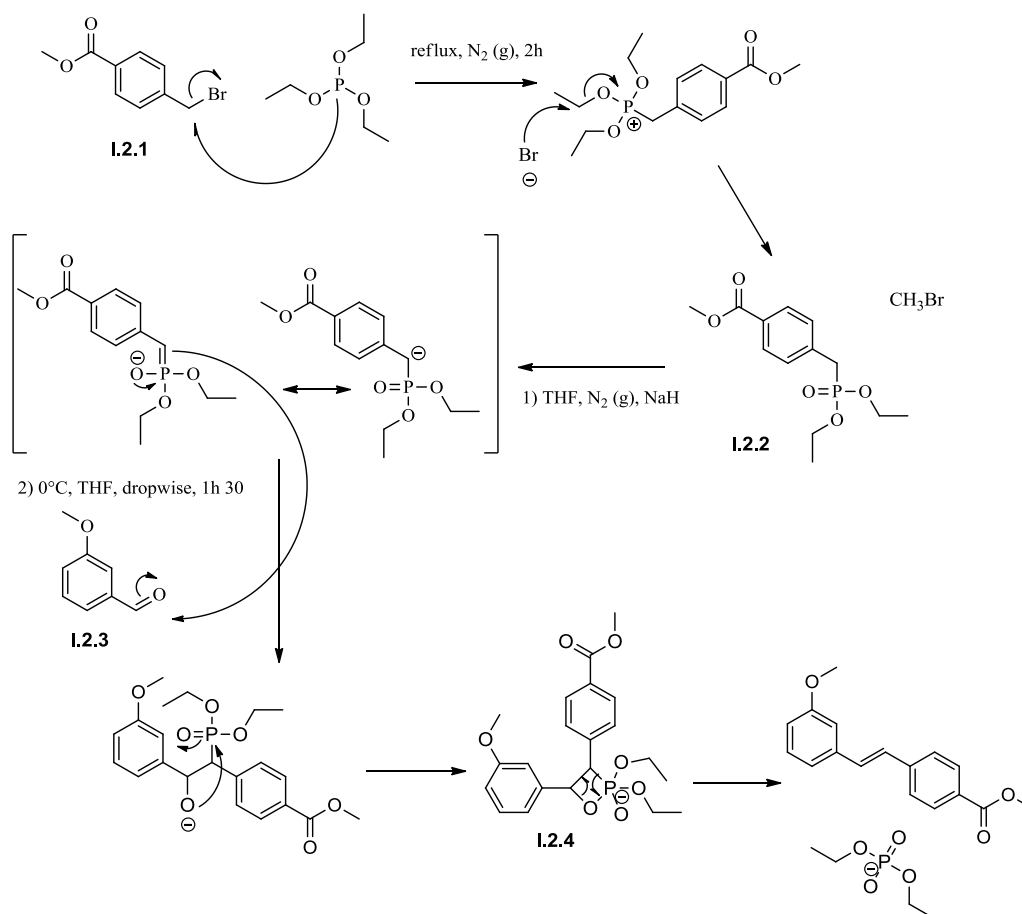
Graph 1. Fluorescence spectra
Absorbance of HGs (3.1 mmol.L^{-1} in water) against wavelength.

2. *Synthesis of I.3*

The synthesis of **I.3** (Scheme 1) required two steps including a Michaelis - Arbusov reaction (Scheme 2) to form an intermediate **I.2.2** containing a phosphorus at a stable oxidation state V^[53], followed by a Horner - Wittig reaction (Scheme 2) between the ylide and an aldehyde to give a four-membered ring system known as an oxaphosphetane **I.2.4**, which then collapsed to release the phosphonate and the alkene ester precursor to **I.3**. Reflux in sodium hydroxide solution yielded the required **I.3** (92% for the last single step).



Scheme 1. Preparation of **I.3**.



Scheme 2. Mechanism of Michaelis-Arbuzov reaction and Horner-Wittig reaction.

The selectivity in the Horner - Wittig reaction is set by steric approach control. In this case, the antiperiplanar approach of the carbanion to the carbon of the carbonyl group is favoured while the aldehydic hydrogen eclipses the bulky phosphoranyl moiety. The ester group is then placed in syn-position to the aldehyde benzylic group. The formation of the alkene assumes an *E*-orientation of these groups after rotation to form the oxaphosphetane. The coupling constant, $^3J = 16.5$ Hz, given by the NMR spectrum is characteristic of a *trans*-alkene. The resulting phosphate by product is readily separated from the desired products by simply washing with water.

II. Choice of different tail groups

Once the head group was chosen, tail groups were chosen according to their pK_a . Positively charged species form strong hydrogen bonds as well as ionic bonds with phosphate anions of DNA but ionic compounds may have difficulties crossing the lipophilic cell membranes and may therefore require active uptake into the cell. Thus, in order to understand which properties are important for the tail group, a range of pK_a s was investigated.

Another problem is associated with basic species that bind to the potassium ion channel known as Herg^[54]; blocking the potassium ion channel can lead to fatal disorders such as fatal heart arrhythmias. Hence it is important to control the pK_a of the tail group such that it does not bind to Herg, while keeping the antibacterial properties of MGBs against targeted cells. Figure 22 below shows the different tail groups used for this project:

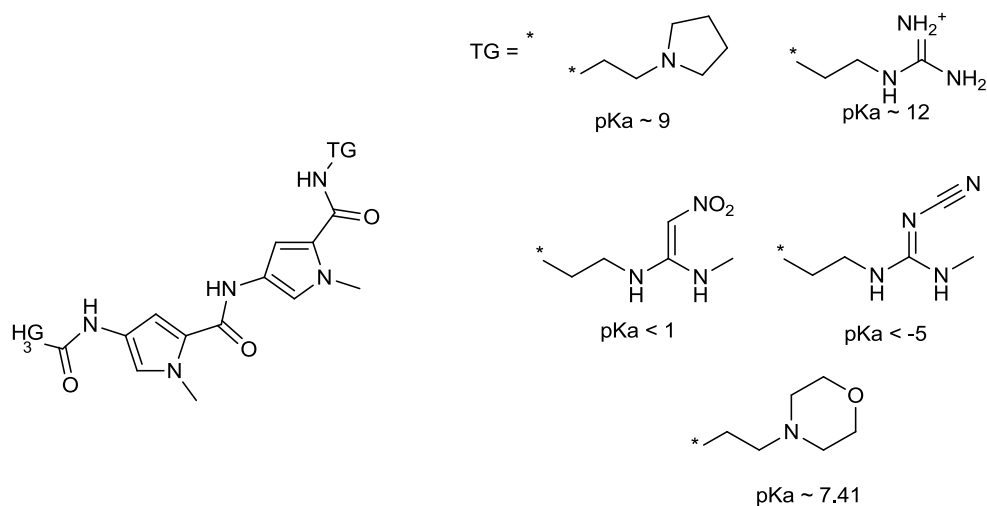


Figure 22. Tail groups selected for study.

The pyrrolidine and morpholine tail groups are protonated at physiological pH (~7) but both ionized and free base forms can be present since their respective pK_as are about 9 and 7.41. These groups should be capable of passing through the lipophilic membrane. On the other hand, the guanidinium tail group is essentially fully protonated at physiological pH and forms strong hydrogen bonds and ionic bonds with the phosphate bases of DNA. The major disadvantage comes from the permanently charged tail group which leads to poor solubility. For the synthesis, this drawback is a minor issue since the molecule is prepared from the BOC protected intermediates, allowing reduction and coupling reactions to be carried out before the introduction of the tail group. However membrane permeation is unlikely and active transport may well be required. The favoured species of the nitro-alkene and cyano-alkene tail groups are highly dipolar but unprotonated at physiological pH. Thus, they should not have any membrane permeation problems and might still bind to DNA.

III. Synthesis of MGBs

The targeted molecules are described below:

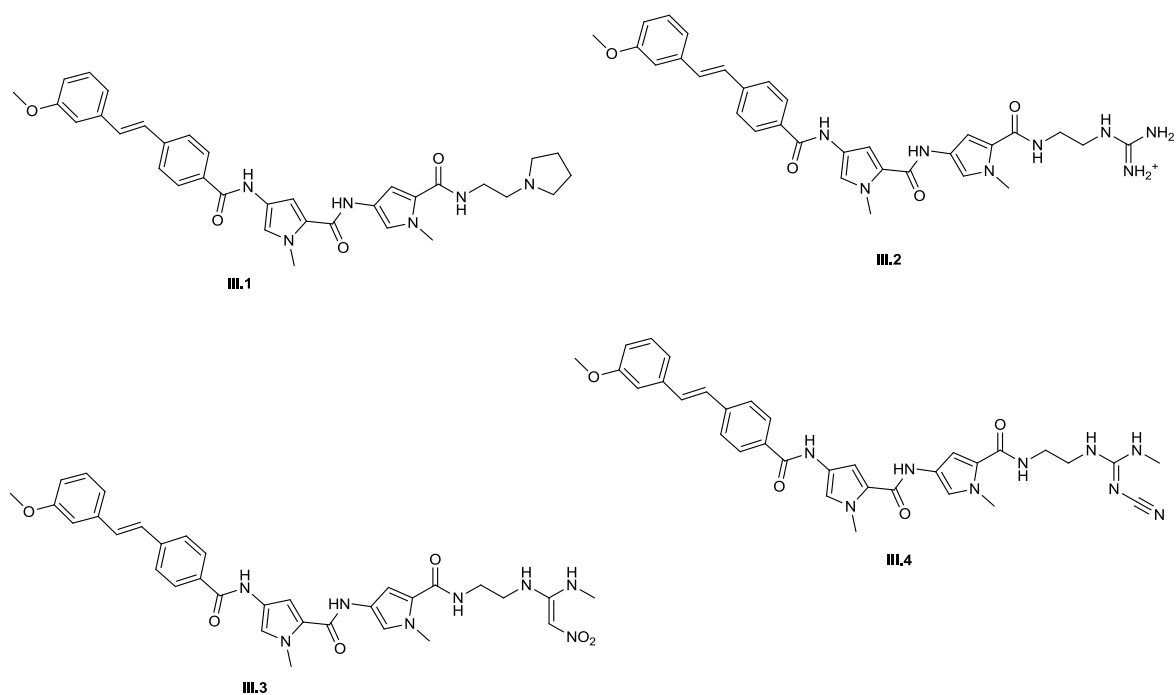
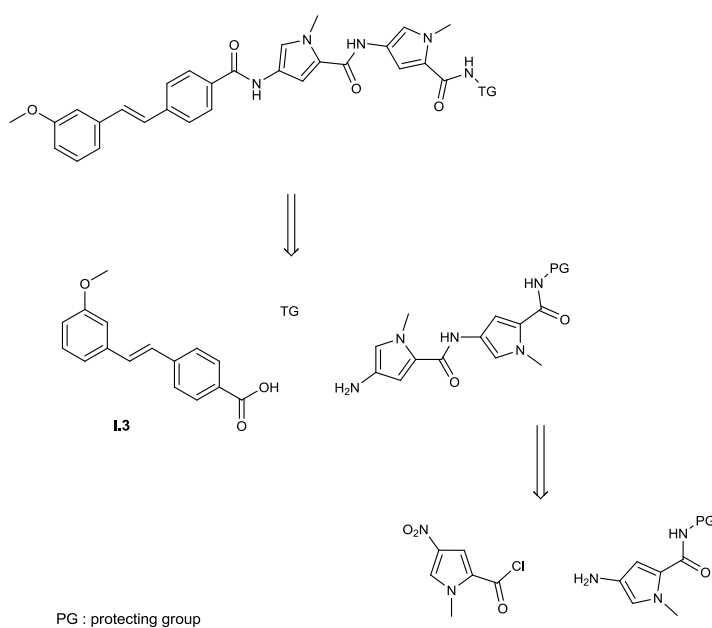


Figure 23. Final fluorescent targeted molecules.

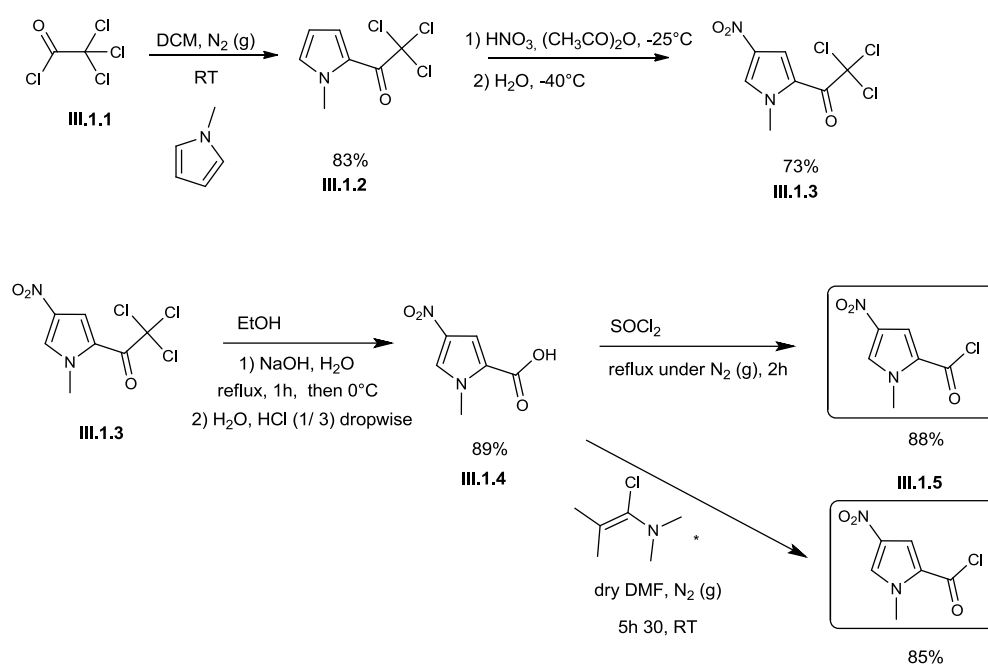
The retrosynthetic analysis (Scheme 3) shows how these compounds could be synthesized. Molecules containing BOC or acetoxy protected tail groups are used as precursors and the use of selective protection and deprotection strategy of those protecting group leads to the final target molecules.



Scheme 3. Retrosynthetic analysis of synthesis of fluorescent MGBs with different tail groups.

1. Preparation of 1-methyl-4-nitro-1H-pyrrole-2-carbonyl chloride III.1.5
(Scheme 4)

The acid chloride **III.1.5** was synthesized from commercially available trichloroacetyl chloride **III.1.1** reacting with *N*-methylpyrrole under Friedel-Crafts conditions to give **III.1.2** (83%). Nitration of **III.1.2** with nitric acid/acetic anhydride gave **III.1.3** (73%), which was then hydrolysed with aqueous sodium hydroxide under reflux to give carboxylic acid **III.1.4** (89%). The acid chloride **III.1.5** was obtained from **III.1.4** in two ways, firstly using thionyl chloride^[8] and secondly using Ghosez's reagent^[56], 1-chloro-*N,N*,2-trimethylpropenylamine. The two procedures gave similar yield. However, the first one was easier to work up since the excess of Ghosez reagent was difficult to remove and could be seen in the NMR spectrum of the final product **III.1.5**.

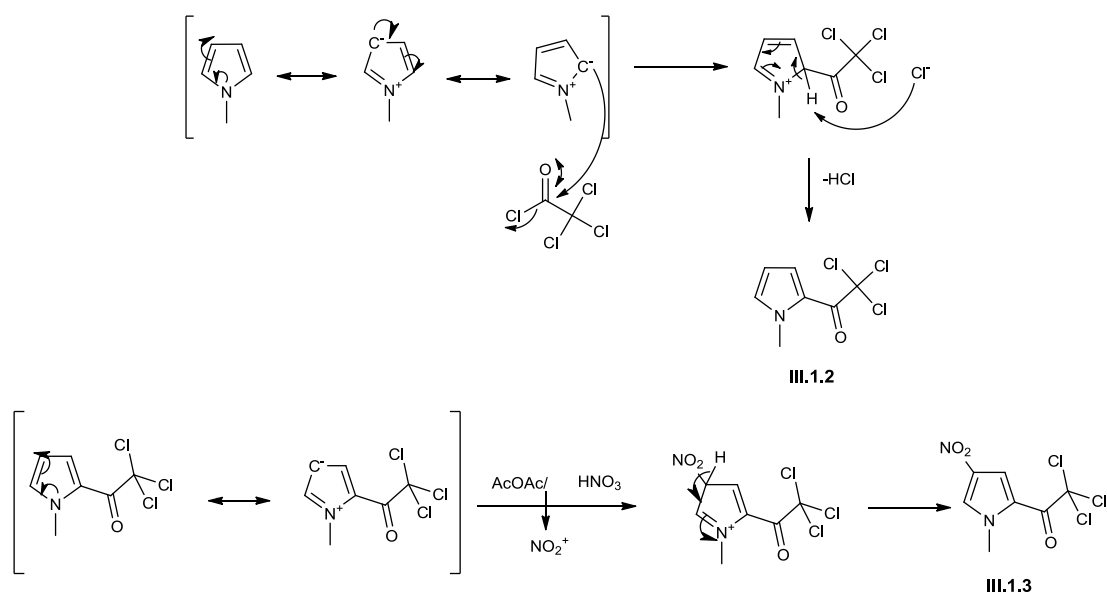


Scheme 4. Preparation of *N*-methylpyrrole precursors.

a) *Aromatic substitutions: Friedel – Crafts' reaction followed by Nitration*
(Scheme 5.)

No catalyst is needed for the Friedel-Crafts reaction (1st step), because pyrrole is very reactive to electrophilic substitution. This can be understood since the pyrrole is a heterocyclic aromatic ring that has very low basicity due to the delocalization of the lone pair of the nitrogen atom in the aromatic ring. The resonance contribution provides insight to the reactivity of the pyrrole ring towards aromatic substitution because the donation of the

nitrogen lone pair into the ring stabilizes the positive charge of the intermediate carbenium ion. The relative stability of the possible intermediates justifies the regioselectivity of the Friedel-Crafts substitution occurring essentially at C2 or C5 (α -positions).



Scheme 5. Successive aromatic substitutions: Friedel-Crafts reaction and nitration.

Following the first substitution of the pyrrole ring, the subsequent nitration is an aromatic substitution of a C2-substituted pyrrole ring. This substitution raises the problem of regioselectivity which is determined by the intermediates formed (Figure 24). In this case, there are now three non equivalent positions where substitution by the nitroso can take place: C3, C4 or C5. The ketone inserted at position C2 through the Friedel-Crafts reaction is electron-withdrawing; hence the aromatic system is deactivated. This destabilizes the intermediate cation located at C2 when the reaction occurs at C3 or C5. The C4 position is the most likely position for electrophilic aromatic substitution, and the intermediate cation is stabilized by the lone pair of the nitrogen. At the end of the reaction, a proton is removed to restore aromaticity.

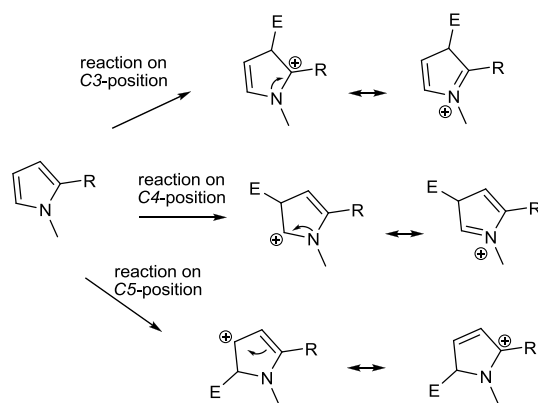
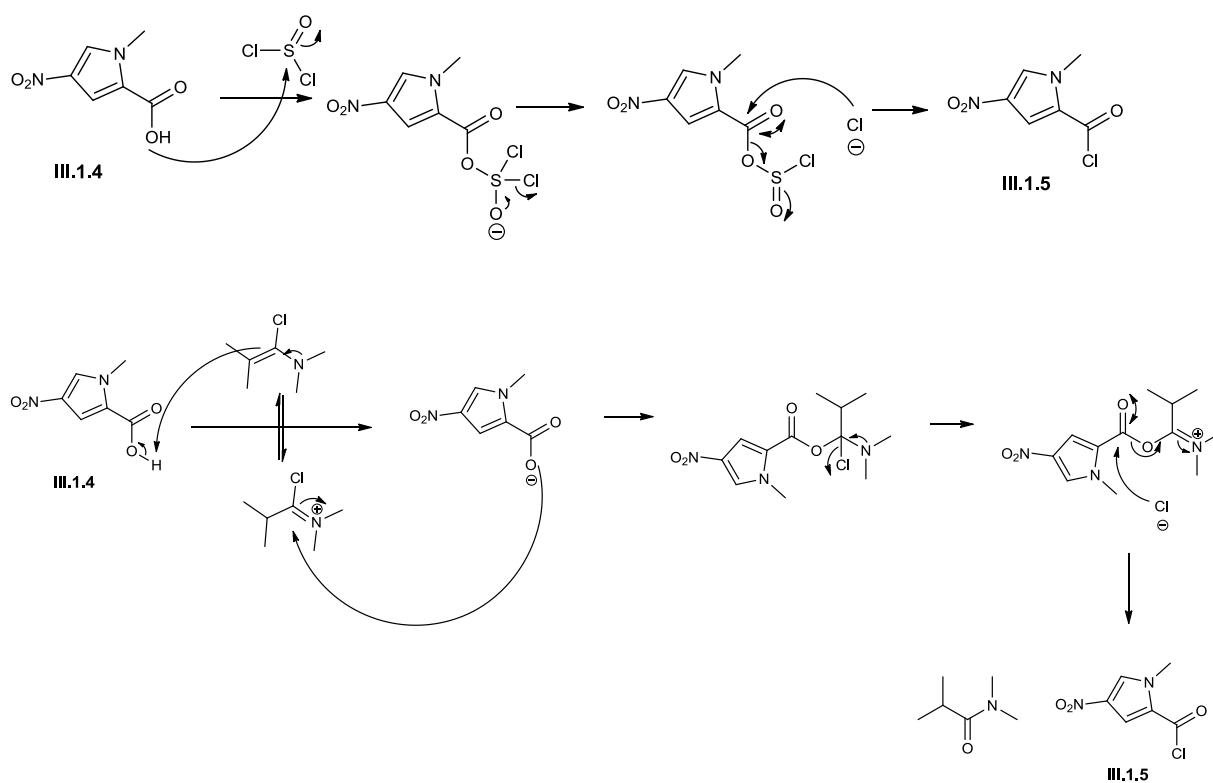


Figure 24. Nitration : regioselectivity.

*b) Preparation of the 1-methyl-4-nitro-1H-pyrrole-2-carboxylic acid **III.1.4** and 1-methyl-4-nitro-1H-pyrrole-2-carbonyl chloride **III.1.5***

The hydrolysis of **III.1.3** was carried out under reflux using sodium hydroxide to give the carboxylic acid (**III.1.4**). The two reagents used for the preparation of the acid chloride **III.1.5**, share the property of forming a reactive intermediate that undergoes substitution by chloride (Scheme 6.).



Scheme 6. Formation of 9 through two different pathways.

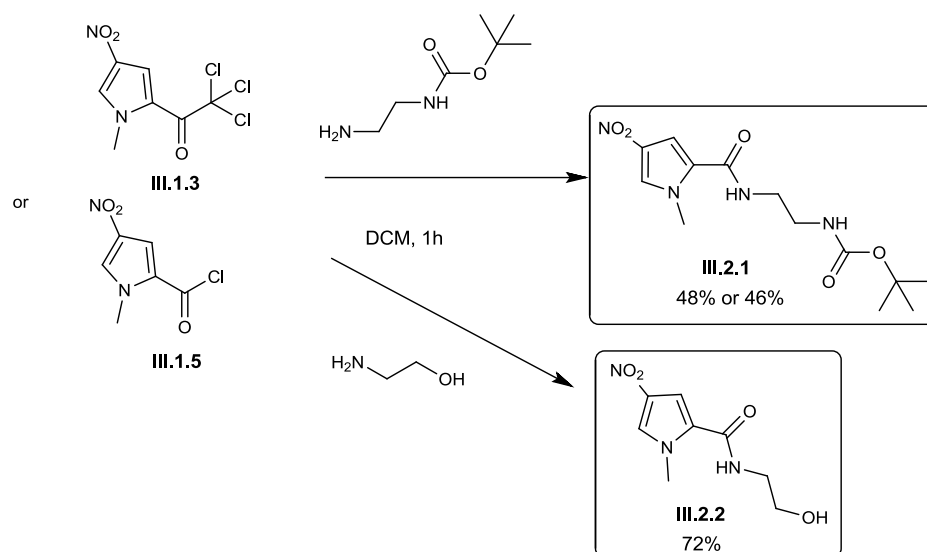
In the reaction of thionyl chloride, the oxygen attacks the sulfur atom of thionyl chloride since the latter is an oxophile and releases chloride. The chloride ion then attacks the carbonyl bond to yield the molecule desired, as well as sulfur dioxide and hydrochloric acid as by-products.

In the reaction using Ghosez's reagent, the nitrogen delocalises its lone pair to give the quaternary ammonium salt, and allows the double bond of the enamine to pick a proton from the carboxylic acid to give the carboxylate ion. This anion reacts with the ammonium to give the lone pair back to the nitrogen. This lone pair is then delocalised again and removes the chlorine as a chloride ion, which reacts then with the ester.

In contrast to using thionyl chloride, Ghosez's reagent allows the conversion of the carboxylic acid to an acid chloride using mild and non acidic conditions. Thanks to its high volatility, the excess reagent introduced is removed under high vacuum and without further work up, allowing **III.1.5** to be recovered. However, the two syntheses showed similar yield (85% or 88%), and Ghosez reagent appeared to be much more difficult to remove than expected.

2. Preparation of N-methylpyrroles with functionalized tail groups

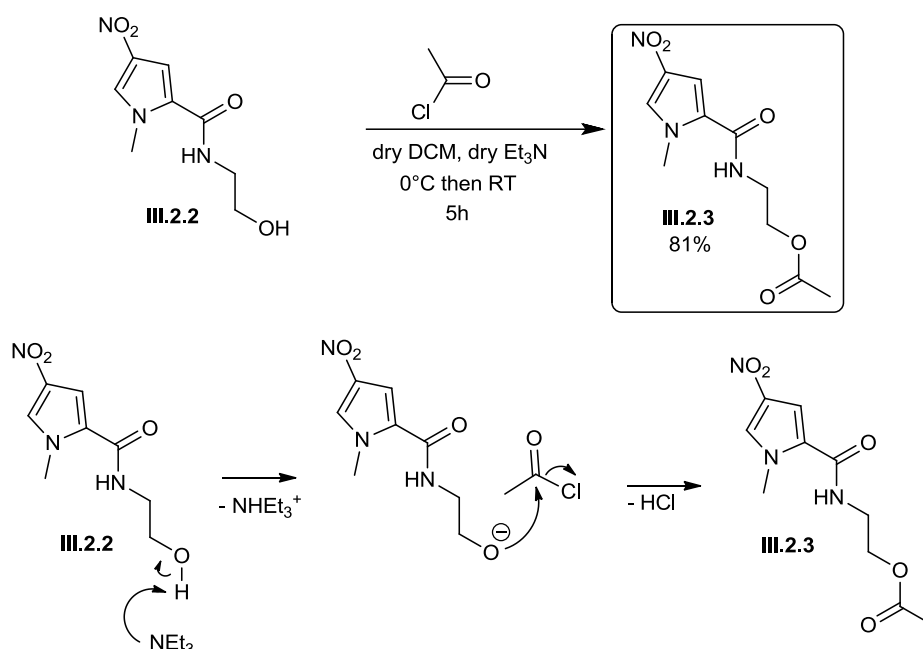
Once the carbonyl chloride **III.1.5** was formed, functionalized monomers with the different tail groups or their precursors were synthesized. Amide formation with *tert*-butyl-2-aminoethyl carbamate gave **III.2.1**, a monomer containing a BOC protected amine (Scheme 7). Similarly, the reaction with 2-aminoethanol gave a monomer containing a primary alcohol **III.2.2** that needed to be protected before further reactions.



Scheme 7. Preparation of functionalized tail groups.

The monomer **III.2.1** was synthesized from both **III.1.3** and **III.1.5**, and the yields obtained were quite similar. Both the chloride and the trichloromethyl moieties are good leaving groups as a result of the nucleophilic attack of the primary amine to give the amide. The primary amine reacts with the carbonyl group to form the amide while releasing the good leaving group CCl_3^- which is then protonated by the protonated primary amine RNH_2^+ to give chloroform which is easily evaporated (Scheme 7).

The primary alcohol tail group in **III.2.2** had to be protected to avoid any side reactions during the subsequent stages of the synthesis. Treatment with acetyl chloride to give the acetate ester **III.2.3** in good yield (81%) (Scheme 8). However, most of the time the esterification was not complete and the ester **III.2.3** was separated from unreacted **III.2.2** by flash chromatography on silica using ethyl acetate and hexane as eluents.



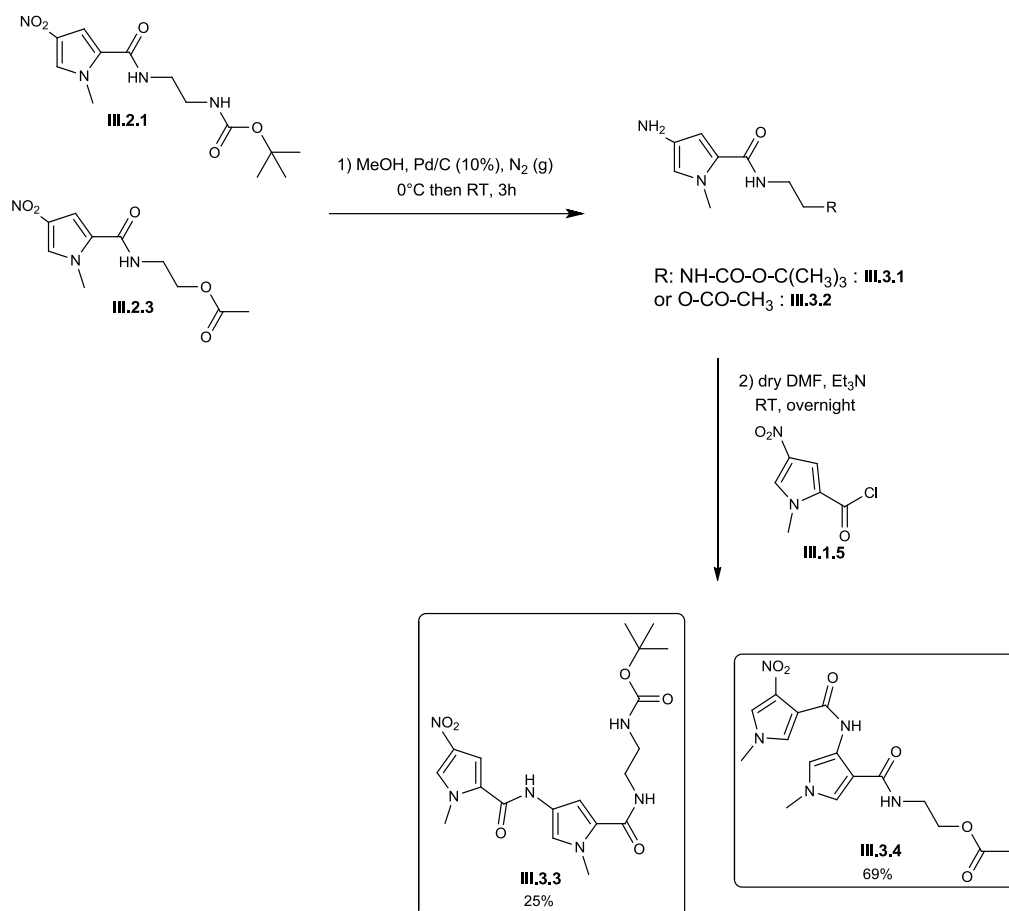
Scheme 8. General scheme and mechanism of protection of primary alcohol tail group by acetyl chloride.

The lone pair of the oxygen in the primary alcohol attacks the acetyl chloride to form the ester. The triethylamine helps to remove the proton and gives back the lone pair of electrons to the oxygen to give **III.2.3** protected with the acetyl group (Scheme 8).

Both **III.2.1** and **III.2.3** are key intermediates in the global synthesis of the required MGBs. The protecting groups are maintained until before the last step to avoid any likely side reactions.

3. Coupling with a second N-methylpyrrole

After obtaining the functionalized monomers, a second pyrrole ring was added in two steps. First, the functionalized monomer was hydrogenated using palladium on charcoal to reduce the nitro group to a primary amine. This amine is not stable so the amide formation has to be set up as soon as possible using the acid chloride **III.1.5** (Scheme 9).



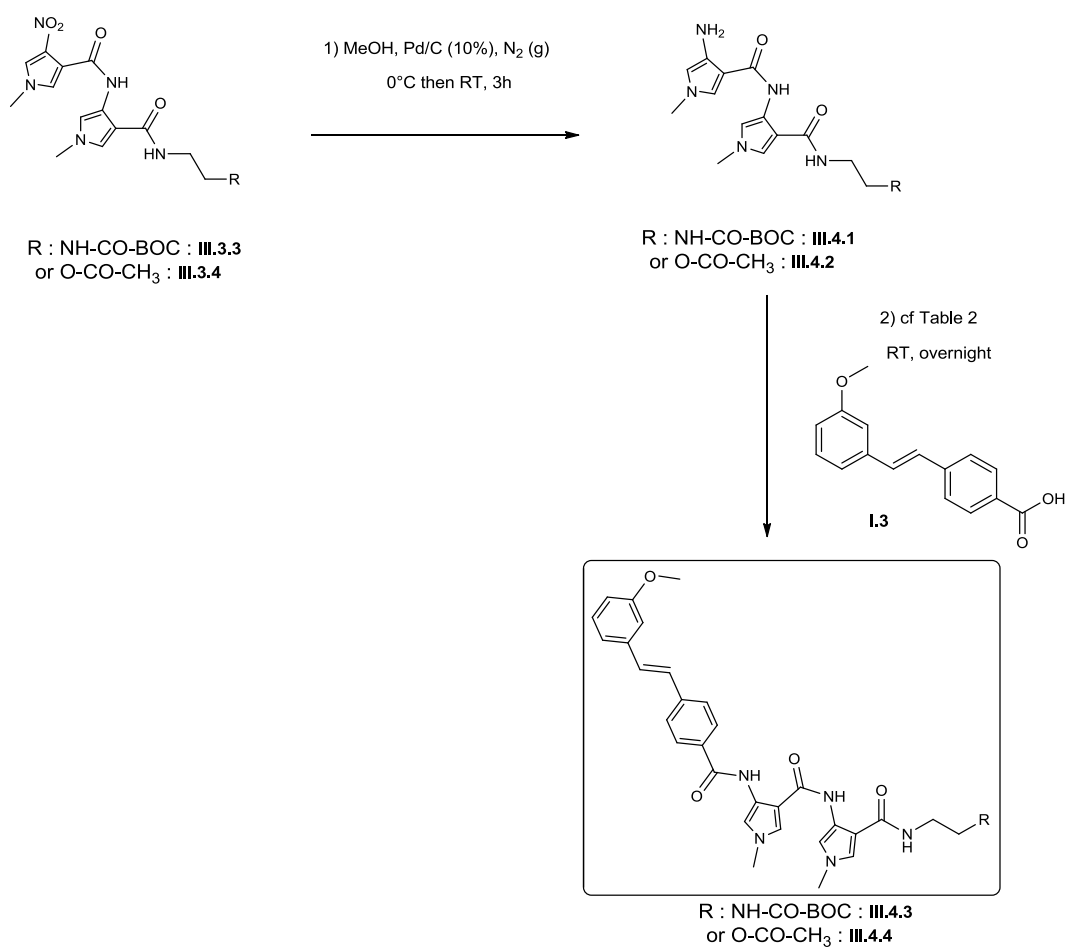
Scheme 9. Coupling with a second pyrrole ring.

The hydrogenation over Pd on charcoal transforms the nitro group into a primary amine (**III.3.1** & **III.3.2**), which then reacts with the carbonyl chloride **III.1.5** to form a new peptide bond with a second pyrrole ring (**III.3.3**, **III.3.4**). Compounds **III.3.3** and **III.3.4** were purified by recrystallisation using ethyl acetate and hexane.

4. Coupling of the pyrrole dimer to the head group

The first step was hydrogenation of the nitro group of the protected dimer to give the reactive primary amine (**III.4.1** and **III.4.2**) and the second step consisted of coupling **I.3**

with the different protected dimers **II.4.3** and **III.4.4** to give the full length compounds **III.4.3** and **III.4.4** (Scheme 10).



Scheme 10. Coupling with the head group.

In previous work ^[12], many coupling reactions had been carried out but the yields were generally poor. It was important, therefore, to find conditions for the preparation of **III.4.4** that were easily worked up and resulted in good yields (Table 2).

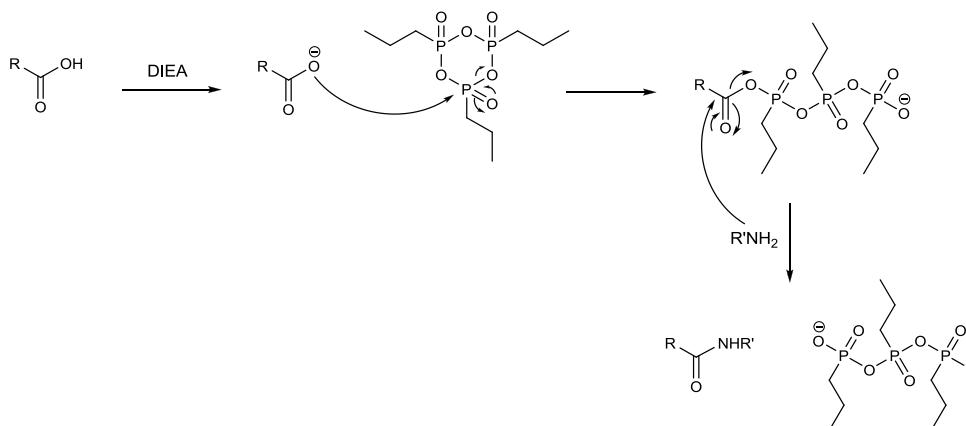
REACTION	SOLVENTS	BASE	COUPLING REAGENT	TEMPERATURE	TIME	WORK UP	PURIFICATION	YIELD
1	dry DCM, dry DMF	NEt ₃		25°C	overnight			failed
2	dry DMF	DIEA	HBTU	25°C	overnight		HPLC	31%
3	dry DMF	DIEA	Ghosez	25°C	overnight			failed
4	dry DMF	DIEA	T ₃ P (50% in DMF)	0°C then 25°C	overnight	NaHCO ₃		62%

Table 2. Summary of results of coupling reactions.



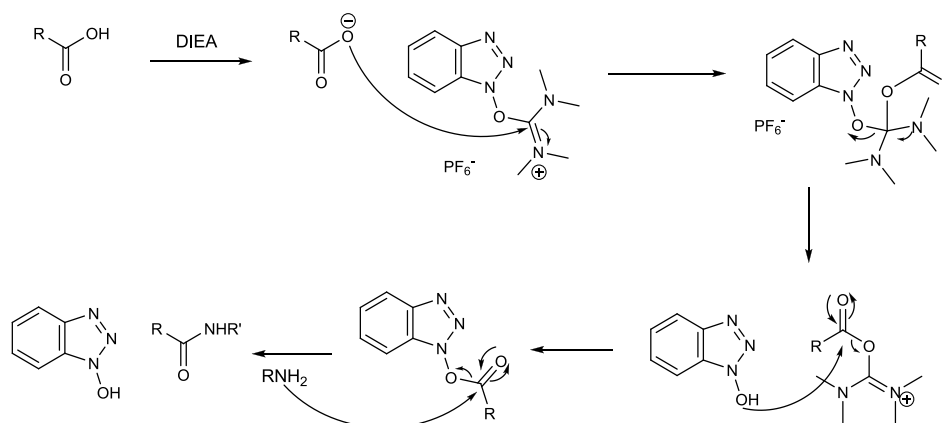
Figure 25. Structure of HBTU and T₃P.

Propane phosphonic acid anhydride, T₃P, is known to be a mild reagent with low toxicity, which gives high yielding reactions for amide bond formation with low epimerization and an easy work up ^[56]. It converts the oxygen of the carboxylic acid into an ionic leaving group (Scheme 11).



Scheme 11. Amide formation in presence of T₃P.

2-(1*H*-Benzotriazole-1-yl)-1,1,3,3-tetramethyluronium hexafluorophosphate, HBTU, is also a coupling reagent (Scheme 12) that gives high yields in the synthesis of peptides ^[56]. However HBTU is more toxic than T₃P and has sensitizing properties; the purification of the resulting product is usually costly because of the use of HPLC.



Scheme 12. Amide formation in presence of HBTU.

The procedure using HBTU as an *in situ* coupling reagent along with DIEA, gave a higher yield (31%) than the previous conditions tried with HBTU along with 4-methylmorpholine in anhydrous DMF (27%). However, the coupling reagent T₃P gave an increase of up to 62% yield, and a pure product was recovered (NMR and LC/MS spectra) after pouring the solution into aqueous sodium hydrogen carbonate solution from which **III.4.4** precipitated. Sometimes the yield obtained was apparently above 100% because of contamination with phosphates, which were removed by dissolution of crude **III.4.4** in ethyl acetate and washing the organic layer with water.

The two procedures that gave good yields of **III.4.4** were used for the formation of **III.4.3**, as shown in Table 3.

REACTION	SOLVENT	BASE	COUPLING REAGENT	TEMPERATURE	TIME	WORK UP	PURIFICATION	YIELD
1	dry DMF	dry NEt ₃	HBTU	25°C	overnight		HPLC	71%
2	dry DMF	DIEA	T ₃ P (50% in DMF)	0°C then 25°C	overnight	NaHCO ₃		81%

Table 3. Preparation of full length MGB precursor **III.4.3**.

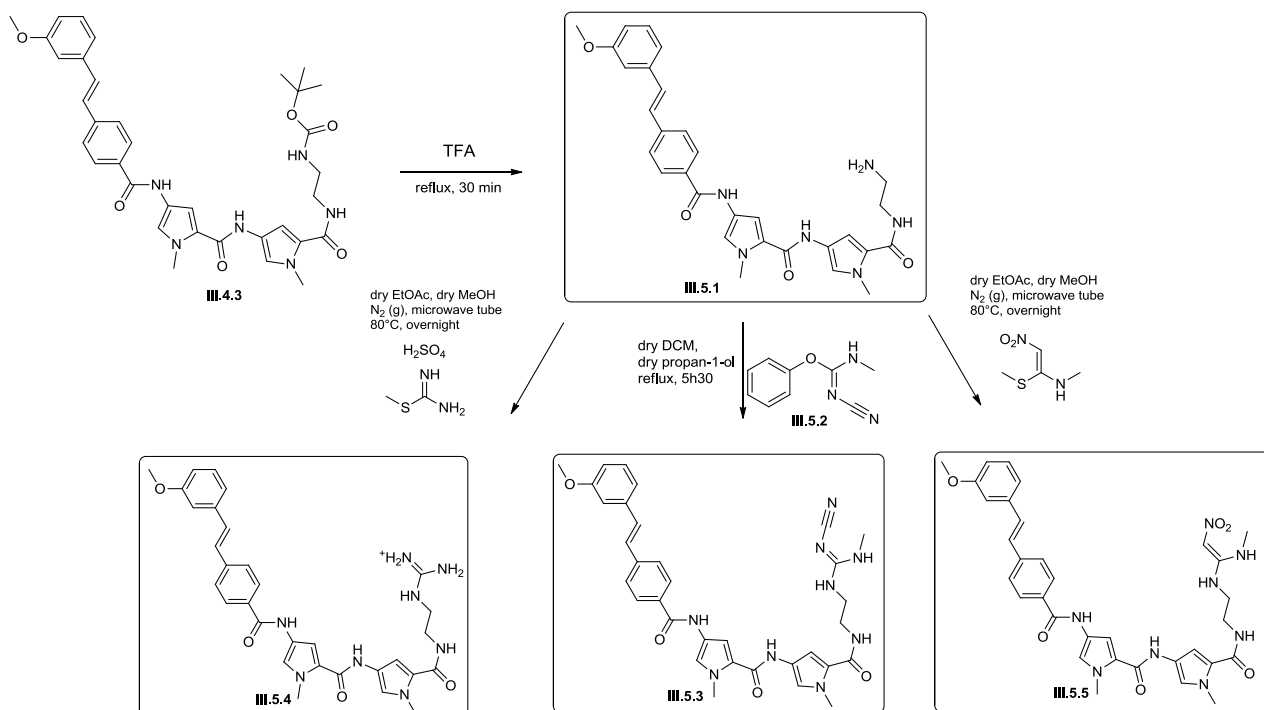
Both procedures worked and the one using T₃P gave higher yields and allowed the use of the carboxylic acid **I.3** instead of the associated carbonyl chloride. The yield obtained was five-fold higher (81%) than that obtained using HBTU and 4-methylmorpholine in anhydrous DMF (yield = 15%)^[52]. The substantial improvement in yield is a major advance in the synthesis of MGBs of this class.

5. Elaboration of tail groups from **III.4.3** and **III.4.4**

III.4.3 and **III.4.4** are key intermediates for the synthesis of MGBs differing at the tail group. As mentioned before, the variation of tail has significant interest due to its influence both on binding with DNA and cell membrane permeation. The final step in the synthesis involves removal of the protecting group located on the tail group, either BOC (**III.4.3**) or acetoxy (**III.4.4**), and then a substitution reaction. The products obtained will enable the investigation of the significance of the tail group on the antibacterial activity of these compounds.

a) Tail group variation from **III.4.3**

As explained in section II, most of the MGBs that have been prepared bear basic tail groups that will be protonated at physiological pH. Scheme 13 describes the transformation of **III.4.3** to **III.5.4**. Compound **III.5.4** contains an amidine tail group, permanently charged at physiological pH. Several active MGBs contained this tail group, and it is partly responsible for the anti-*oncolytic* properties of these compounds. On the other hand, compound **III.5.5**, with the nitroalkene tail group, has a special interest in our study since it has a largely neutral tail group which is nevertheless strongly dipolar and may form several hydrogen bonds with DNA.



Scheme 13. Tail group transformation.

The solubility of amino(methylsulfanyl) methaniminium sulphate and (*Z*)-*N*-methyl-1-(methylthio)-2-nitroethenamine caused experimental difficulties in the preparation of **III.5.4** and **III.5.5**. The best conditions were found using anhydrous ethyl acetate and methanol heated in a microwave tube at 80°C, instead of dry DMF under reflux at 120°C. Too high a temperature was probably causing degradation of some of the product. In previous work, the purification of related compounds by HPLC using acetonitrile/water/TFA was routinely successful. Unfortunately the world shortage of acetonitrile during the course of this work forced the use of methanol instead of acetonitrile and led to the degradation of our molecules. The purification of **III.5.4** and **III.5.5** was tried by flash chromatography, eluting with ethyl acetate/hexane/methanol, to remove the main impurities. However, the complete

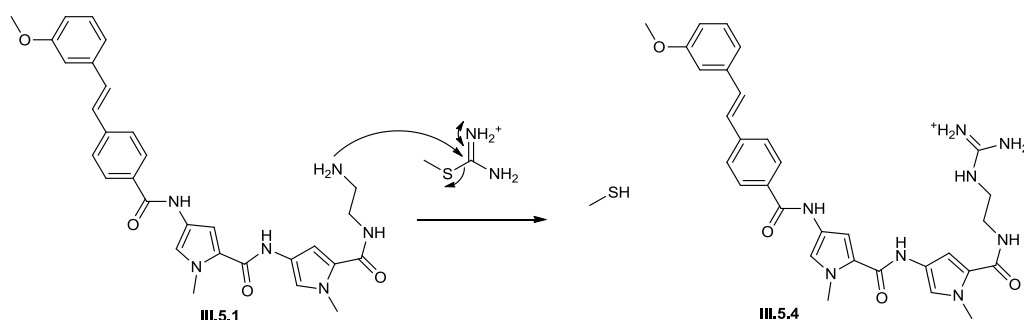
separation of amidine **III.5.4** and nitroalkene **III.5.5** from the precursor **III.5.1** failed. Finally the last attempt to purify both **III.5.4** and **III.5.5** using reverse phase flash chromatography with water/methanol/TFA as eluents was successful (51% and 15%).

The substitution of **III.5.5** with (*E*)-phenyl-*N'*-cyano-*N*-methylcarbamimidate **III.5.2** was undertaken in propan-1-ol and dichloromethane under reflux ^[57]. The purification was carried out on silica gel chromatography using ethyl acetate and hexane as eluents to give 48% of molecule **III.5.3**.

i. Boc deprotection leading to III.5.1

TFA is a perfluorinated carboxylic acid containing three very electronegative fluorine atoms that are responsible for the strong acidity of this reagent. The nitrogen atoms of **III.4.3** are not nucleophilic since they are part of amide or urethane functions. The TFA enables the release of carbon dioxide and a tertiary carbocation that deprotonates at room temperature to give isobutene - a gaseous product.

ii. Preparation of the guanidine tail group III.5.4



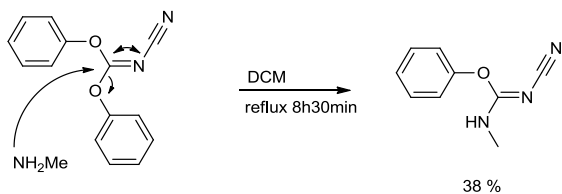
Scheme 14. Mechanism of the guanidine tail group formation.

Since the primary amine is nucleophilic, it reacts with the carbon-nitrogen double bond of the amino(methylsulfanyl) methaniminium sulphate to form a tetrahedral intermediate from which methyl thiolate - a good leaving group - is eliminated (Scheme 14). The mechanism leading to molecule **III.5.5** is similar to the above.

iii. Preparation of the cyano-alkene tail group III.5.3

The formation of **III.5.3** required the preparation of (*E*)-phenyl *N'*-cyano-*N*-methylcarbamimidate **III.5.2** from the commercially available diphenyl cyanocarbonimidate and methylamine in dichloromethane under reflux. The addition of the nucleophilic

methylamine displaces the electrons of the π bond between carbon and nitrogen, creating an electron-deficient quaternary carbon linked to four electronegative atoms (two nitrogens and two oxygens). The electrons on the nitrogen then reform the π bond and release the phenoxide ion which is a good leaving group. Only one phenoxide is lost since only one equivalent of methylamine was added ^[57].

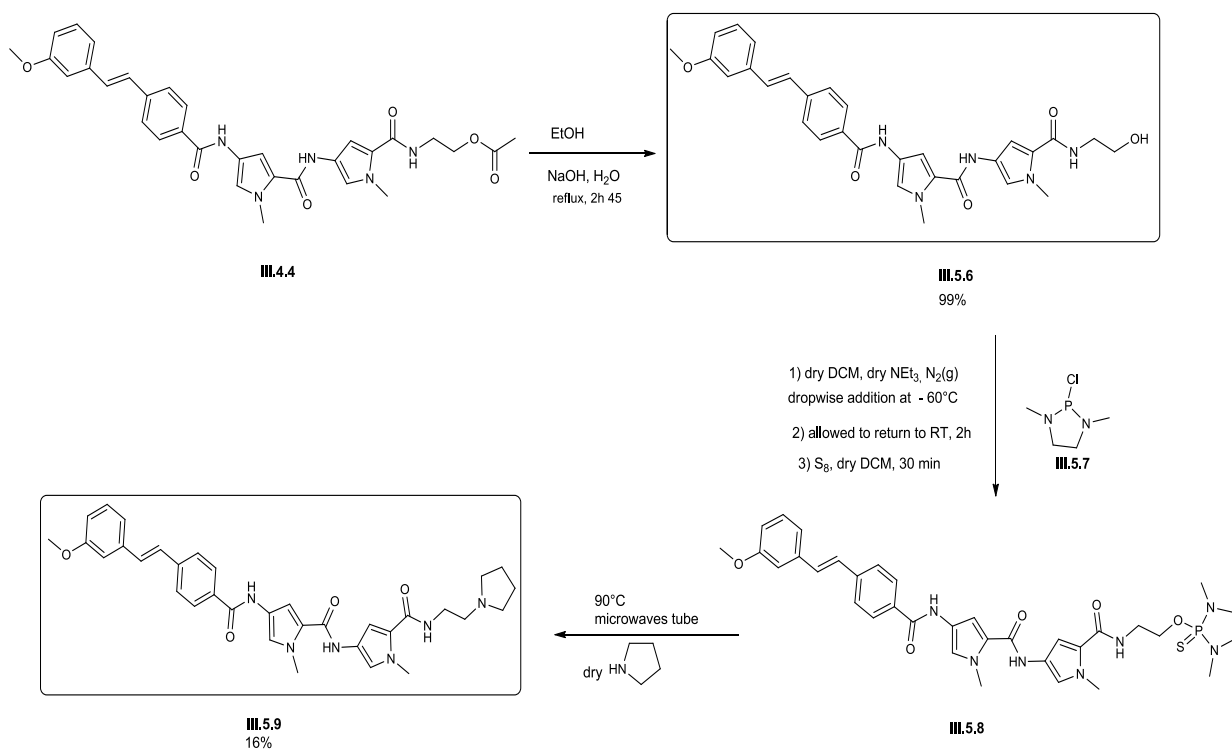


Scheme 15. Formation of **III.5.2**.

The reaction of **III.5.2** with the primary amino group of **III.5.1** occurs by the same mechanism to give structure **III.5.3**.

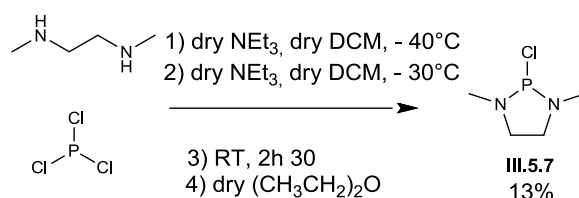
Compounds **III.5.1**, **III.5.3**, **III.5.4** and **III.5.5** were submitted for biological assays to test their antibacterial activity and penetration into cells.

b) Tail group variation from III.4.4



Scheme 16. Route to pyrolidinyl tail group MGB **III.5.9**.

The first step in the conversion of the acetate tail group in **III.4.4** into the pyrrolidinyl amine present in **III.5.9** was deprotected to give the corresponding primary alcohol **III.5.6**. This was achieved in 99% yield using sodium hydroxide in aqueous ethanol (Scheme 16). Following this, a number of steps were required in which a recently discovered amination reaction^[52] was tested using structure **III.5.7** (Scheme 17).



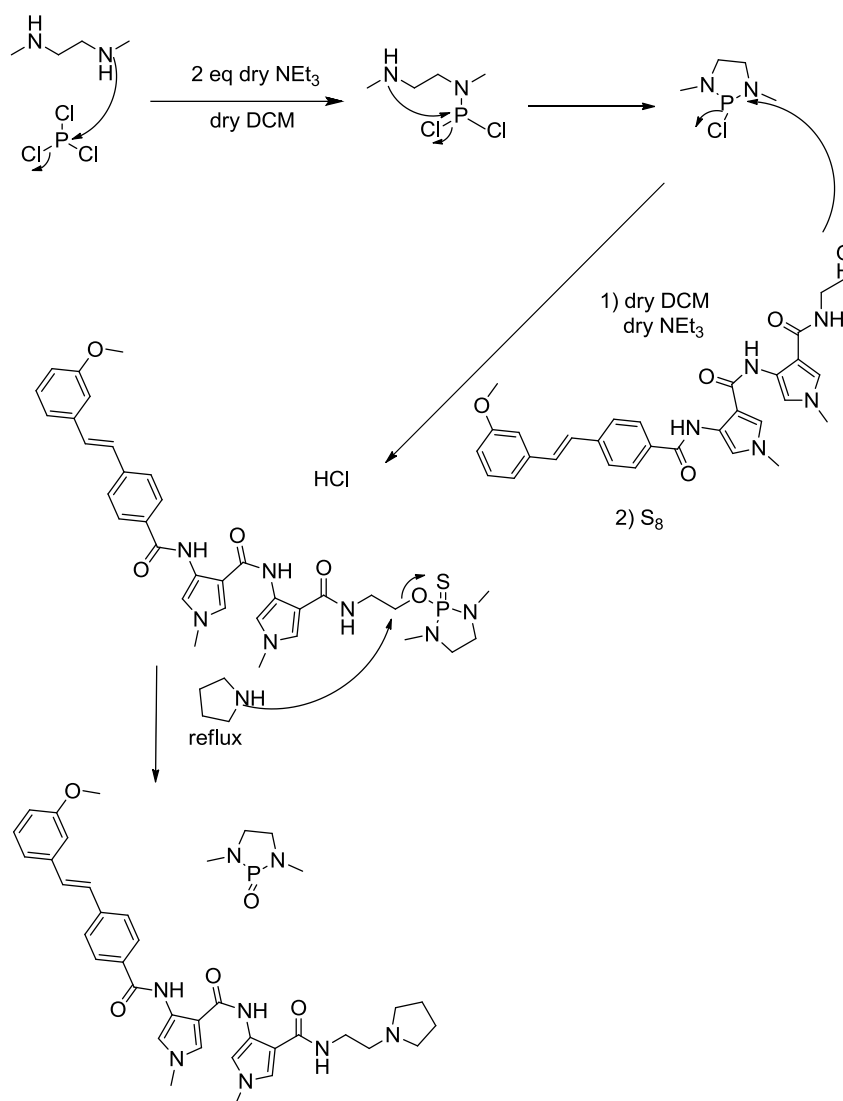
Scheme 17. Preparation of the pyrrolidinyl MGB **III.5.9** using phosphorus containing intermediates.

The synthesis of **III.5.9** required extremely anhydrous conditions, especially for the first two steps since an intermediate containing phosphorus III is involved, such a structure is extremely unstable and reacts with the water contained in the atmosphere. In contrast, intermediate **III.5.8** is more stable, containing phosphorus V, and was converted by thermolysis to give the required MGB **III.5.9**, albeit in low yield. The conditions required for this amination had not been optimized and further experiments were therefore carried out.

The third step leading to **III.5.9** was investigated with Lewis acid catalysis. Using anhydrous THF in the presence of ZnCl₂, heated at 150°C in a sealed tube, the reaction failed and the starting material was recovered (NMR and LC/MS 540 g.mol⁻¹). Zinc chloride is a Lewis acid whose role is to coordinate with the sulfur to make the 5 membered ring a better leaving group, and make the structure more susceptible to be attacked by pyrrolidine. The separation of product **III.5.9** was carried out by basic flash chromatography using triethylamine as base. Since the primary aim of the project was to understand the influence of tail groups on biological activity, no further work was carried out on this reaction; others are taking it forward.

The mechanism below describes a double nucleophilic substitution of *N,N'*-dimethylethane-1,2-diamine on phosphorus trichloride. Triethylamine accepts the proton from each secondary amine formed. Another substitution of a chloride by the primary alcohol **III.5.6** then occurs to give the phosphorus III, intermediate which is then stabilized to phosphorus

V by adding sulfur flowers. Finally, the pyrrolidine adds to split the carbon-oxygen bond to give **III.5.9**.



Scheme 18. Chemical pathway to **III.5.9**.

The intermediates **III.5.7** and **III.5.8** were recovered, but the next step was not successful. The NMR spectrum and the LRMS and HRMS spectra did not correspond to **III.5.9**, and the starting material **III.5.6** or **III.5.8** was recovered, as well as degradation products. The reflux was probably carried out at too high a temperature, or left too long. However, the pyrrolidine should attack the phosphorus easily since it is nucleophile. Further reactions monitored by TLC or LRMS and changing the experimental conditions could be investigated in future work.

Compounds **III.4.4** and **III.5.6** were submitted for biological assays to test their antibacterial activity and penetration into cells.

6. *Other variations of the tail group*

Although six new compounds with a range of pK_as have been prepared, more possibilities were considered. For example, another idea was to develop a molecule containing a tail group bearing an oxetane moiety through a spirocyclic carbon. This structure is similar to the morpholine tail group - a tail group used successfully in potent antibacterial MGBs ^[2]. It would have been interesting to compare the effects of azaoxetane and morpholine on bonding to DNA and antibacterial activity. The position of the spiro carbon could have been varied and the different physical and chemical properties arising from different *N*-substituents could have been evaluated. Earlier studies suggested that oxetane and aliphatic carbonyl groups are good H-bond acceptors ^{[58][59]}, so the oxetane tail group could enhance the bonding with DNA. Furthermore, oxetanes are known to be chemically stable at pH 1-10, and the introduction of the oxetane moiety lowers the basicity of the cyclic amine ^[60]. Therefore, a comparison between azaoxetane and pyrrolidine containing compounds would have been of real interest. It has also been proved that the lipophilicity increases as the oxetane unit is positioned closer to the nitrogen atom; hence it should have a better cell penetration. The oxetane moiety itself is polar and enhances the solubility of the molecule. Generally, oxetane derivatives are stable molecules; however, when located at the α position to the basic amine functionality, the stability decreases ^[61].

Before starting the synthesis of oxetane-containing MGBs, studies involving molecular dynamics were carried out with these compounds to see if they could fit and stay in the minor groove of the double-stranded DNA.

Molecular dynamics provides information about the dynamics and flexibility of nucleic acids. Relative binding affinities to various DNA sequences (A:T-rich DNA sequences in our case) can be predicted. The simulation allows observation of the flat and crescent shape of our MGB fitting into the helical minor groove of DNA. During the relaxation - the first phase of molecular modeling simulation - the system changes its conformation compared to the initially constructed and energetically optimal one. Secondly, the system ligand-DNA oscillates reproducing the effect due to thermal fluctuation around the structure ^[62].

Starting with the crystal structure of the distamycin-DNA complex (2:1), the head and tail groups were modified to get the desired molecules shown in Figure 26, with the same stoichiometry (2:1 ratio), and the same DNA oligo. The ligand was then manually positioned in the central portion of the DNA minor groove (5'GTATATAC...) and the complex DNA:MGB was allowed to breath.

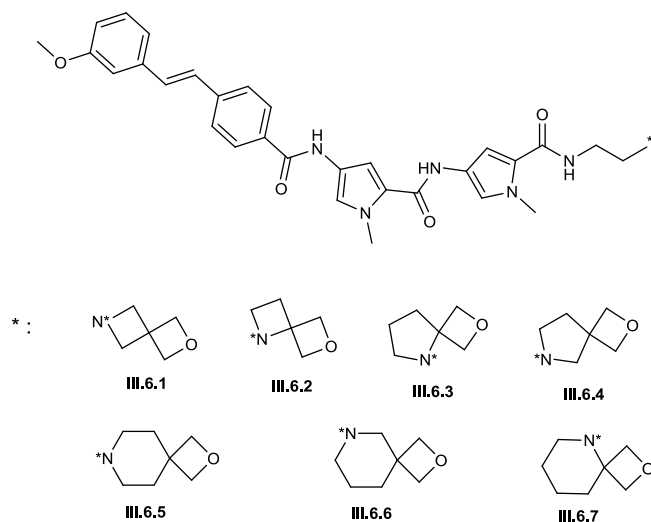


Figure 26. Variation of oxetane tail groups.

In the case of the oxetanes **III.6.1** and **III.6.2**, the two ligands were sitting head to head together in the minor groove. However, when the ring containing the nitrogen is expanded (oxetanes **III.6.3**, **III.6.4**, **III.6.5**, **III.6.6**, **III.6.7**), the two ligands lie head to tail inside the minor groove to prevent steric hindrance. This head to tail configuration still retains the π -stacking interactions occurring between two aromatic rings. In this case, the stacking occurs between pyrrole and benzyl rings instead of pyrrole-pyrrole and benzyl-benzyl interactions observed for the 4 membered ring oxetanes (**III.6.1** and **III.6.2**).

This experiment showed that the ring containing the oxygen is located out of the DNA minor groove (Figure 27) and that no steric clashes occur with the second molecule of MGB in the minor groove. All ligands managed to stay in the groove side-by-side while the DNA was breathing, which is a good sign for binding to DNA.

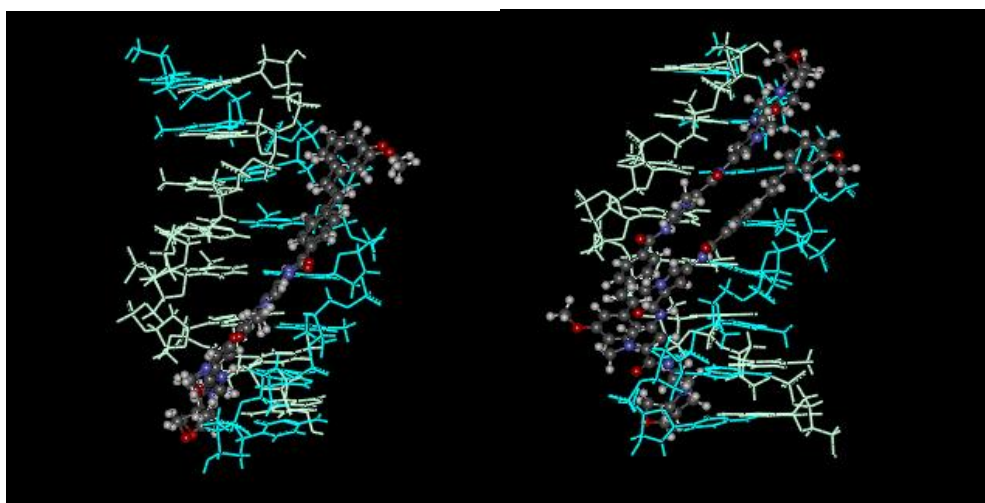
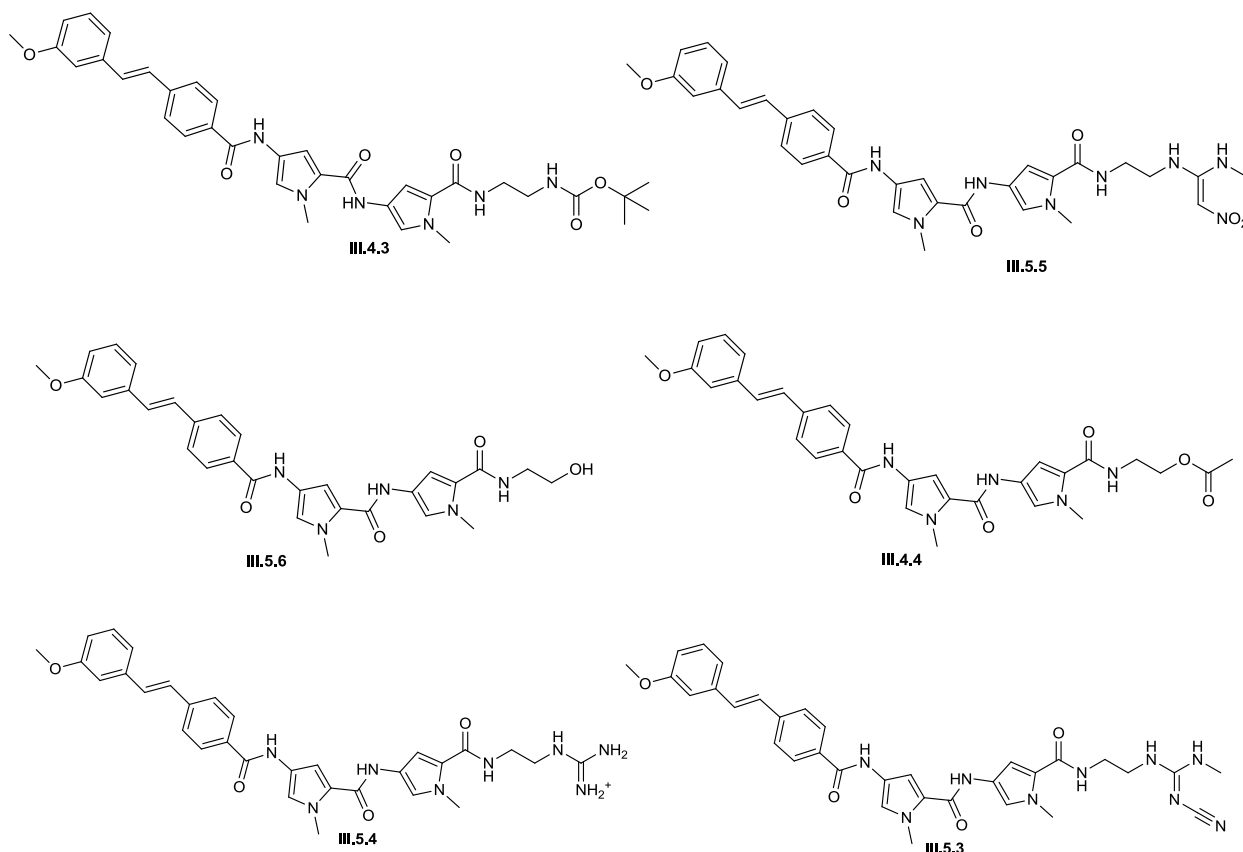


Figure 27. Oxetanes **III.6.1** and **III.6.6** fitting in the DNA minor groove (2 :1 ratio).

MGBs containing an oxetane tail group rather than an amidine tail group, represent another possibility for study. The molecular modeling suggests that this kind of MGB would fit into the minor groove; unfortunately no synthetic work was carried out due to lack of time.

IV. Conclusion

A series of new compounds have been made with fluorescent heads, and tails covering a range of pK_a from < 0 to 14. Biological testing in bacterial and mammalian cells would now enable the understanding of the relationship between biological activity and the structure. So far, some of the best compounds discovered are highly toxic to Gram positive bacteria but show little mammalian cell toxicity. The biological assays and microscopy should enable us to understand these results. The structures of the molecules sent for biological testing are drawn below (Figure 28). Some of those molecules were available from earlier work (**IV.1, IV.2, IV.3, IV.4, IV.5, IV.6, IV.7**) and some had already been tested and were used as controls (**IV.2, IV.3, IV.4**).



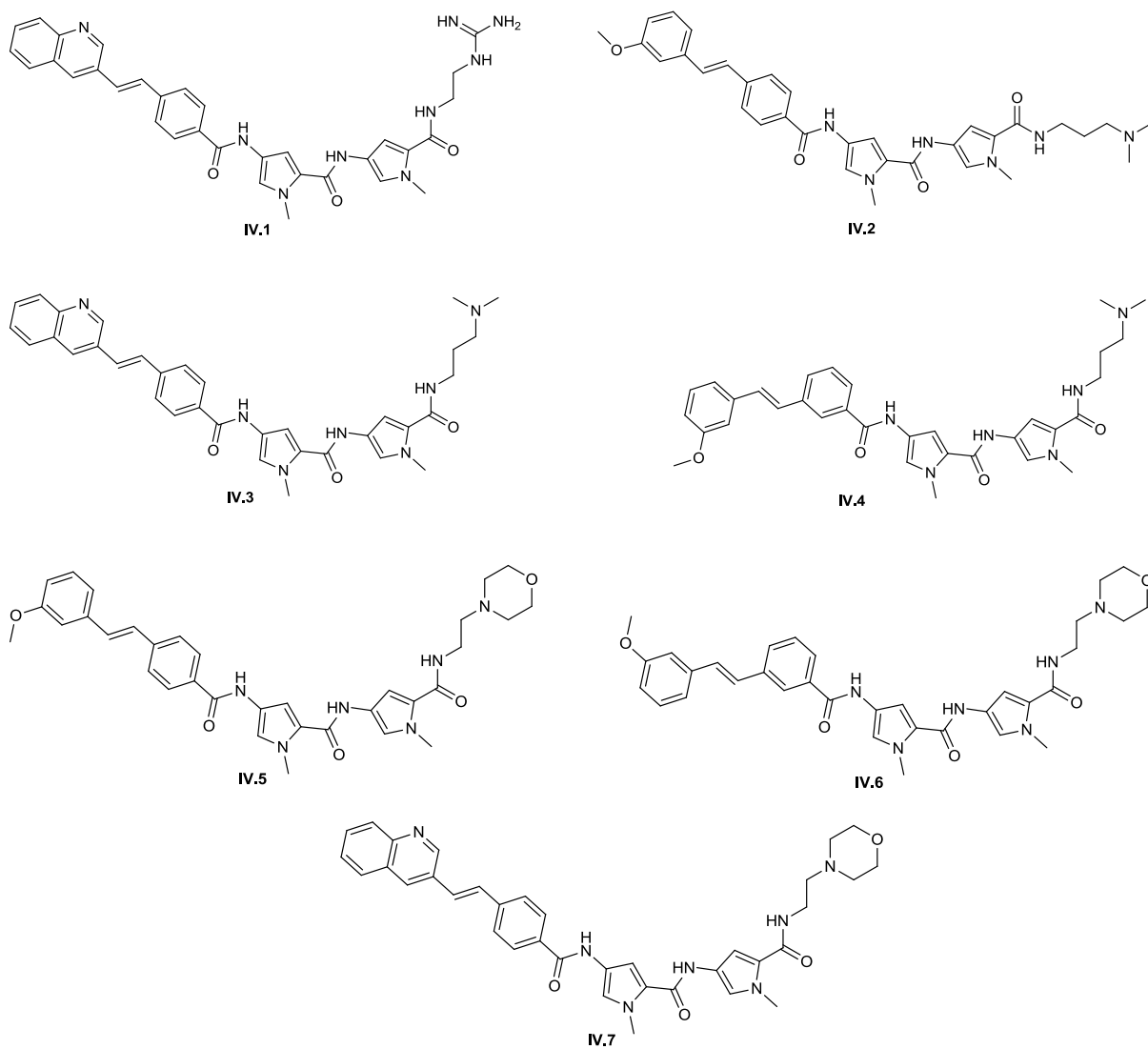


Figure 28. Structural features of biologically tested molecules.

C. BIOLOGICAL TESTING

I. Introduction

Several biological tests were undertaken with the molecules shown in Figure 28 to understand their action against Gram positive and Gram negative bacteria and the correlation between activity, cell selectivity, and permeation into mammalian cells (V79).

1. The Gram stain ^[63].

The Gram stain broadly differentiates bacteria into Gram-positive and Gram-negative groups differing drastically in the organization of the structures outside the plasma membrane but below the capsule (Figure 29): in Gram-negative organisms these structures constitute the cell envelope, whereas in Gram-positive organisms they are called a cell wall.

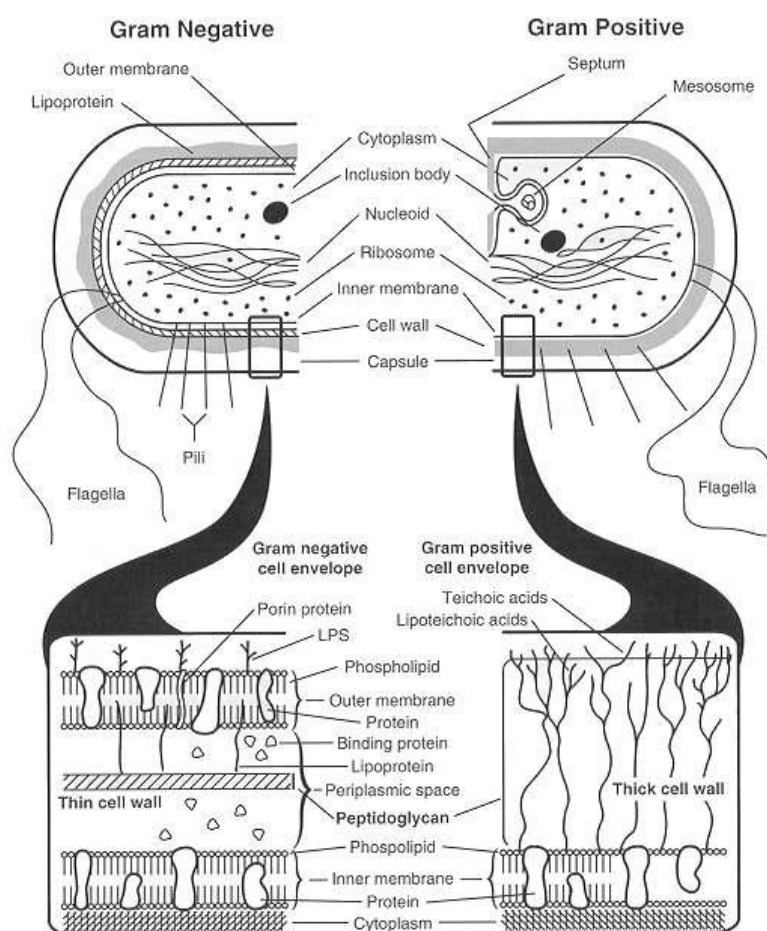


Figure 29. Comparison of Gram bacteria: cell wall structure ^[64].

Gram positive bacteria are able to retain the crystal violet stain of Gram stain because of the high amount of peptidoglycan in the cell wall and the lack of outer membrane. On the other

hand, Gram negative bacteria cannot retain the crystal violet stain, instead taking up the counterstain and appearing red or pink. In these studies, *E. coli*¹ was used as a Gram negative bacterium, and *Staph. aureus*² was used as a Gram positive bacterium.

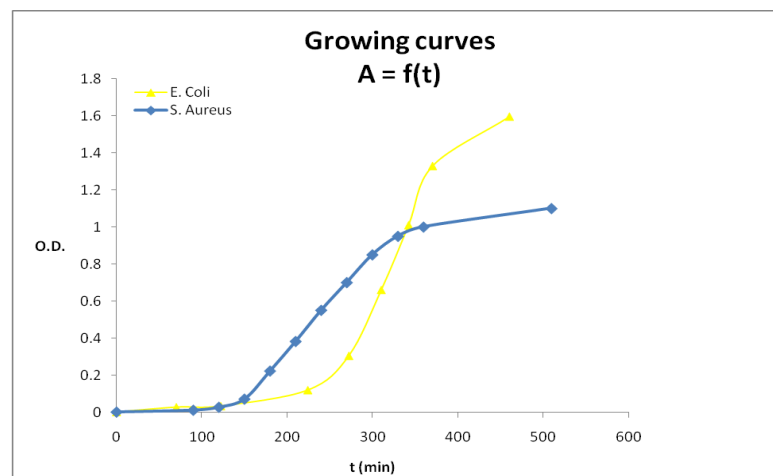
2. Mammalian cells

The mammalian cells used were a Chinese hamster lung fibroblast cell line known as V79. This type of cell synthesizes the extracellular matrix and collagen, the structural framework for animal tissues, and plays a critical role in wound healing. Fibroblasts are the most common cells of connective tissue in animals. They have a branched cytoplasm surrounding an elliptical, speckled nucleus having one or two nucleoli.

II. Killing Curves of Gram positive and Gram negative bacteria

1. Growth curves of bacteria

Using appropriate media, cells were inoculated into 10 ml of sterile medium and placed in a stirring incubator at 140 rpm at 37 °C. 1 mL of the medium was withdrawn from the flasks and the optical density (O.D.) was measured at 600 nm. A graph of absorbance against time (minutes) was plotted. The absorbance for the starting point of the experiment was chosen at 0.2 or 0.4, a value at which the bacteria are still growing.



Graph 2. Growth of Gram bacteria.

¹: *Escherichia coli*

²: *Staphylococcus aureus*

2. Killing curves of bacteria ^[65]

Resazurin (Figure 30), also known as 7-hydroxy-3*H*-phenoxazin-3-one 10-oxide, a blue dye used as a redox indicator, was used to determine the potential killing effect of the MGBs shown in Figure 28.

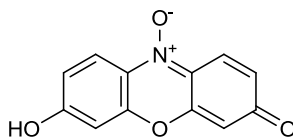


Figure 30. Structure of Resazurin.

Resazurin (blue) is reduced by living cells to resorufin resulting in a pink color, which itself is further reduced to hydroresorufin (colorless). The absorbances were measured at 540 nm. The more cells are alive, the more resazurin is reduced to give a pink or colorless color, resulting in a high absorbance at this wavelength. In the case of dead cells, the measured absorbance should be low since no reduction of resazurin occurs.

Ampicillin was used as a reference drug for comparison with the killing effect of our molecules. Ampicillin is a beta-lactam antibiotic (Figure 31) that has been used extensively to treat bacterial infections ^[66].

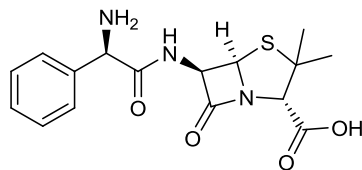


Figure 31. Structure of Ampicillin.

Belonging to the penicillin group of beta-lactam antibiotics, ampicillin is able to penetrate Gram positive and some Gram negative bacteria. The amino group helps the drug penetrate the outer membrane of Gram negative bacteria. Ampicillin acts as a competitive inhibitor of the enzyme transpeptidase, which is needed by bacteria to make their cell walls. As a result, inhibition of the transpeptidase stops the final stage of bacterial cell wall synthesis, which ultimately leads to cell lysis ^[67].

Colonies of Gram bacteria were left growing overnight, and then plated in 96 well plates. Then a varying concentration of MGB was added: 0.5, 1, 2, 3, 4, 5, 10, 20 $\mu\text{g/mL}$ with resazurin. The plates were then incubated overnight and absorbances were measured at different times to give the curves below.

a) Gram positive bacteria: *Staphylococcus Aureus* RN4220

i. Tertiary alkyl amine tail group series

The molecules MGB bearing a tertiary alkyl amine (Figure 31) were tested against the Gram positive bacterium *Staph. aureus*.

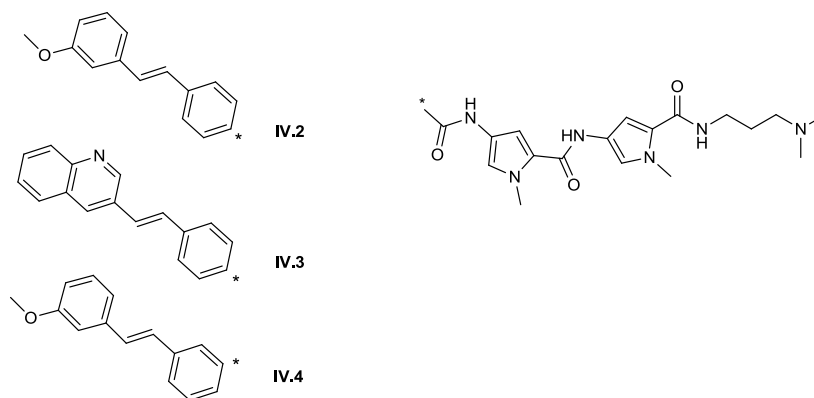
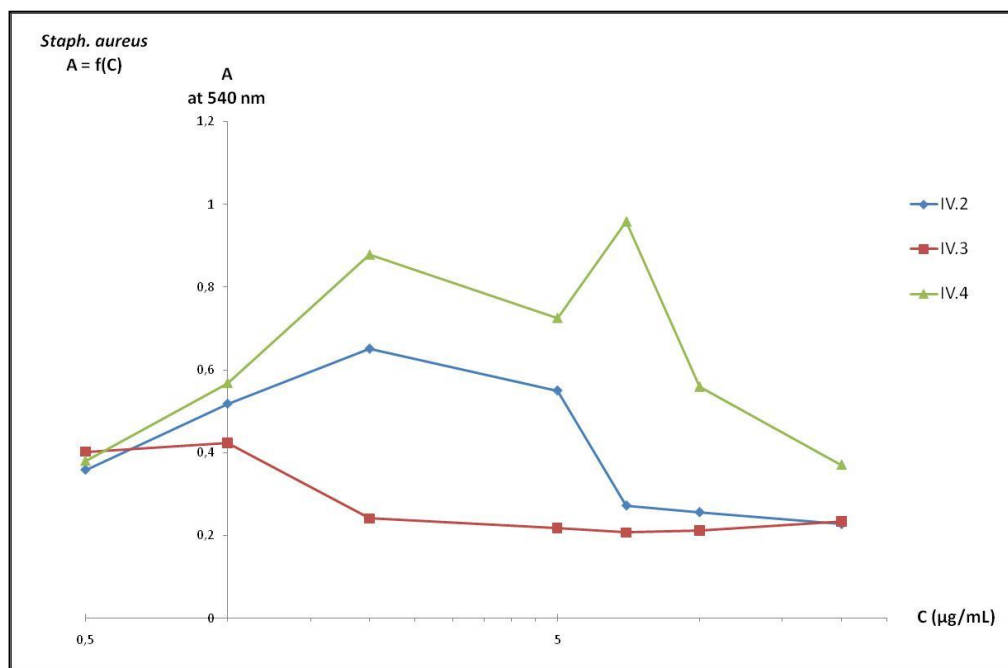


Figure 31. Tertiary amine tail group series.

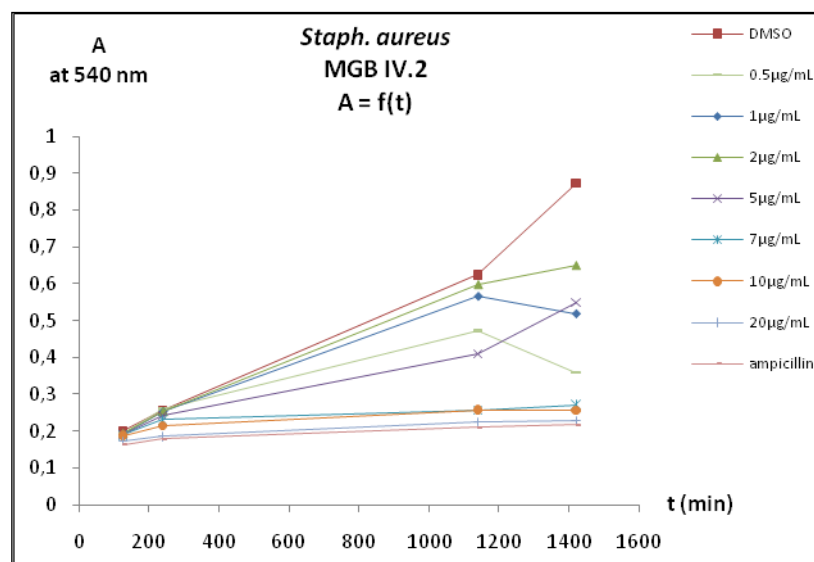


Graph 3. Killing curve of the tertiary amine tail group series against *Staph. aureus*.

The curves from Graph 3 show globally a decrease of absorbance corresponding to the death of bacteria. However the concentration of molecule at which the cells seem to die vary. Molecule **IV.3** seem to have the most important killing effect on *Staph. aureus* since the absorbance decreases significantly between 1 to 2 µg/mL of molecule added. In the case of MGB **IV.2**, the bacteria keep growing (A increases) until reaching a concentration of

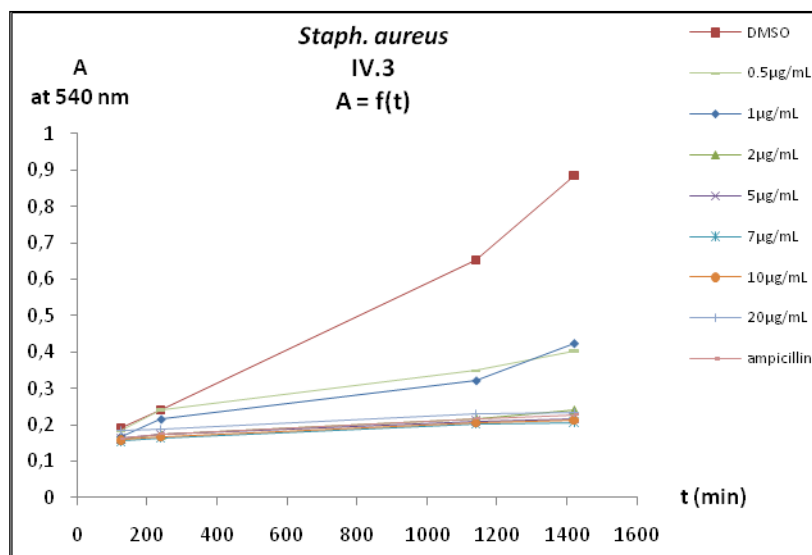
molecules introduced at 2 $\mu\text{g/mL}$. The curve corresponding to **IV.4** also show a slight killing effect.

To confirm those results, graphs of absorbance against the time were plotted to assess not only the potential killing affect of molecules of the tertiary amine tail group series but also to see the behaviour of the bacteria in the presence of those molecules during a long period of time. The following graphs show absorbances against time for different concentrations of tested molecules introduced.



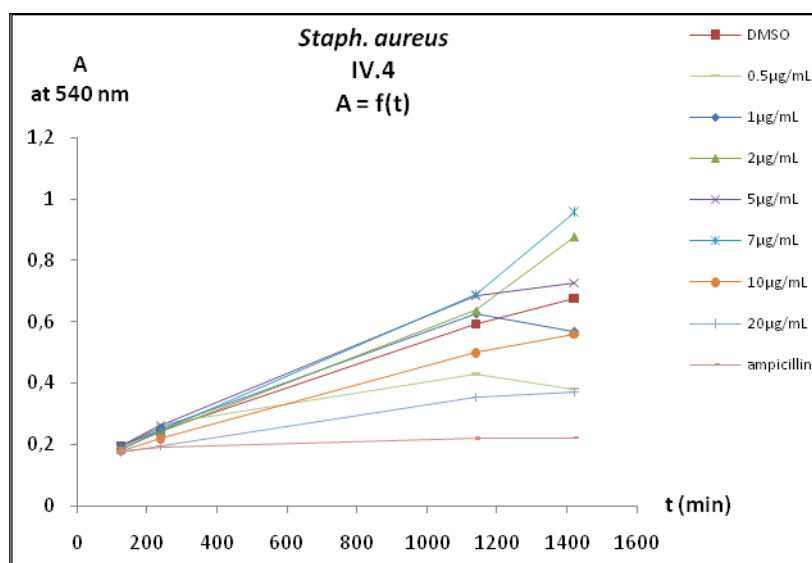
Graph 4. Anti-bacterial effect of **IV.2** against *Staph. aureus*.

Graph 4 above stresses the fact that below 5 $\mu\text{g/mL}$, molecule **IV.2** has no killing effect on Gram positive bacteria, and even after 1500 min (25h) almost no cells have died. However the comparison between the curve of ampicillin with the curves corresponding to 7 $\mu\text{g/mL}$, 10 $\mu\text{g/mL}$ and 20 $\mu\text{g/mL}$ of molecule **IV.2** introduced with the bacteria, those curves are quite similar. So above a concentration of 7 $\mu\text{g/mL}$ of MGB **IV.2**, *Staph. aureus* bacteria die and this killing effect occurs before 240 min (4h) after the molecule was added.



Graph 5. Anti-bacterial effect of **IV.3** against *Staph. aureus*.

Graph 5 confirms the hypothesis made from Graph 3. First of all the curves are lower in absorbance than the one at which no molecule of **IV.3** was added (DMSO). It clearly demonstrates that below a concentration of 1 µg/ml the bacteria are dying, since the curves corresponding to 2 µg/ml, 5 µg/ml, 7 µg/ml, 10 µg/ml and 20 µg/ml are similar to the curve for ampicillin.



Graph 6. Anti-bacterial effect of **IV.4** against *Staph. aureus*.

At first glance, it seems that the antibacterial properties of molecule **IV.4** are not that obvious (Graph 6). However, at a concentration of 20 µg/mL the absorbance is lower than

for any other concentration, so bacteria are either slowly dying or the introduction of molecule **IV.4** delays their growth.

Finally, Graph 3 and Graph 5 prove that MGB **IV.3** kills the Gram positive bacteria quickly and below a concentration of only 1 $\mu\text{g/ml}$. MGB **IV.2** kills bacterial but its antibacterial activity is lower than MGB **IV.3** since the killing concentration is below 5 $\mu\text{g/ml}$. Then comes MGB **IV.4**, which has a poor killing effect on *Staph. aureus*, and to see any killing effect similar to ampicillin, a higher concentration of this molecule needs to be introduced.

ii. Morpholine tail group series

The molecules MGB bearing a morpholine tail group (Figure 32) were tested against the Gram positive bacterium *Staph. aureus*.

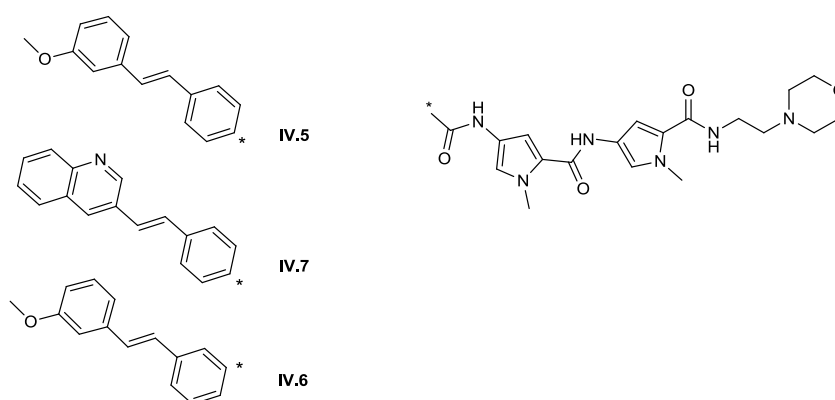
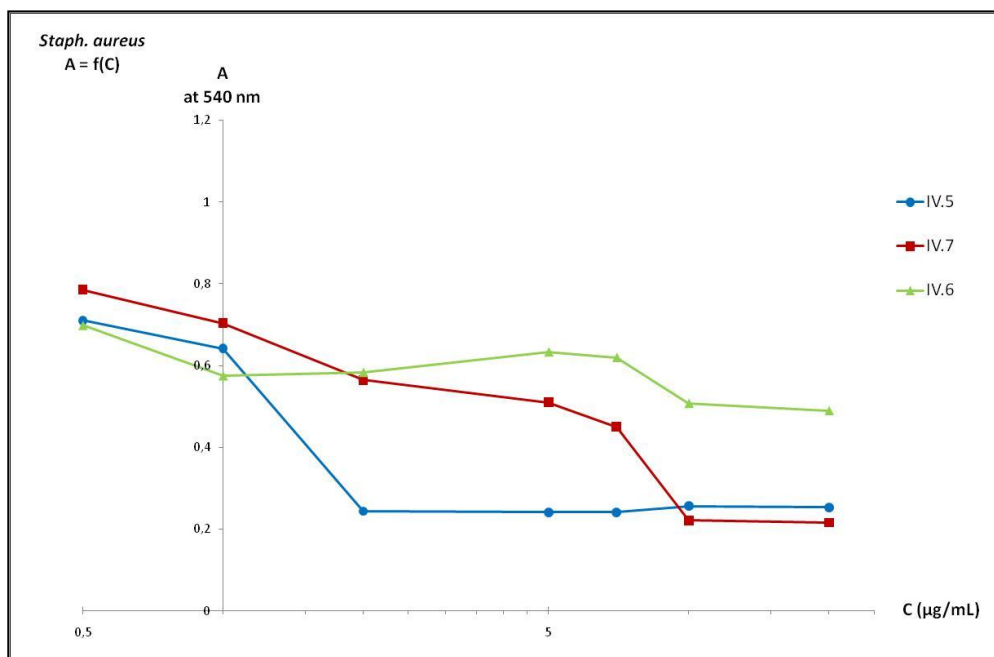


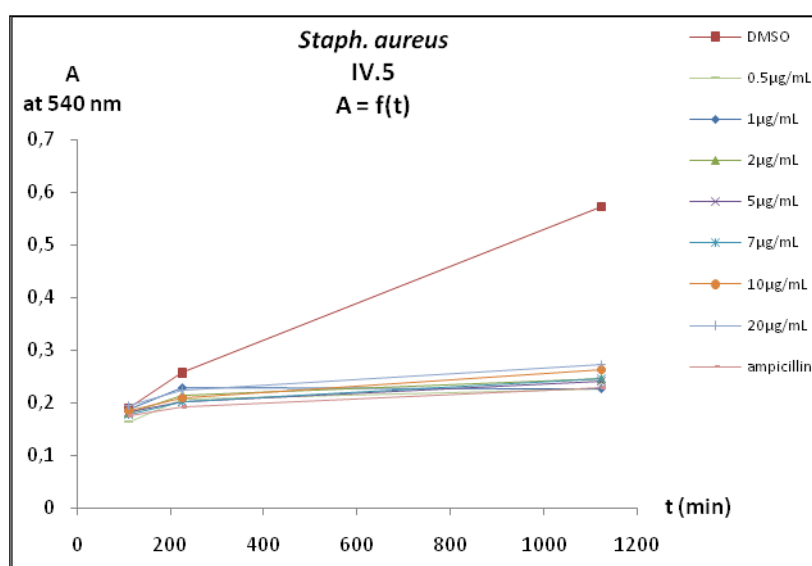
Figure 32. Morpholine tail group MGB series.



Graph 7. Killing curve of the morpholine tail group MGB series against *Staph. aureus*.

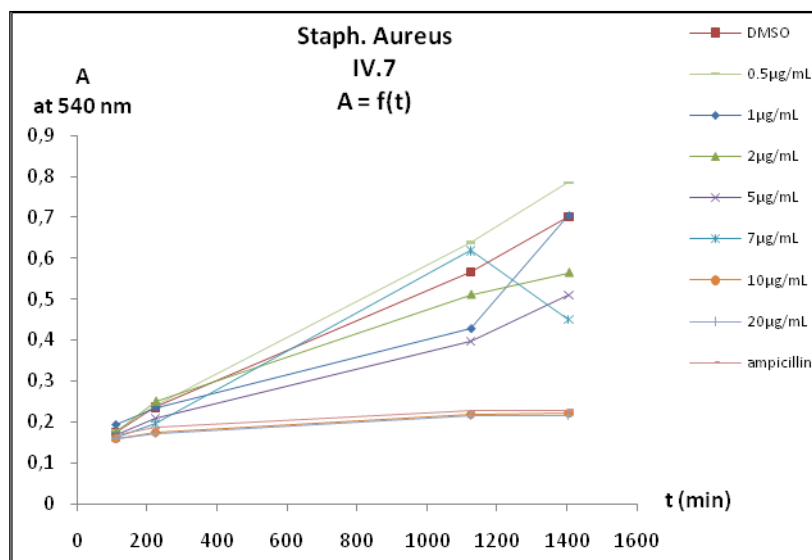
According to the graph above, both MGB **IV.5** and MGB **IV.7** seem to have antibacterial behaviour. Both curves indicate a decrease in absorbance due to poor reduction of resazurin by bacteria. Molecule **IV.5** seems to kill bacteria when more than 1 $\mu\text{g}/\text{ml}$ is introduced into the media. In comparison, the bacteria seem to either grow slower than usually or die slowly with molecule **IV.7**, until reaching a concentration of 7 $\mu\text{g}/\text{ml}$ at which the drop in absorbance suggests the death of *Staph. aureus*. Graph 7 does not suggest a significant killing effect related to the introduction of molecule **IV.6**.

To determine the behaviour of *Staph. aureus* in the presence of different concentrations of molecules from the morpholine tail group series, the graphs below were plotted with A measured against time.



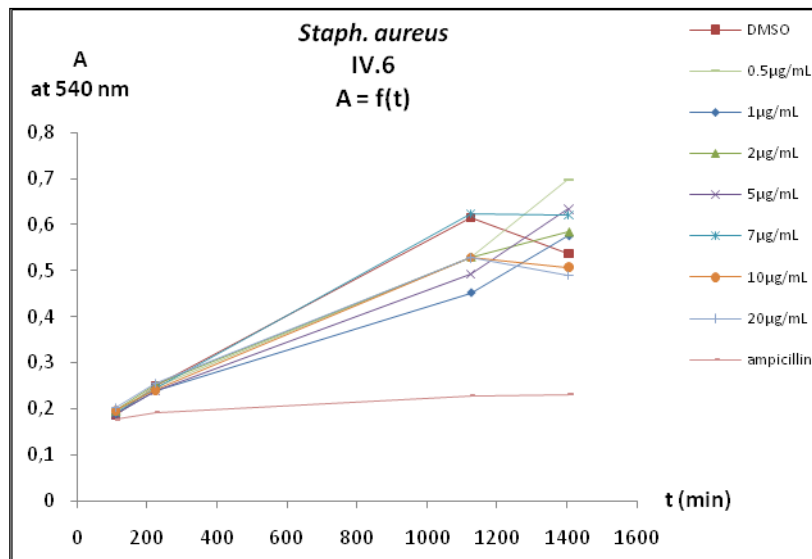
Graph 8. Anti-bacterial effect of **IV.5** against *Staph. aureus*.

This first graph (Graph 8) confirms the extremely good killing effect of **IV.5** against *Staph. aureus* noticed in Graph 7. The curve corresponding to the concentration of 0.5 $\mu\text{g}/\text{mL}$ is quite low in absorbance and follows the curve of the ampicillin. The bacteria seem to grow extremely slowly after 225 min (3h45min), ie. they are dying quite fast in the presence of **IV.5**.



Graph 9. Anti-bacterial effect of **IV.7** against *Staph. aureus*.

MGB **IV.7** kills *Staph. aureus* above a concentration of 7 µg/ml. The curves corresponding to concentrations of 10 µg/ml and 20 µg/ml are similar to that of ampicillin. In comparison, at 7 µg/ml of molecule **IV.7** the Gram positive bacteria are still healthy and growing well up to 1125 min (18h45min) at which the absorbance drops, suggesting that bacteria start dying at that point.



Graph 10. Anti-bacterial effect of **IV.6** against *Staph. aureus*.

In the case of molecule **IV.6**, no killing effect is seen even at 20 µg/ml. This molecule does not have any antibacterial effects on *Staph. aureus*.

To conclude, these results prove that **IV.5** is a really potent antibacterial molecule against *Staph. aureus* since its killing effect is evident even at 0.5 µg/ml. In comparison, molecule **IV.7** kills bacteria quickly above 7 µg/ml, but even at 7 µg/ml bacteria seem to die significantly after a certain time, however without reaching the levels observed for ampicillin curve. Finally, the experiment undertaken with **IV.6** does not allow to see its killing concentration which is obviously above 20 µg/ml, so it has no interesting antibacterial effect.

iii. Intermediate MGBs series

The molecules synthesized as intermediate MGBs (Figure 33) were tested biologically against the Gram positive bacterium *Staph. aureus*.

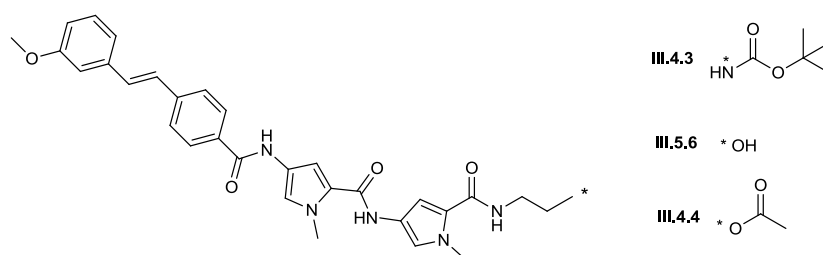
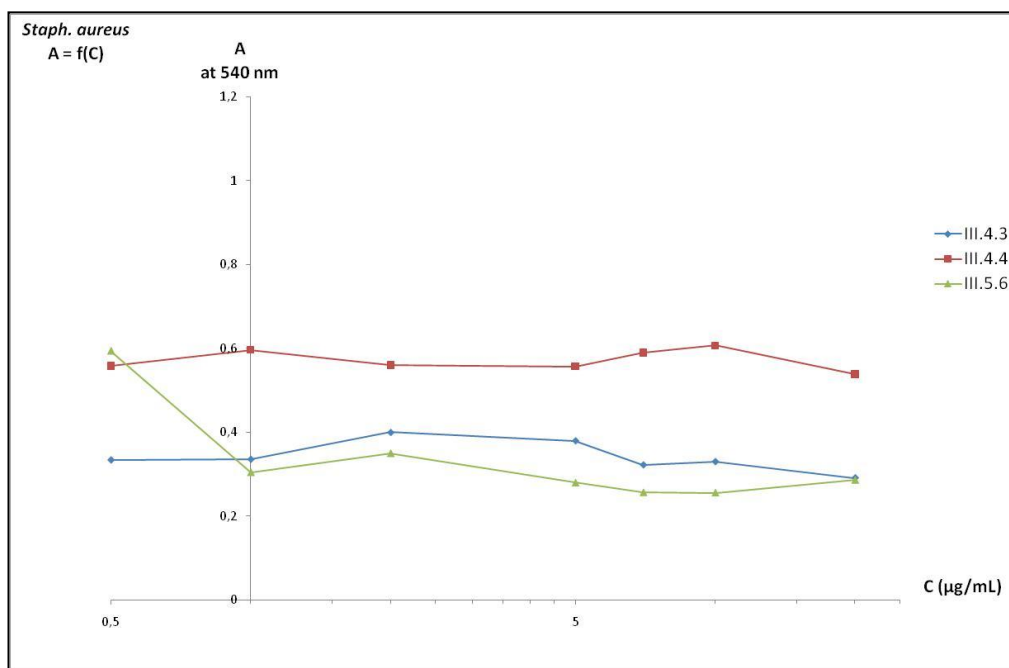
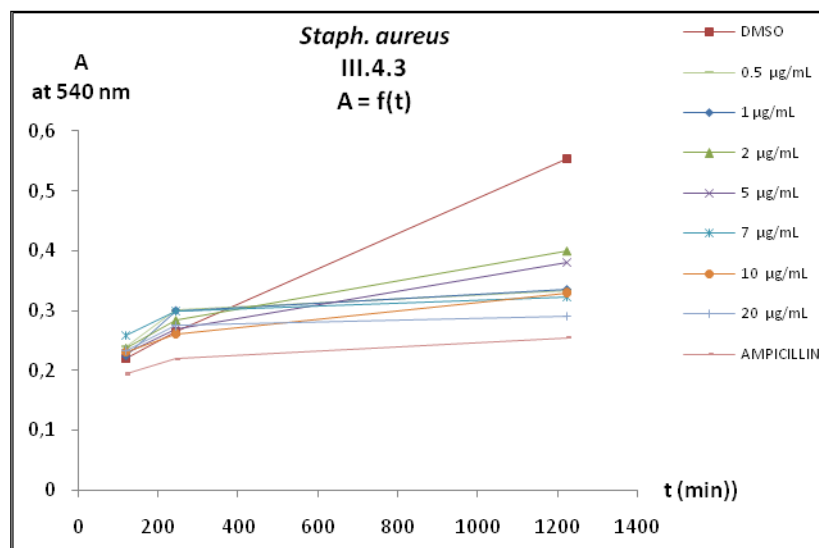


Figure 33. Structural features of intermediate MGBs series.

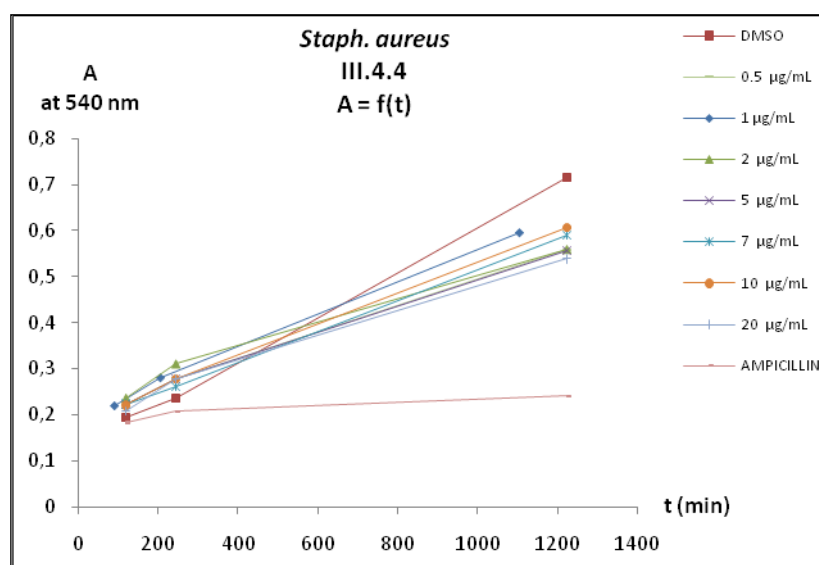


Graph 11. Killing curve of intermediate MGBs against *Staph. aureus*.

Graph 11 suggests that **III.4.3** and **III.4.4** have no impact on the cell growth whichever the concentration is. This can be confirmed by the two graphs below (Graph 12 and Graph 13) in which no curve is similar or even close to the ampicillin one.



Graph 12. Anti-bacterial effect of **III.4.3** against *Staph. aureus*.

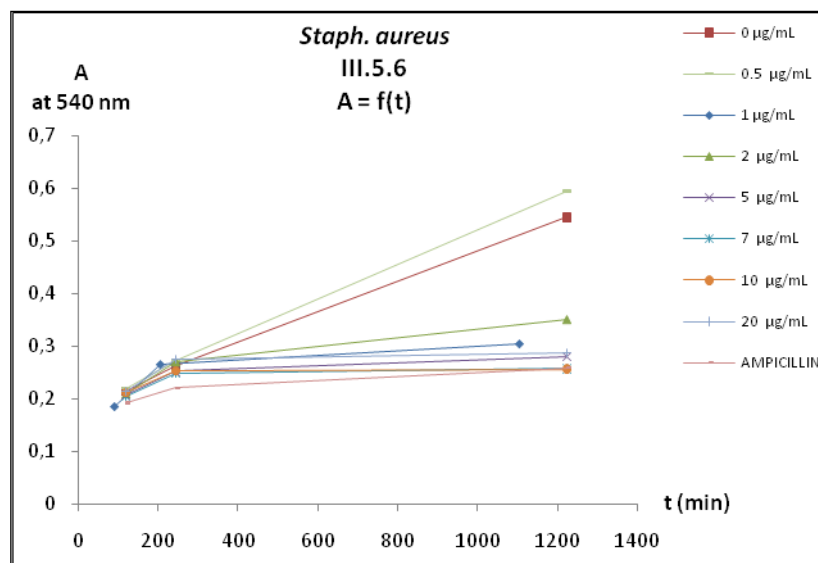


Graph 13. Anti-bacterial effect of **III.4.4** against *Staph. aureus*.

In comparison with molecule **III.4.4** (Graph 13), molecule **III.4.3** (Graph 12) seems to slow the growth of Gram positive bacteria since all the curves are significantly below the one corresponding to no treatment by **III.4.3** (DMSO). However, no killing is observed.

The curve of molecule **III.5.6** (Graph 11) drops significantly in absorbance above 0.5 µg/ml. Further studies gave the graph below (Graph 14) confirming this hypothesis. Only the 0.5

$\mu\text{g/ml}$ curve is similar to the one corresponding to the untreated bacteria (DMSO), but even the 1 $\mu\text{g/ml}$ curve, low in absorbance, suggests some effect of **III.5.6** against *Staph. aureus* after 245 min (4h05min).



Graph 14. Anti-bacterial effect of **III.5.6** against *Staph. aureus*.

The intermediate MGBs **III.4.3**, **III.4.4** and **III.5.6** have different effects on *Staph. aureus* bacteria. While the first two do not show any antibacterial effect below 20 $\mu\text{g/ml}$, molecule **III.5.6** has an impact on bacteria growth above 0.5 $\mu\text{g/ml}$.

iv. New MGBs and MGB IV.1 series

The new molecules and **IV.1** (Figure 34) were tested against the Gram positive bacterium *Staph. aureus*.

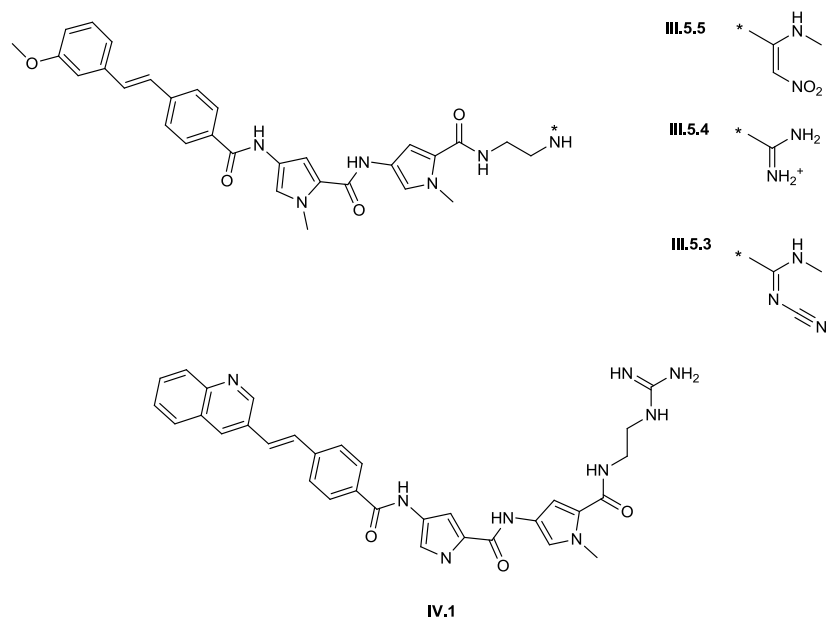
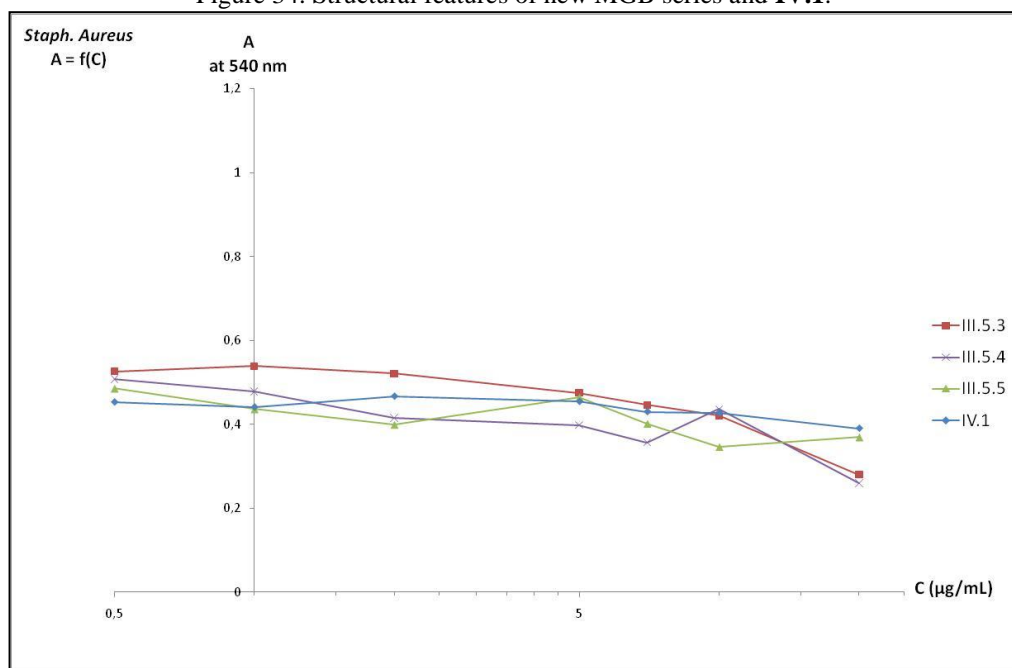
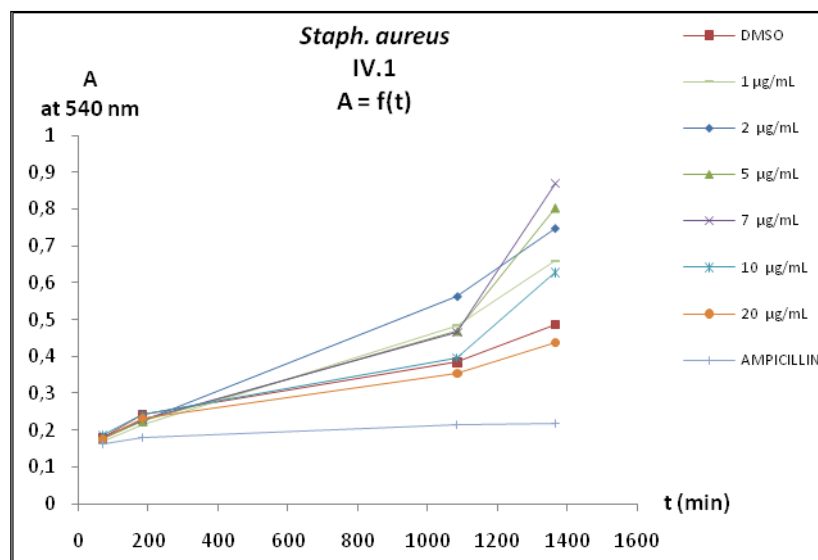


Figure 34. Structural features of new MGB series and IV.1.



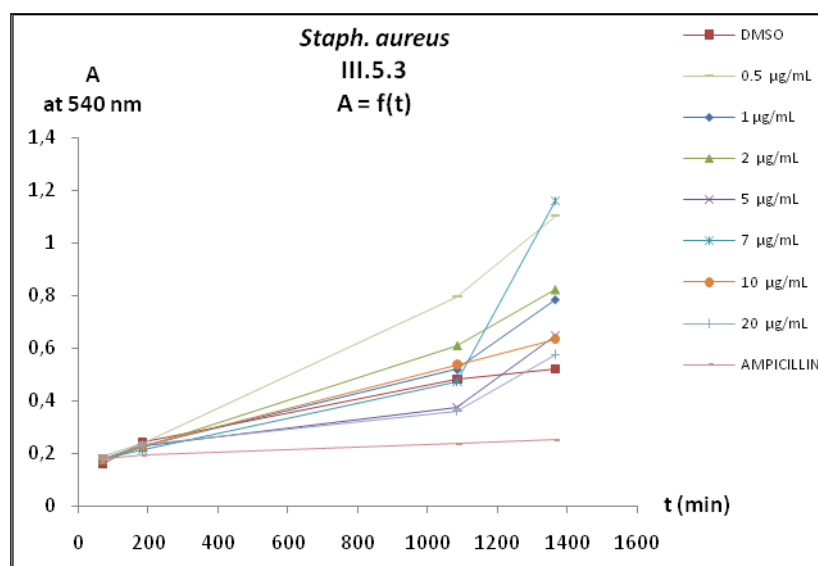
Graph 15. Killing curves of new MGBs series and IV.1.

All MGBs curves for the MGBs except molecule **IV.1** show a decrease of absorbance when the concentration increased, meaning that the bacteria are affected by molecules **III.5.3**, **III.5.4** and **III.5.5**. Graph 16 confirms the curve of molecule **IV.1** obtained above (Graph 15), ie. no significant effect on *Staph. aureus*.

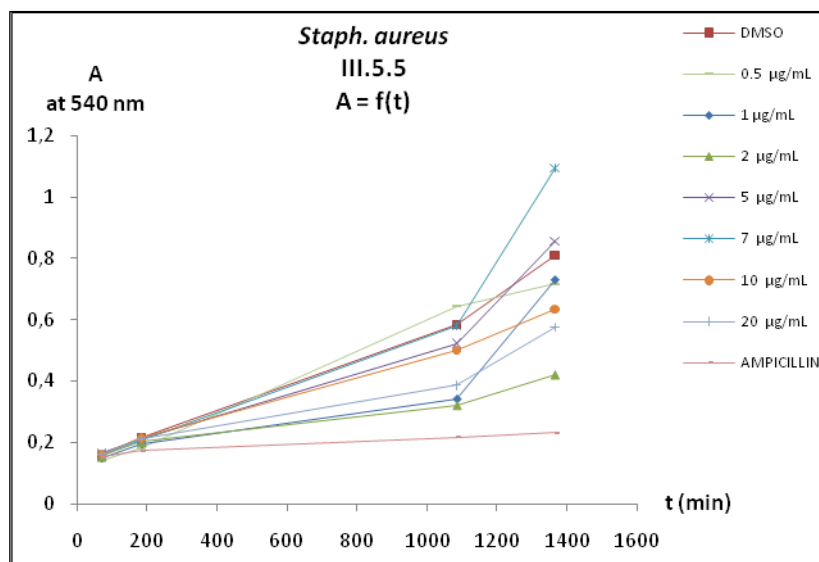


Graph 16. Anti-bacterial effect of MGB IV.1 against *Staph. aureus*.

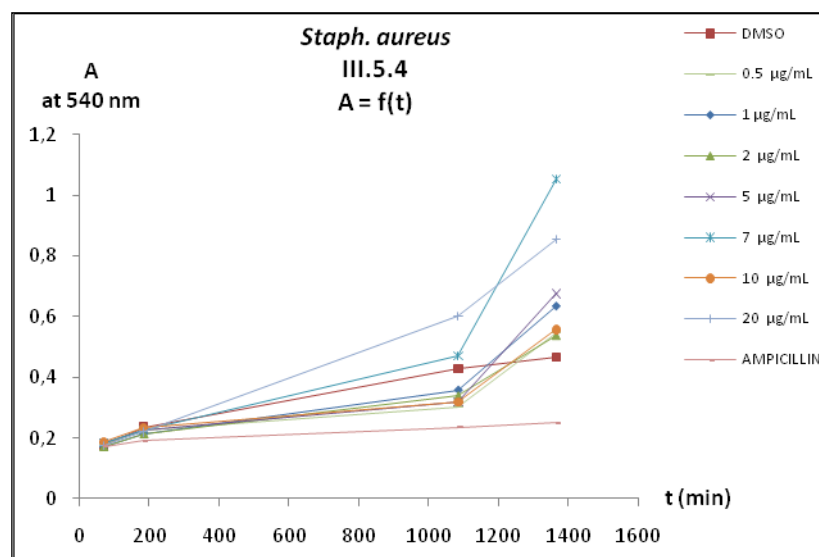
The effect on *Staph. aureus* seems to be slightly less important in the presence of molecule III.5.5 (Graph 15). To understand the behaviour of bacteria in the presence of these MGBs, graphics of the absorbance against the time were plotted.



Graph 17. Anti-bacterial effect of III.5.3 against *Staph. aureus*.



Graph 18. Anti-bacterial effect of **III.5.5** against *Staph. aureus*.



Graph 19. Anti-bacterial effect of **III.5.4** against *Staph. aureus*.

These three graphs are quite similar and do not confirm what is shown on Graph 15. Any concentration seems to be toxic to *Staph. aureus* bacteria for all three molecules. However, it seems that the growth of the bacteria is slightly slower before 1185 min (18h05min) and increases after. Comparing the absorbance values from Graph 17-19, **III.5.5** is the one that least affecting the growth of the bacteria.

v. **CONCLUSION**

Regarding the toxicity against Gram positive bacteria, the MGBs tested have different effects.

The most toxic agents against *Staph. aureus* bacteria are molecules **IV.3** and **IV.5**. These have different head groups and respectively, a tertiary alkyl amine and a morpholine tail group. They both show the best antibacterial effect at low concentration, ie. below 1 µg/ml, resulting probably from the basic tail group.

Molecule **III.5.6**, the intermediate MGB containing the free primary alcohol, affects Gram positive bacteria above 0.5 µg/ml.

Molecule **IV.2** shows antibacterial effect below 5 µg/ml, whereas MGB **IV.4** does not kill bacteria at or below a concentration of 20 µg/ml; however it has an effect on the growth rate of bacteria at 20 µg/ml. This difference in antibacterial effects could be related to the position of the substitution of the head group ((*E*)-1-methoxy-3-styrylbenzene) with the rest of the molecule,

MGB **IV.7**, bearing a morpholine tail group and (*E*)-4-(2-(quinolin-3-yl)vinyl)benzamide as head group, shows antibacterial properties from 7 µg/ml, in contrast to molecules **IV.6** (morpholine tail group and (*E*)-3-(3-methoxystyryl)benzamide head group), **III.4.3** (BOC tail group), **III.4.4** (acetate tail group) and **IV.1** (guanidine tail group and (*E*)-4-(2-(quinolin-3-yl)vinyl)benzamide head group) which have no effect on *Staph. aureus*, even at 20 µg/ml. MGBs **III.4.3** and **III.4.4** bear protected tail groups which could prevent either the membrane permeation of Gram positive bacteria or the interaction with DNA.

Molecules **III.5.3** (cyano alkene tail group), **III.5.4** (guanidine tail group) and **III.5.5** (nitro alkene tail group), all have the same head group and differently affect the growth rate of Gram positive bacteria without apparently killing them, suggesting that these molecules do not interact with the DNA of bacteria.

Similar experiments were undertaken with *Escherischia coli* to assess the antibacterial properties of MGBs against Gram negative bacteria.

b) *Gram negative bacteria: Escherischia coli* NM522

i. **Tertiary alkyl amine series**

The molecules MGB bearing a tertiary alkyl amine (Figure 35) were tested against Gram negative bacterium *E. coli*.

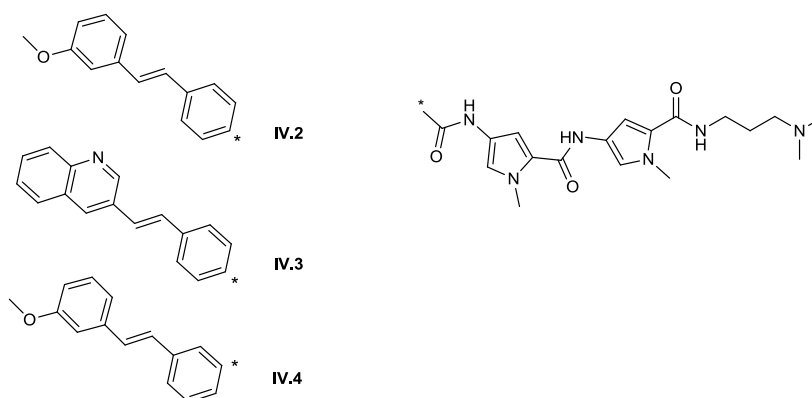
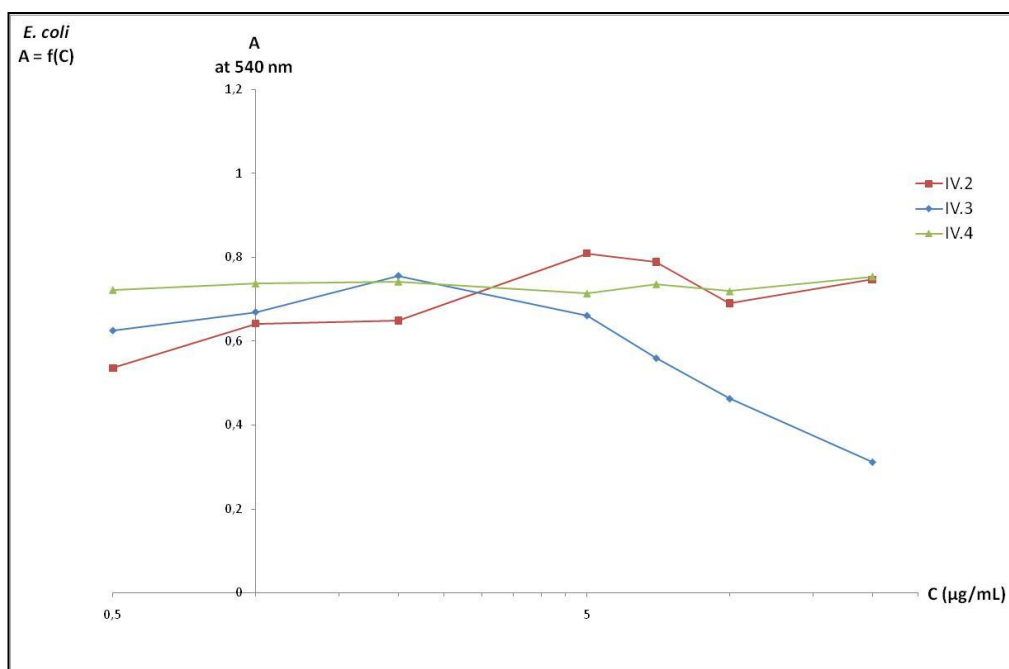
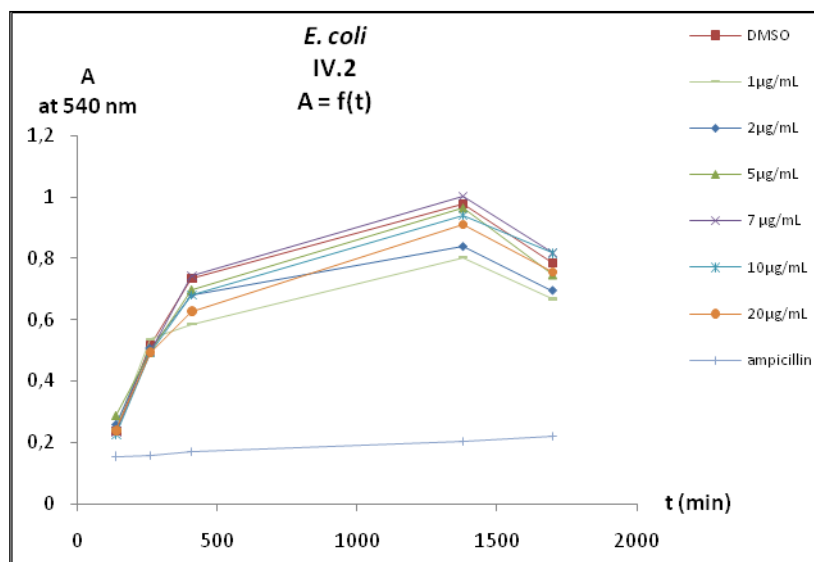


Figure 35. Tertiary alkyl amine tail group series.

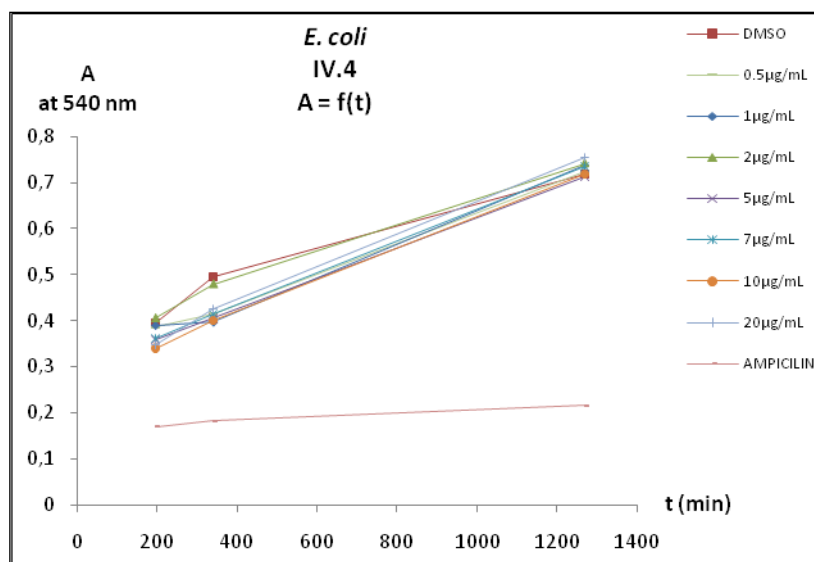


Graph 20. Killing curves of tertiary alkyl amine series.

Graph 20 suggests that **IV.3** slows and then stops the growth of *E. coli* above a certain concentration which still has to be evaluated from Graph 23. In comparison **IV.2** and **IV.4** do not seem to stop the *E. coli* bacteria from growing since the corresponding curves are almost straight. This behaviour is confirmed by Graph 21 and Graph 22, which show no difference between the curves at different concentrations and the curve for which the Gram negative bacteria have not been treated, even after 1700 min (28h20min).

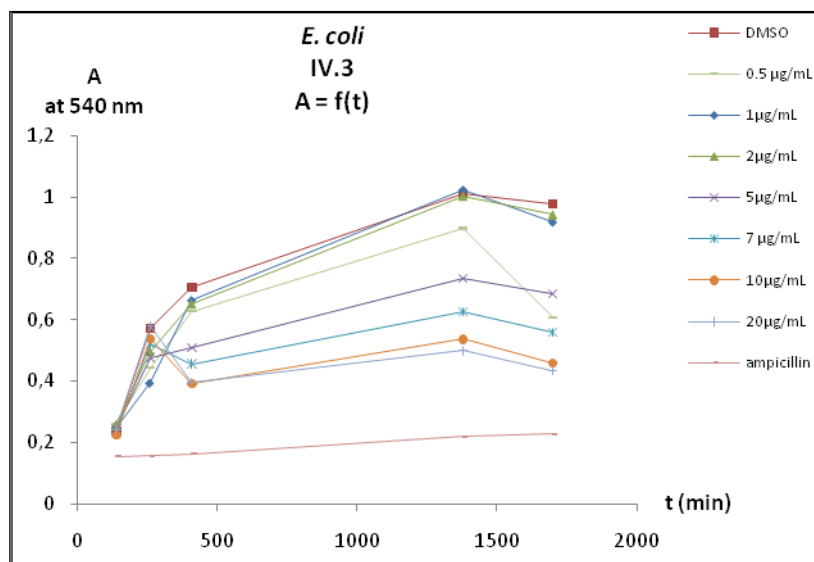


Graph 21. Anti-bacterial effect of **IV.2** against *E. coli*.



Graph 22. Anti-bacterial effect of **IV.4** against *E. coli*.

Graph 23 shown below is in accordance with Graph 20 since the curves at different concentrations are lower in absorbance than the one corresponding to the untreated bacteria. From 5 µg/ml to 20 µg/ml, the addition of **IV.3** slows down the growth rate of bacteria without killing them.



Graph 23. Anti-bacterial effect of **IV.3** against *E. coli*.

None of these molecules of the tertiary alkyl amine series kills *E. coli* below a concentration of 20 µg/ml; however **IV.3** slows the growth of *E. coli* above a concentration of 2 µg/ml.

ii. Morpholine tail group series

The molecules MGB bearing a morpholine tail group (Figure 36) were tested against the Gram negative bacterium *E. coli*.

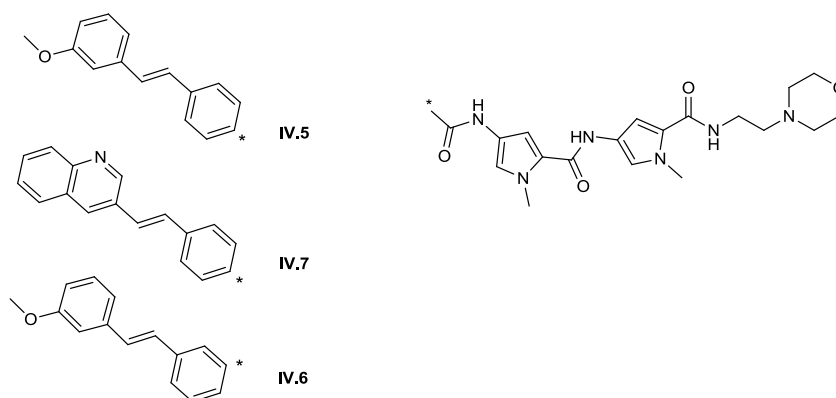
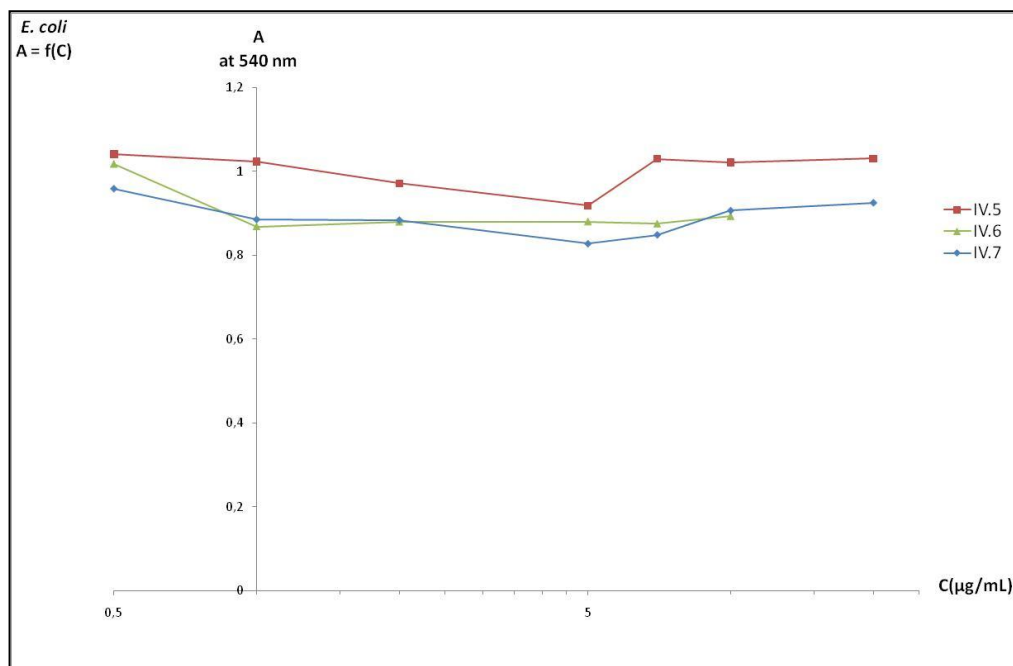
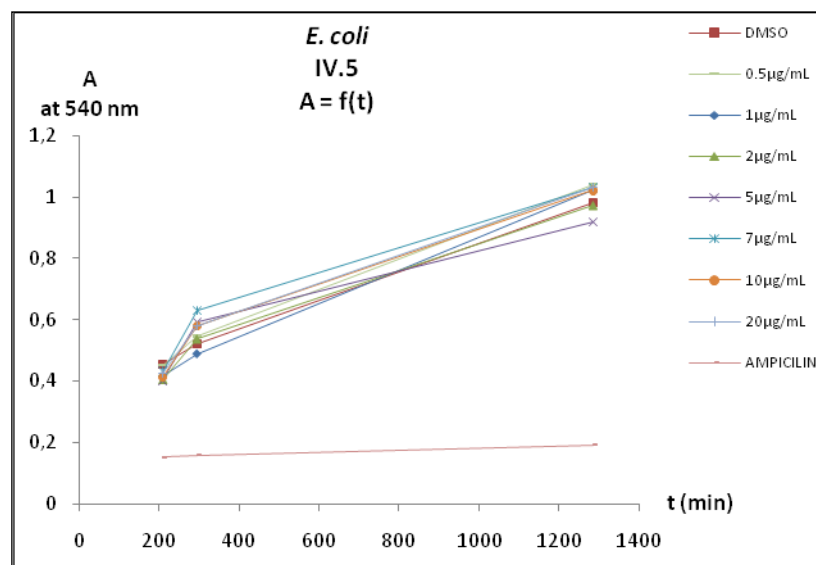


Figure 36. Morpholine tail group MGB series.

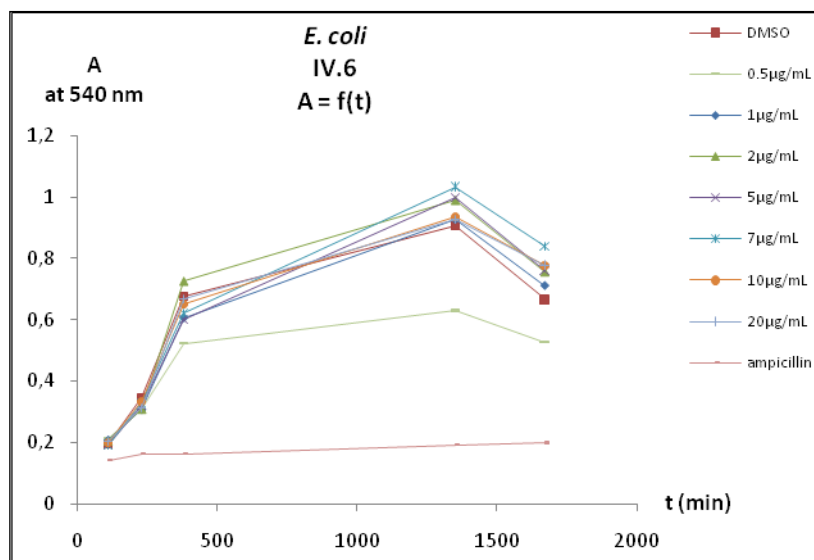


Graph 24. Killing curves of morpholine tail group series.

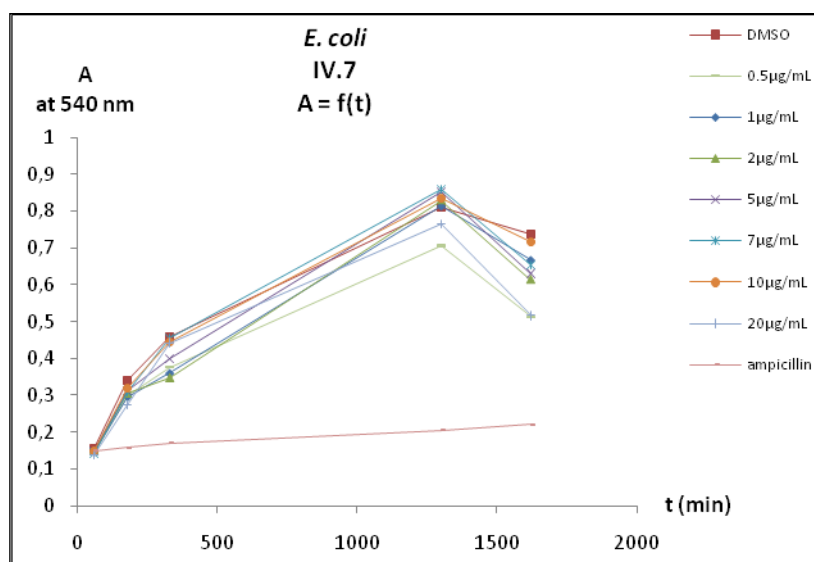
The curves of Graph 24 are in accordance with the ones showed in Graph 25-27. These curves suggest that the molecules bearing a morpholine tail group do not have any antibacterial effect against the Gram negative bacterium *E. coli* below 20 µg/ml.



Graph 25. Anti-bacterial effect of **IV.5** against *E. coli*.



Graph 26. Anti-bacterial effect of **IV.6** against *E. coli*.



Graph 27. Anti-bacterial effect of **IV.7** against *E. coli*.

iii. Intermediate MGBs and IV.1 series

The molecules synthesized as intermediate MGBs (Figure 37) were tested biologically against the Gram negative bacterium *E. coli*.

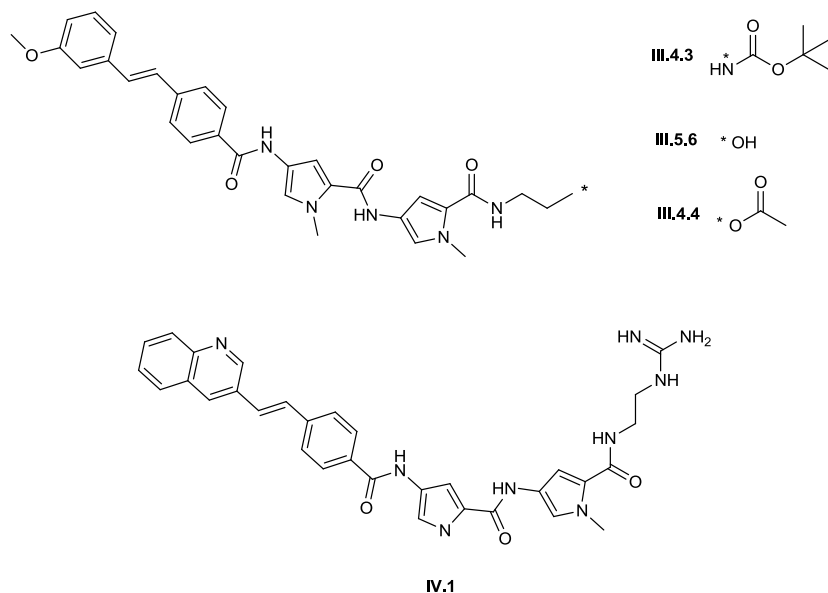
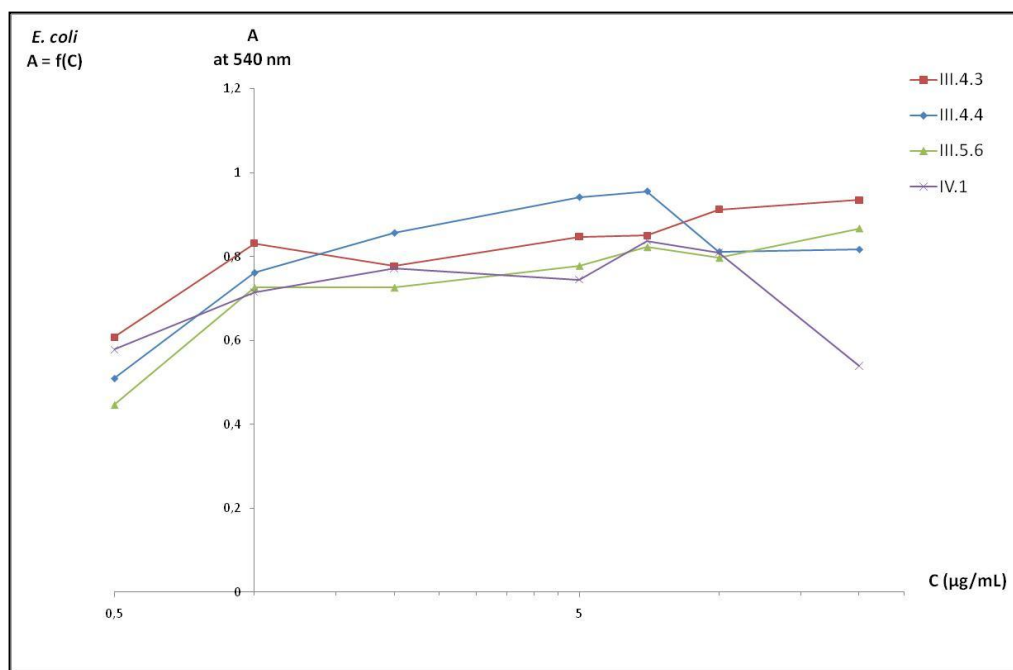
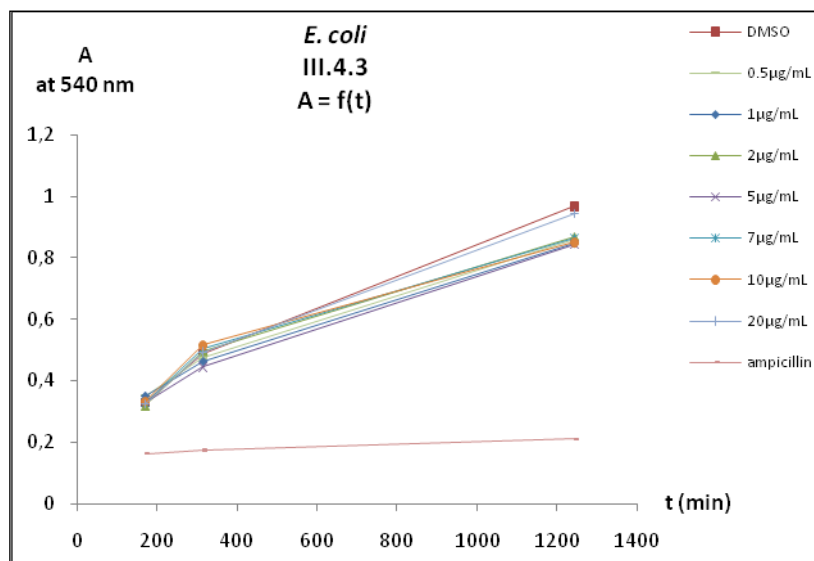


Figure 37. Structural features of intermediate MGBs and IV.1 series.

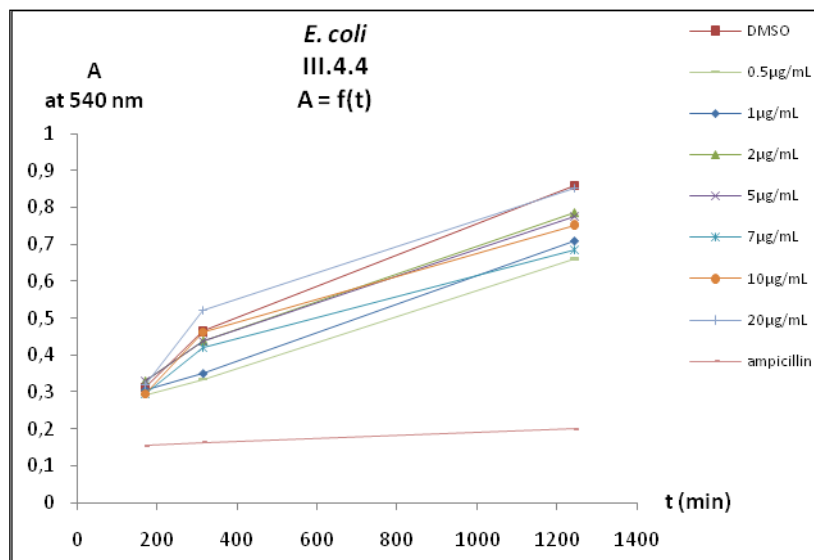


Graph 28. Killing curves of intermediate MGBs and IV.1.

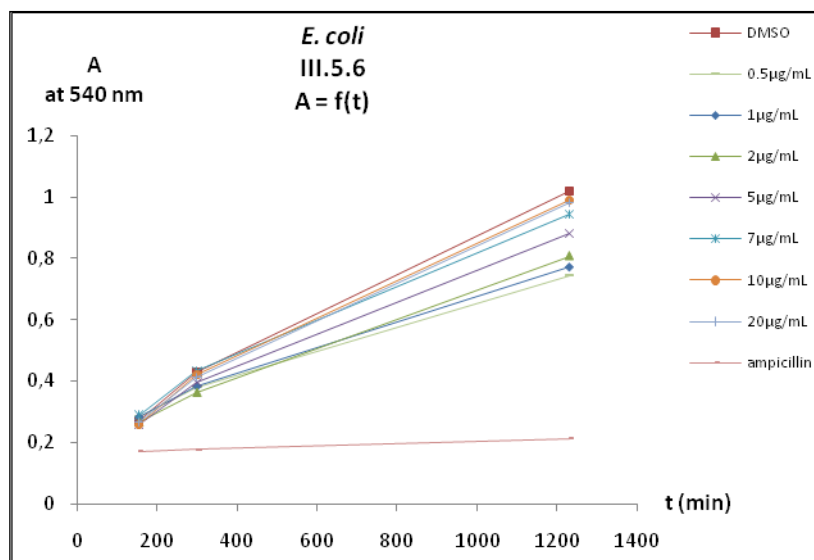
No difference of absorbance is observed between the lowest and the highest concentrations. Molecules **III.4.3**, **III.4.4**, **III.5.6**, **IV.1** do not seem to stop *E. coli* from growing. These results can be confirmed by the Graph 29-30 which show similar curves for all concentrations as the one corresponding to no treatment of the bacteria (DMSO). In the case of **IV.1**, the growth seems, however, to be affected above a certain concentration that can be determined from Graph 32.



Graph 29. Anti-bacterial effect of **III.4.3** against *E. coli*.

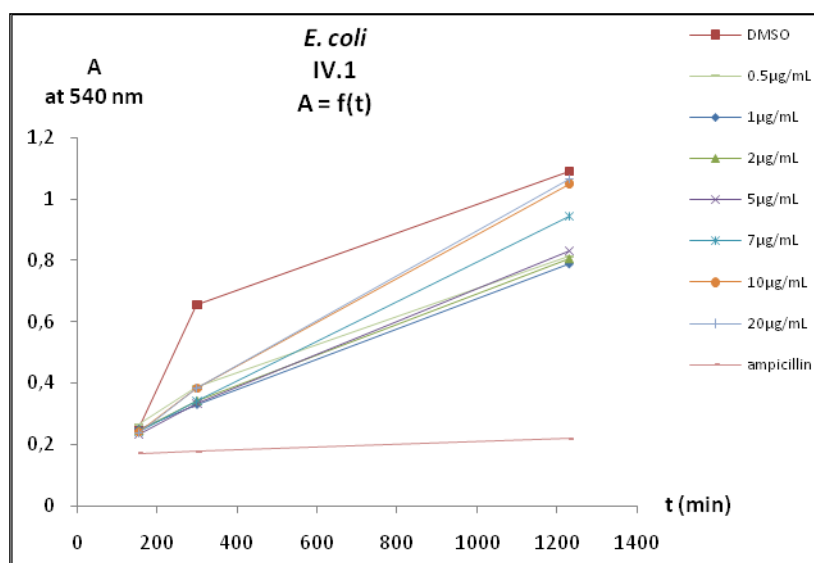


Graph 30. Anti-bacterial effect of **III.4.4** against *E. coli*.



Graph 31. Anti-bacterial effect of **III.5.6** against *E. coli*.

Graph 32 proves that the effect of molecule **IV.1** against *E. coli* is not significant, since even at 20 µg/ml, the absorbance value shows that bacteria are still growing healthily.



Graph 32. Anti-bacterial effect of **IV.1** against *E. coli*.

In summary, none of the intermediate MGBs synthesized nor **IV.1** were toxic towards *E. coli*.

iv. New MGBs series

The new molecules (Figure 38) **III.5.3-III.5.5** were tested against the Gram negative bacterium, *E. coli*, to assess their antibacterial activity.

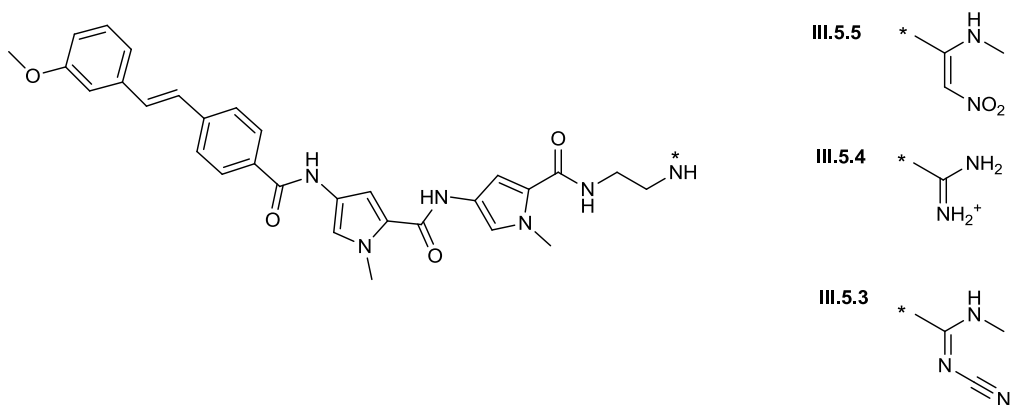
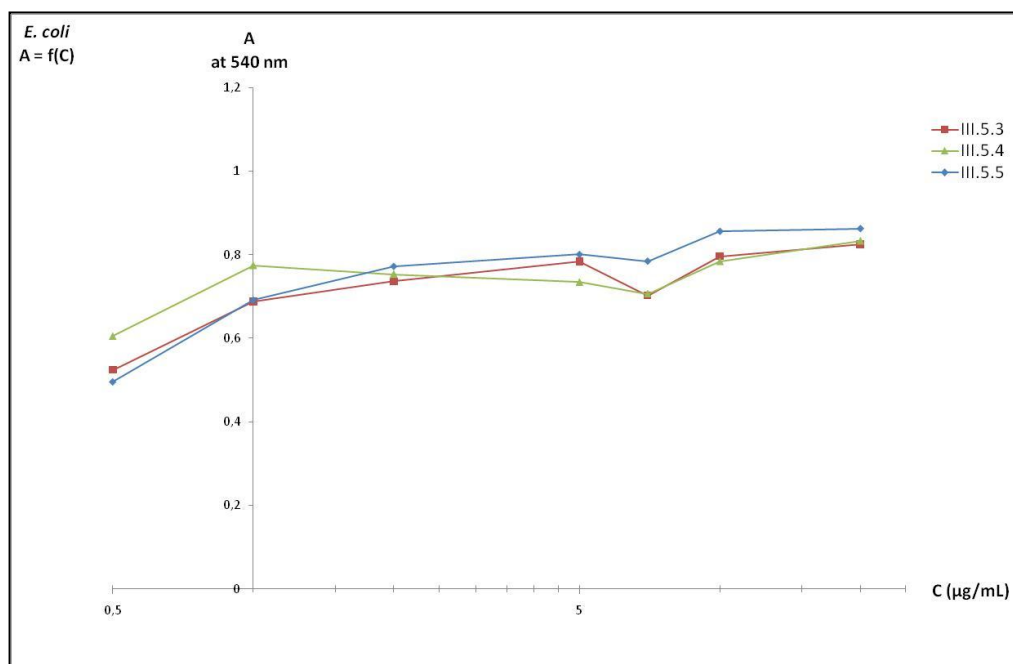
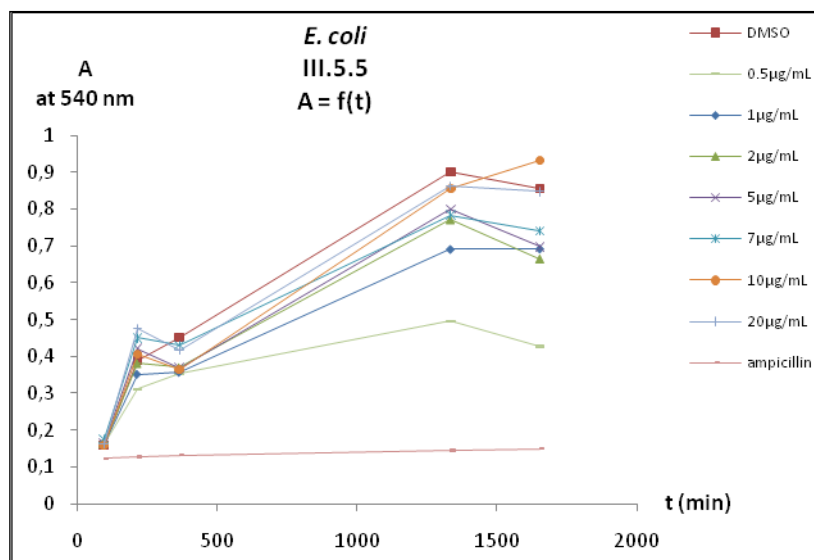


Figure 38. Structural features of new MGBs series.

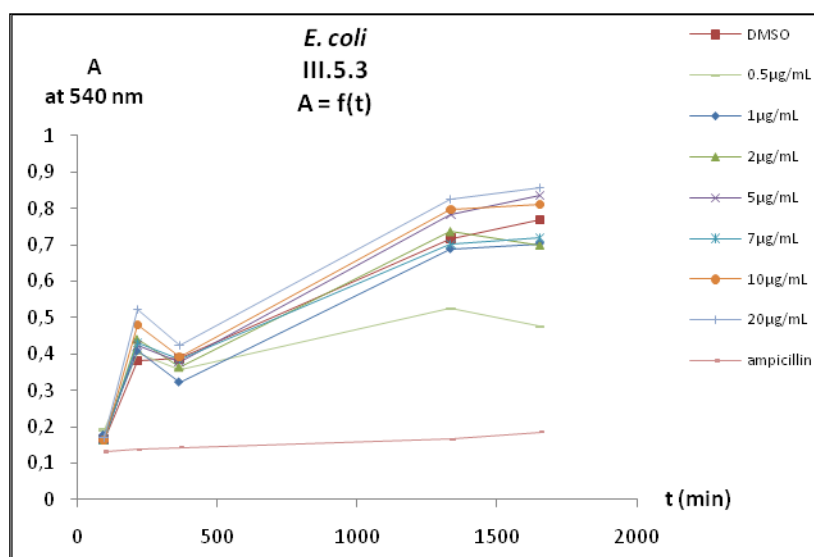


Graph 33. Killing curves new MGBs series.

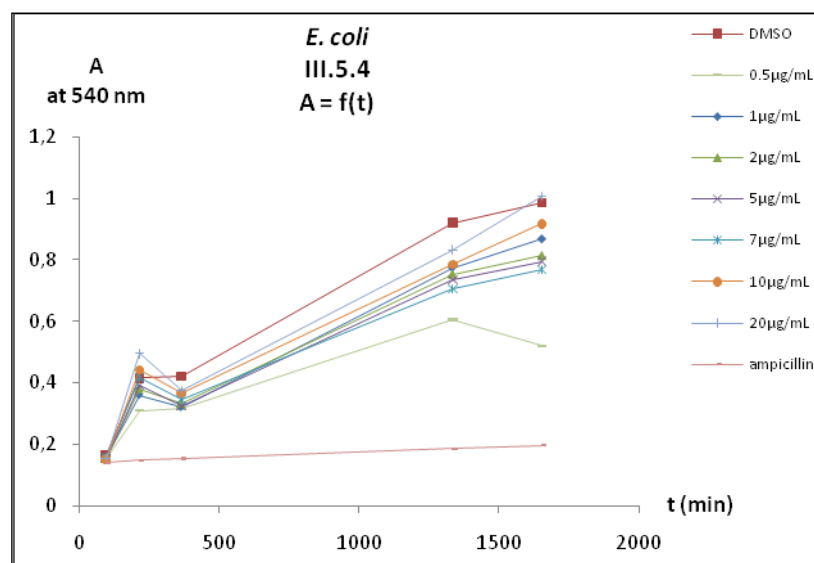
Again in this case, Graph 33 clearly indicates that **III.5.5**, **III.5.3**, **III.5.4** have no effect on bacterial growth, not even slowing down the growth rate. These results are confirmed by the graphs below (Graph 34-36) which show no difference in absorbance between the different concentrations of drug and when the bacteria is treated only with the solvent vehicle (DMSO).



Graph 34. Anti-bacterial effect of **III.5.5** against *E. coli*.



Graph 35. Anti-bacterial effect of **III.5.3** against *E. coli*.



Graph 36. Anti-bacterial effect of **III.5.4** against *E. coli*.

v. **CONCLUSION**

These experiments demonstrate that Gram negative bacteria, represented by *E. coli*, are not affected by the MGBs tested below the highest concentration introduced, ie. 20 µg/ml. Most of the time bacteria still grow as they would if they had not been treated by MGBs. However, in the case of molecule **IV.3**, bearing the (*E*)-4-(2-(quinolin-3-yl)vinyl)benzamide head group and tertiary alkyl amine tail group, the growth is slowed down at concentrations above 2µg/ml.

c) *Discussion*

The experiments with Gram positive and Gram negative bacteria were necessary to get an idea of the antibacterial effect of MGBs. The toxicity of MGB molecules is likely to be related to the cell wall permeation which in turn is likely to be related to the structure of the MGB.

Molecules **IV.5** and **IV.7**, bearing the morpholine tail group and, respectively, the (*E*)-4-(3-methoxystyryl)benzamide and the (*E*)-4-(2-(quinolin-3-yl)vinyl)benzamide head groups, inhibited the growth of Gram positive bacteria, at a concentration respectively above 0.5 µg/ml and above 7 µg/ml, but had no toxicity against Gram negative bacteria at or below 20 µg/ml. This can be probably explained by the difference in structure between Gram positive and Gram negative bacteria. Due to the lack of an outer membrane in Gram positive bacteria,

IV.5 may permeate the cell wall of Gram positive bacteria relatively easily, whereas the outer membrane in Gram negative bacteria may prevent the molecule from entering the bacteria. This permeation hypothesis will be evaluated by microscopy (see section IV p84).

No killing effect was shown by molecule **IV.6** ((*E*)-3-(3-methoxystyryl)benzamide and morpholine) against Gram negative bacteria, but Graph 10 suggests a slower growth of *Staph. aureus* at a concentration of 20 µg/ml. The same results were observed for **IV.4** bearing the same head group but the tertiary alkyl amine tail group. In comparison, **IV.2** ((*E*)-4-(3-methoxystyryl)benzamide and tertiary alkyl amine) did not have any effect on Gram negative cells, but did kill Gram positive bacteria above 5 µg/ml. Again, the different cell wall structures of the two kinds of bacteria probably influence the accumulation of MGBs into the cell.

The molecules with the (*E*)-4-(3-methoxystyryl)benzamide head group, **III.4.3** (BOC tail group), **III.4.4** (OAc tail group), **III.5.3** (cyano alkene tail group), **III.5.4** (guanidine tail group), **III.5.5** (nitro alkene tail group), as well as molecule **IV.1** (*E*)-4-(2-(quinolin-3-yl)vinyl)benzamide and guanidine) did not show any toxicity against either *E. coli* or *Staph. aureus* at or below 20 µg/ml. We could assume that they are not entering the bacterial cell. However, the inactivity of compounds containing a neutral tail group, and particularly the inactivity of **IV.1**, is surprising since the parent compounds, distamycin (**II.1.1**) and netropsin (**II.1.6**), contain amidines and showed anti-bacterial activity. In comparison, **III.5.6** ((*E*)-4-(3-methoxystyryl)benzamide and OH) probably enters Gram positive bacterial cells since it seems to slow down the bacteria growth at a concentration of 20 µg/ml.

Finally, molecule **IV.3** is the only MGB that seemed to have an effect on both *E. coli* and *Staph. aureus* according to Graph 5 and Graph 23. It was toxic towards Gram positive bacteria above a concentration of 1 µg/ml, and only affected bacterial growth above 5 µg/ml.

III. Cytotoxicity assay using V79 Chinese Hamster cells

For an MGB to be a potential drug, it is essential that it should have selective toxicity for the bacteria and not be toxic to mammalian cells. It is therefore important to investigate toxicity to a mammalian cell line as well as to bacteria.

1. MTT assay : Experimental

The MTT assay was carried out in order to determine any potential toxicity of MGBs against V79 mammalian cells. The tetrazole 3-(4,5-dimethylthiazol-2-yl)-2,5-diphenyltetrazolium bromide (MTT) (Figure 39) is yellow and is reduced to purple formazan in living cells. These reductions take place only when reductase enzymes are active, and therefore the colour conversion is often used as a measure of living cells.

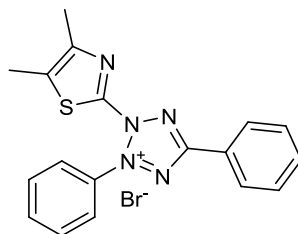
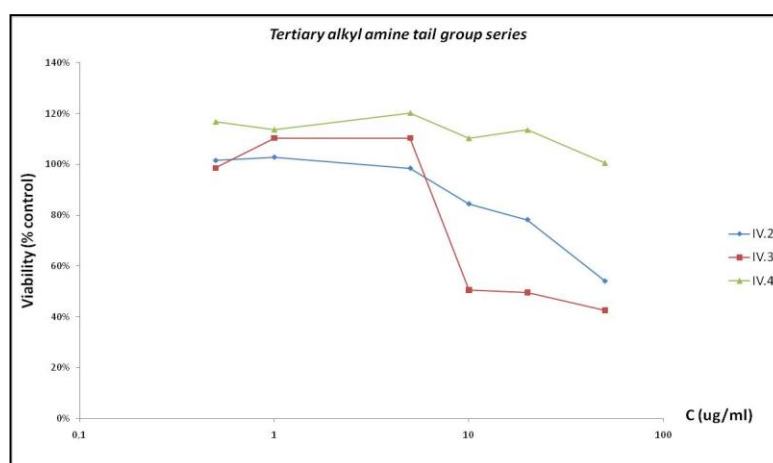


Figure 39. Structure of MTT.

During this assay, the cells were in contact with a MGB for 24hrs, at which time the MTT dye was added to the medium. After 2hrs of exposure, the dye was removed and DMSO was added to dissolve the crystal of the dye that had accumulated in the cells and to give a purple color. The absorbance was recorded at 540 nm to give the curves below from which the viability of cells was determined.

2. Results

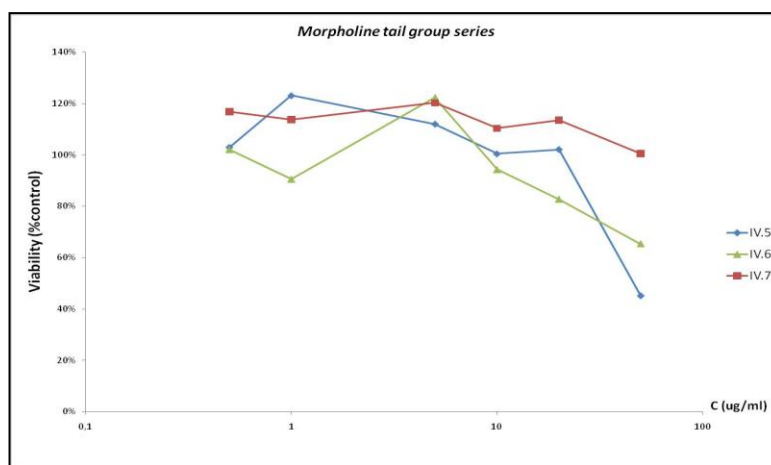
a) *Tertiary alkyl amine tail group series*



Graph 37. Killing curves of tertiary alkyl amine tail group series in the presence of V79 mammalian cells.

The curve corresponding to **IV.3** drops significantly and indicates that 67% of the V79 cells die as the concentration of the molecule increases. The killing concentration seems to be between 5 to 10 $\mu\text{g/ml}$. This could have been evaluated if the absorbance had been measured for several concentrations at different times. The V79 cells also die in presence of **IV.2**, but the process is slower and becomes significant above 20 $\mu\text{g/ml}$. The introduction of **IV.4** does not seem to have any killing effect on mammalian cells, even at a high concentration of 50 $\mu\text{g/ml}$. In the tertiary alkyl amine tail group series, only **IV.3** is highly toxic against V79 fibroblast hamster cells, **IV.2** shows poor toxicity, whereas **IV.4** does not inhibit cells growth.

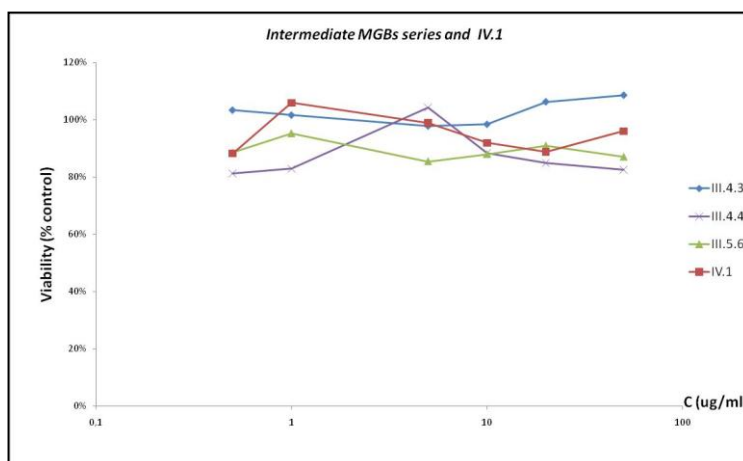
b) Morpholine tail group series



Graph 38. Killing curves of the morpholine tail group series in the presence of V79 mammalian cells.

The three curves indicate that molecules with a morpholine tail group are not toxic against V79 mammalian cells below a concentration of 20 $\mu\text{g/ml}$. This poor toxicity would make molecule **IV.5** and **IV.7** good potential drugs since the previous bacterial assays suggested that they were inhibiting Gram positive bacterial growth.

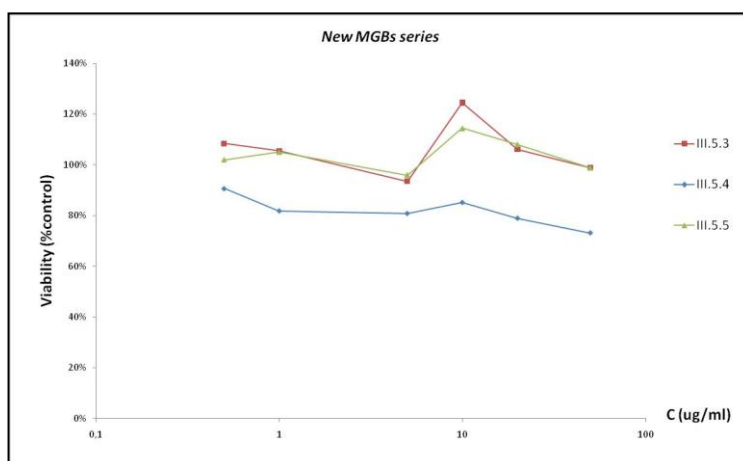
c) *Intermediate MGBs and IV.1 series*



Graph 39. Killing curves of intermediate MGBs and **IV.1** in the presence of V79 mammalian cells.

Again, in this case, V79 cells do not die in the presence of molecules **III.4.3**, **IV.1**, **III.5.6** and **III.4.4**. The curves are almost straight indicating live cells in the media even above 50µg/ml.

d) *New MGBs series*



Graph 40. Killing curves of new MGBs series in the presence of V79 mammalian cells.

According to Graph 40, almost no cell dies in the presence of MGB **III.5.3**, **III.5.4** and **III.5.5**. In conclusion, these molecules are not toxic for the mammalian cells V79.

e) *Discussion*

All MGBs with the exception of **IV.3** (*E*)-4-(2-(quinolin-3-yl)vinyl)benzamide and tertiary alkyl amine) were not toxic towards V79 fibroblast hamster cells. They did not kill the V79 cells below a concentration of 50 µg/ml, which is a high concentration for potential drugs. It

would be interesting to see whether these molecules permeate the cell membrane and if they do, whether they reach the nucleus, and bind to DNA. These studies were undertaken under microscopy (see section IV p84).

In contrast, **IV.3** is highly toxic since it starts inhibiting cell growth at a concentration above 0.5 µg/ml. This molecule already stands out of the range of potential anti-cancer drugs, unless modifying the structural features in order to decrease the cytotoxicity. Being toxic, this molecule very probably permeates the cell membrane and microscopy assay would help to see where it situated in the cell.

Structure **IV.3** has a similar tail group to structures **IV.2** and **IV.4**, but a different head group - the (*E*)-3-styrylquinoline head group. **IV.2** showed some toxicity above 20 µg/ml, but **IV.4** was not toxic, suggesting that the similar tail group, a tertiary alkyl amine, might not be the feature related to the toxicity. On the other hand, **IV.1** has the same head group as **IV.3** without being toxic below 50 µg/ml, so the head group also does not seem to be the reason for toxicity. The toxicity of molecule **IV.3**, therefore, is not related to one specific structural feature but depends upon the balance of several structural units. This is an important conclusion for the design and discovery of selective and potent antibacterial MGBs.

This hypothesis is supported by the fact that **IV.4**, toxic above 20 µg/ml, and having the same tail group as **IV.2** and **IV.3**, has also the same head group as the new MGBs **III.5.3**, **III.5.4** and **III.5.5** which are not toxic against V79 mammalian cells.

IV. Fluorescent Microscopy

Microscopy was used to determine the accumulation of MGBs in Gram positive and Gram negative bacteria, and in mammalian cells. Molecule **III.4.3**, containing the Boc protected primary amine tail group was not studied under microscopy since the *t*-butyl group might be too big to fit in the minor groove of DNA and thus prevent the binding.

During the microscopy assays, the MGBs were mixed with mammalian or bacterial cells and visualized under different filters. 4',6-diamidino-2-phenylindole - DAPI (Figure 40) - was used as a control since it is a fluorescent stain that binds strongly to DNA, and which is used in fluorescence microscopy^[68]. Since DAPI passes through an intact cell membrane, it is usually used to stain both live and fixed cells. For fluorescence microscopy, DAPI is

excited with ultraviolet light. When bound to double-stranded DNA its absorption maximum is at 358 nm and its emission maximum is at 461 nm and appears blue/cyan^[68].

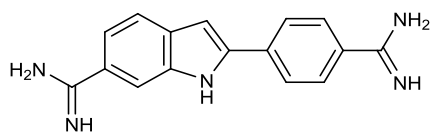


Figure 40. DAPI.

1. Bacteria

The slides were all visualized using the fluorescent microscope 100 x lenses under the bright field (BF) and dark field (using DAPI filter), and the pictures below were obtained. The fluorescence is more or less bright according to the amount of molecule accumulated. Hence the importance of the killing curves assays undertaken earlier, not only to determine their potential activity against *Staph. aureus* and *E. coli* but also to see any potential selectivity towards one family of bacteria.

a) Tertiary alkyl amine tail group series

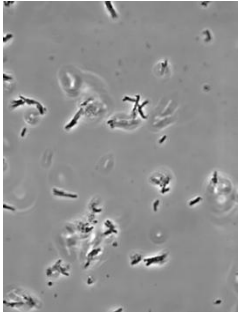
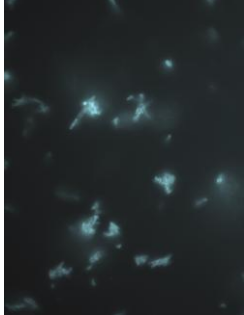
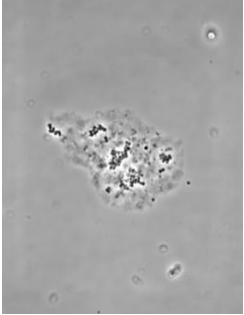
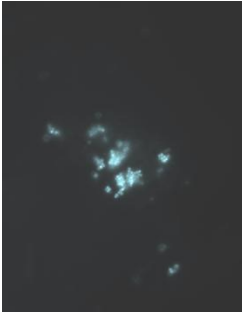
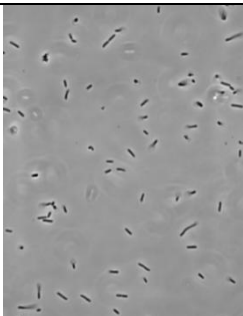
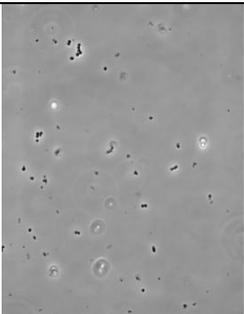
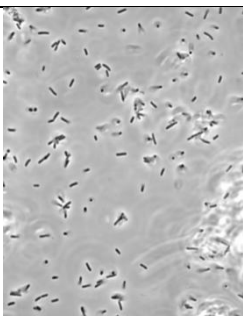
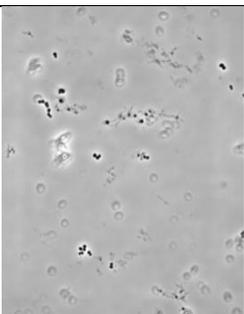
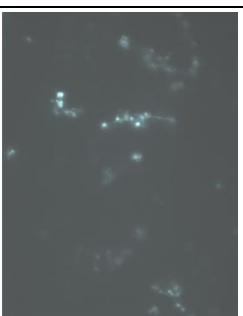
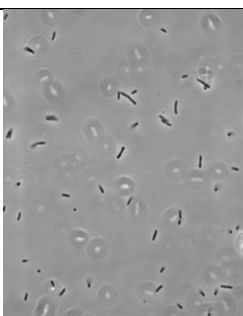
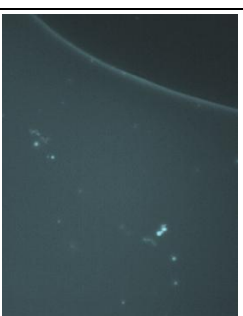
	<i>E. coli</i>		<i>Staph. aureus</i>	
	Brightfield	Fluorescence	Brightfield	Fluorescence
D A P I				
IV.2				
IV.3				
IV.4				

Table 4. Fluorescence of tertiary alkyl amine tail group series under Brightfield and DAPI filters in the presence of Gram positive and negative bacteria.

DAPI enters both Gram positive and Gram negative bacteria, which was expected, and binds to DNA, hence the fluorescence seen under microscopy.

Molecules **IV.2** and **IV.4** permeate into *Staph. aureus*, but not into *E. coli*. These pictures confirm the toxicity of these two molecules against Gram positive bacteria. The lack of toxicity against Gram negative bacteria can be explained since they do not reach the core.

Only molecule **IV.3** seems to enter both Gram negative bacteria (*E. coli*) and Gram positive bacteria (*Staph. aureus*). Nevertheless, the fluorescence seen under the DAPI filter in the presence of *Staph. aureus* is brighter than in the case of *E. coli*, suggesting a better penetration in Gram positive bacteria. This observation can be correlated with the fact that molecule **IV.3** is toxic to both types of bacteria (C.II.2 a) & b) p56 & 68) and the killing effect is most effective against Gram positive bacteria (0.5 µg/ml instead of >20 µg/ml for Gram negative bacteria).

The ability of these molecule to penetrate better into Gram positive bacteria can be easily understood since Gram positive bacteria have only a two layered membrane compared to Gram negative bacteria which have three layers.

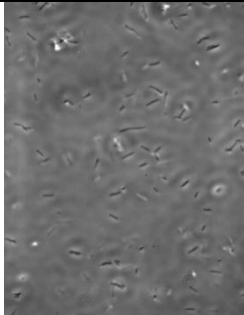
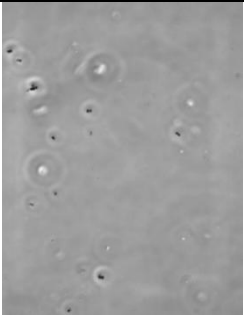
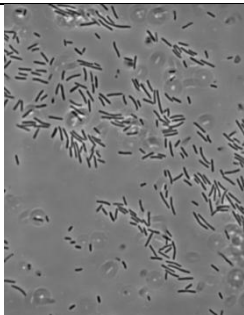
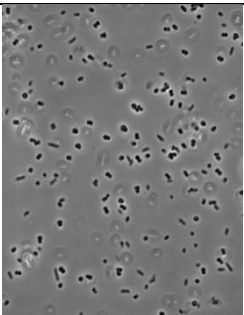
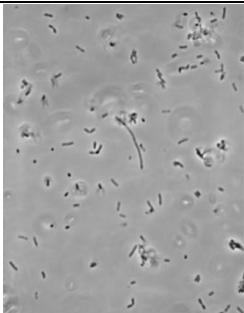
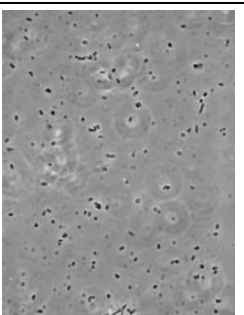
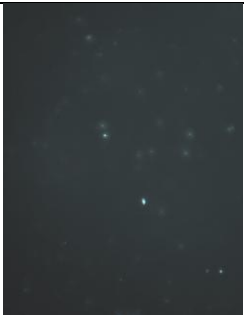
b) Morpholine tail group series				
	<i>E. coli</i>		<i>Staph. aureus</i>	
	Brightfield	Fluorescence	Brightfield	Fluorescence
IV.5				
IV.7				
IV.6				

Table 4. Fluorescence of the morpholine tail group series under Brightfield and DAPI filters in the presence of Gram positive and negative bacteria.

Molecule **IV.5** does not kill *E. coli* (see section C.II.2.b p68), and the pictures above prove that **IV.5** does not cross the bacterial cell wall. However, it does not seem to enter Gram positive bacteria either, though earlier results (see section C.II.2.a p56) indicated significant good toxicity above 0.5 µg/ml with a killing effect. In this case, the conclusion that can be drawn from the microscopy does not appear reliable.

Molecule **IV.7** does not penetrate Gram negative bacteria, hence no killing effect was seen (see section C.II.2.b p68), but it does penetrate Gram positive bacteria quite well, hence the toxicity

evaluated via the curves (see section C.II.2.a p56).

The microscopy pictures of molecule **IV.6** suggest good permeation into *Staph. aureus*, hence the antibacterial effect shown during the assays (see section C.II.2). The picture corresponding to *E. coli* permeation does not show fluorescence for all bacteria present under the Brightfield filter and is quite weak compared to the fluorescence usually obtained. Since the assays in section C.II.2. do not show any toxicity, **IV.6** probably does not enter in Gram negative bacterial cells.

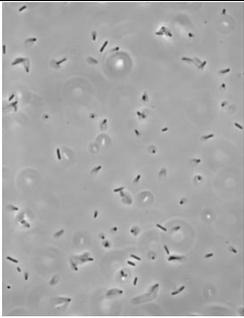
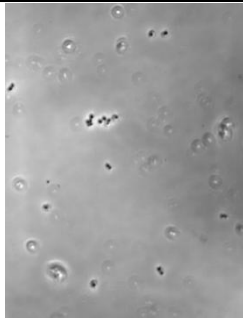
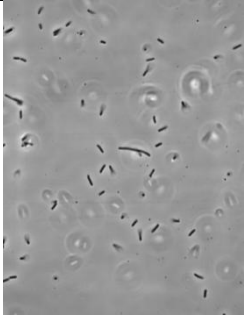
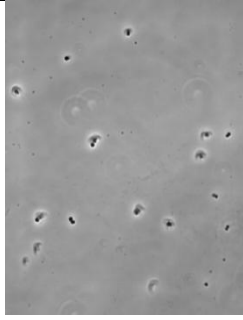
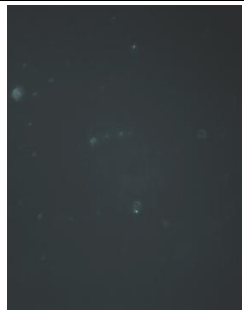
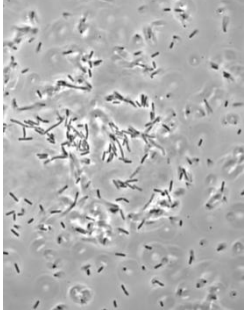
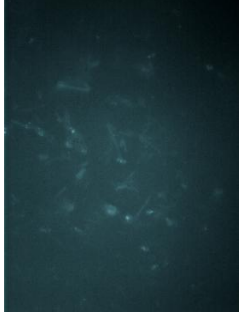
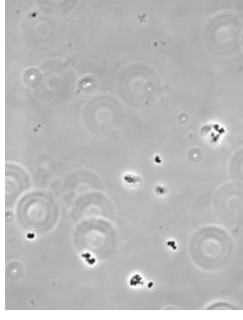
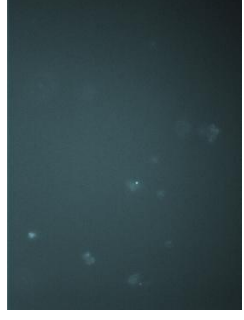
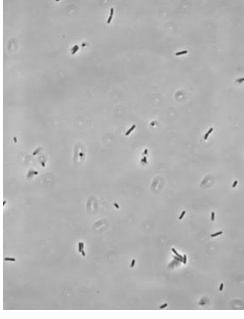
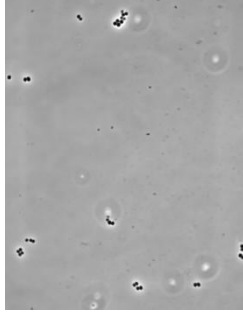
c) Intermediate MGBs and IV.1				
	<i>E. coli</i>		<i>Staph. aureus</i>	
	Brightfield	Fluorescence	Brightfield	Fluorescence
III.5.6				
III.4.4				
III.4.3				
IV.1				

Table 5. Fluorescence of intermediate MGBs and IV.1 series under Brightfield and DAPI filters in the presence of Gram positive and negative bacteria.

At first glance we can say that molecule **IV.1** is not entering into either Gram positive or Gram negative bacteria, and is then not able to kill bacteria, even if it had any antibacterial properties; hence the curves obtained in part C.II.2 show no toxicity.

Molecules **III.5.6** and **III.4.4** do not permeate *E. coli* and so cannot be toxic (see section C.II.2.b), while **III.5.6** does not show any inhibition of Gram positive bacterial growth because it apparently does not accumulate into such bacteria. Molecule **III.4.4** seems to enter slightly into *Staph. aureus*. The latter observation along with the negative results from section C.II.2.a, suggest that **III.4.4** does not have antibacterial properties.

Finally, molecule **III.4.3** accumulates in both Gram positive and Gram negative bacteria; however the curves obtained from the bacterial assays do not show any toxicity at the concentration tested. Therefore, **III.4.3** is not a potential antibacterial molecule.

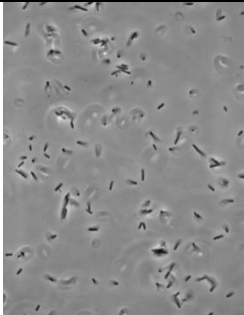
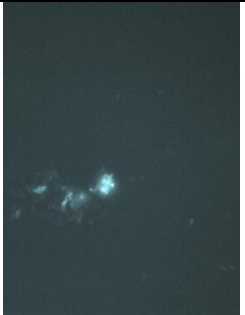
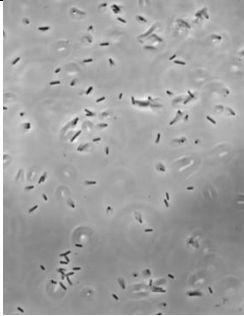
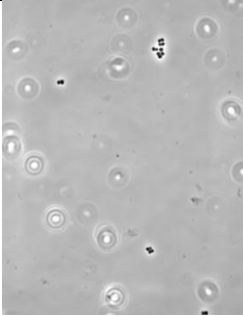
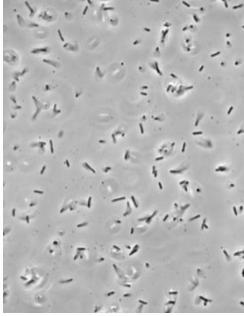
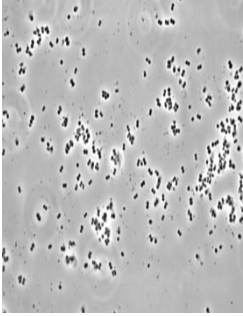
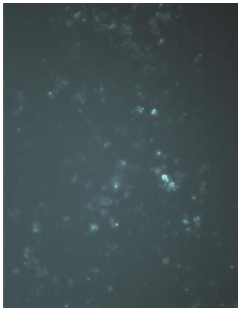
d) New MGBs series				
	<i>E. coli</i>		<i>Staph. aureus</i>	
	Brightfield	Fluorescence	Brightfield	Fluorescence
III.5.4				
III.5.5				
III.5.3				

Table 6. Fluorescence of new MGBs under Brightfield and DAPI filters in the presence of Gram positive and Gram negative bacteria.

Molecule **III.5.4** is the only one of this series which does not accumulate in Gram negative bacteria. And the results from the bacterial assays show that no toxicity is observed (see section C.II.2). However, **III.5.4** accumulates extremely well into *Staph. aureus* since the fluorescence is almost as good as DAPI. Nevertheless, this molecule does not show any antibacterial effect against this organism.

Molecules **III.5.3** and **III.5.5** penetrate into both types of bacteria, and **III.5.5** accumulates the most in *Staph. aureus*. However, the curves obtained from the bacterial assays (see

section C.II.2) suggest no toxicity below 20 µg/ml for both **III.5.3** and **III.5.5**. These two molecules do not have antibacterial properties despite their good accumulation into both bacterial strains tested.

e) Conclusion

All microscopy pictures show a more intense fluorescence in *Staph. aureus* than in *E. coli*, and this is due to easier accumulation of MGBs into two layered cells than three layered cells.

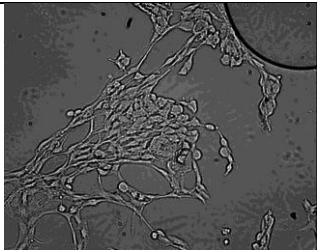
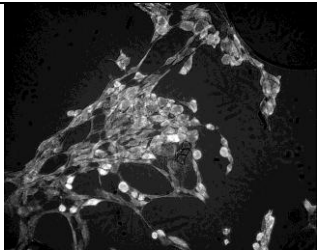
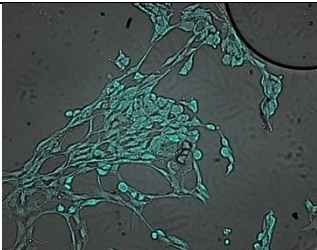
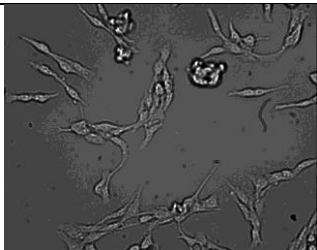
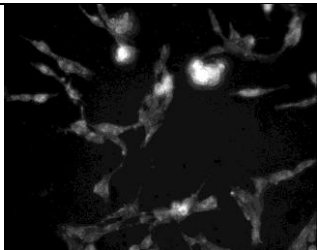
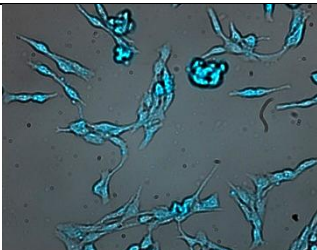
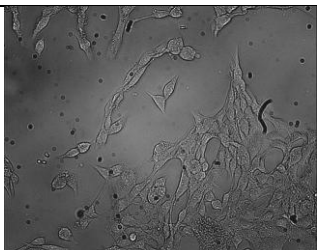
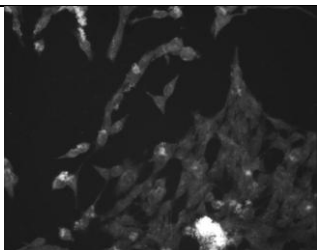
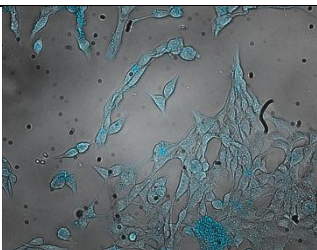
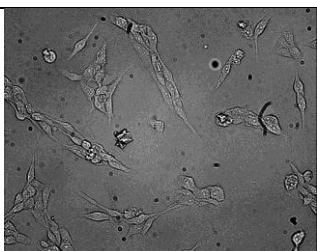
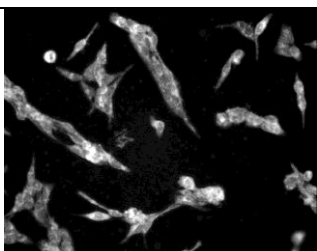
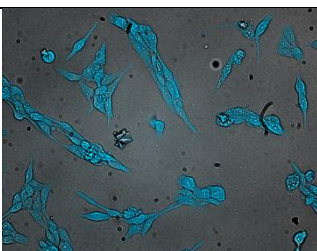
Molecules **III.4.3** (Boc tail group), **III.5.3** (cyano alkene) and **III.5.5** (nitro alkene) show accumulation in both bacteria without showing any toxicity. Only molecule **IV.3** accumulates in both types of bacteria and inhibits them from growing. This molecule bearing a tertiary alkyl amine and (*E*)-3-(4-methylstyryl)quinoline) definitely shows anti-bacterial properties, and the microscopy assays realized with mammalian cells will enable us to make conclusions about its potential anti-cancer activity if it binds to DNA. Accumulation of MGBs in *E. coli* had never been observed in previous microscopy assays.

Molecules **IV.2** and **IV.4**, bearing the tertiary alkyl amine tail group, and molecules **IV.7** and **IV.6**, bearing the morpholine tail group, but all having different head group, accumulate only in one type of Gram positive bacteria and show toxicity, whereas **III.5.4** (guanidine tail group) and **III.4.4** (acetate) penetrate into *Staph. aureus* without being toxic. The first four molecules show selective anti-bacterial activity against Gram positive bacteria.

IV.1 has no effect on both bacteria studied. Since it does not accumulate, its toxicity cannot be assessed, hence the lack of toxicity observed during bacteria assays.

2. Mammalian cells

a) *Tertiary alkyl amine tail group series*

	Brightfield	Fluorescence	Overlay
D A P I			
IV.2			
IV.3			
IV.4			
<p>Table 7. Fluorescence of the tertiary alkyl amine series under Brightfield and DAPI filters in the presence of V79 mammalian cells.</p>			

These molecules are less fluorescent than DAPI, except **IV.4** which is comparable. Nevertheless these pictures suggest the accumulation of the tertiary alkyl amine molecules series in V79 mammalian cells, however they do not reach the nucleus.

Molecule **IV.3** apparently has more difficulties permeating the cells since its accumulation, seen by fluorescence, is weaker. However in this series, **IV.3** is the only molecule that showed toxicity against this mammalian cell line at a concentration below 20 µg/ml.

b) Morpholine tail group series

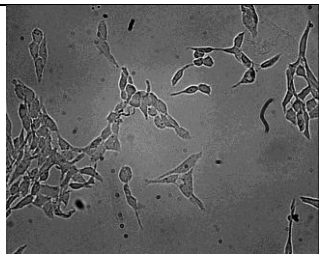
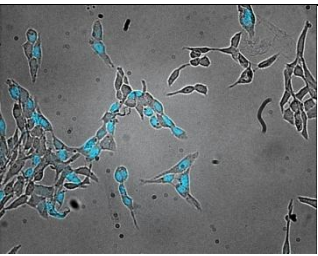
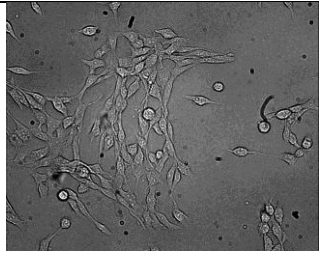
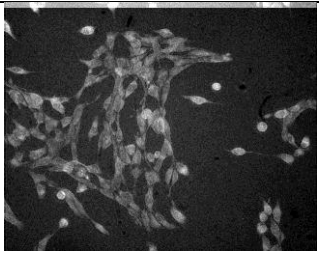
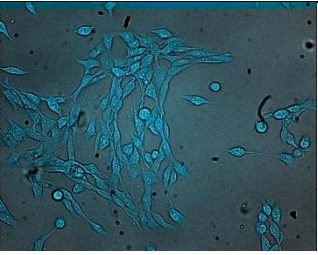
	Brightfield	Fluorescence	Overlay
IV.7			
IV.6			

Table 8. Fluorescence of morpholine tail group series under Brightfield and DAPI filters in the presence of V79 mammalian cells.

This series definitely accumulates into the V79 hamster cell line. However, the fluorescence stain indicates a slight difference in permeation of those two molecules. **IV.6** permeates the cell membrane and seems to reach the nucleus without accumulating into it as much as **IV.7** does. To confirm the conclusion drawn, pictures (Figure 41) at a bigger magnification (x 40 instead of x 20) were taken and are shown below:

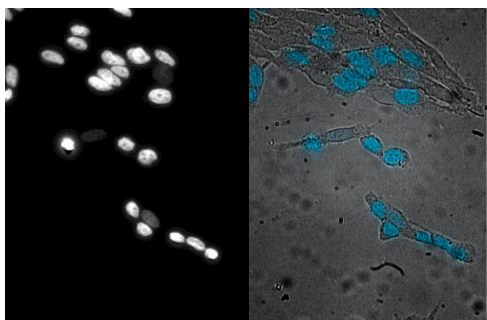


Figure 41. MGB **IV.7** in nucleus of V79 mammalian cells
Magnification X40

No molecule of this series was toxic against V79 hamster cell line below a concentration of 20 $\mu\text{g/mL}$. These two molecules could possibly bind to DNA located in the nucleus and act as anti-cancer drugs.

c) *Intermediates and new MGBs*

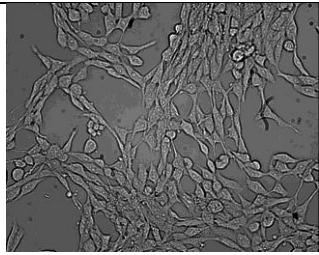
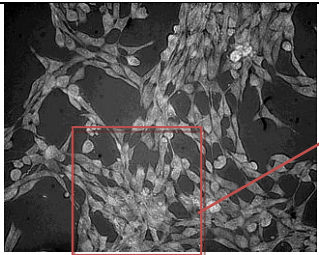
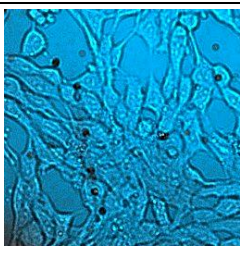
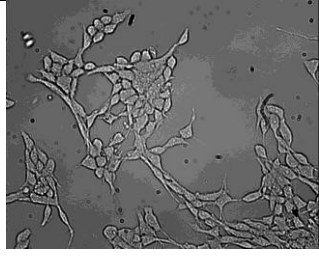
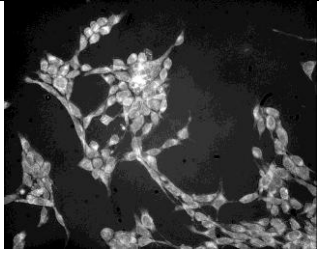
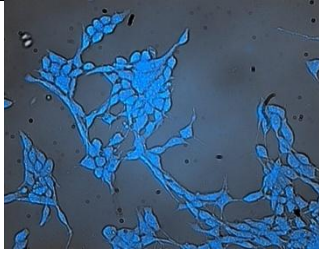
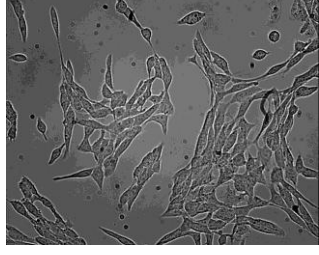
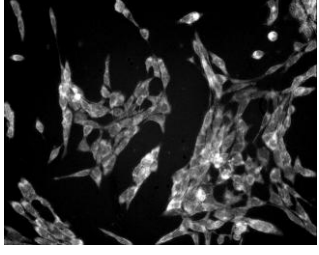
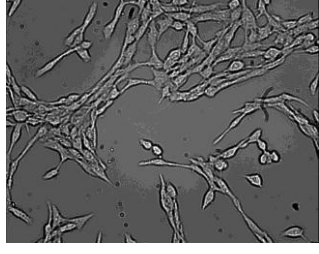
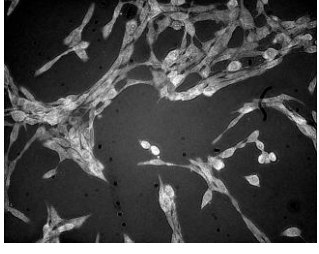
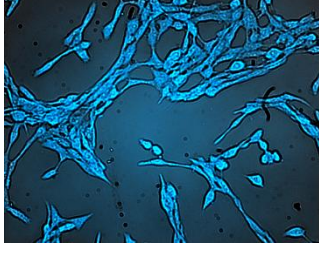
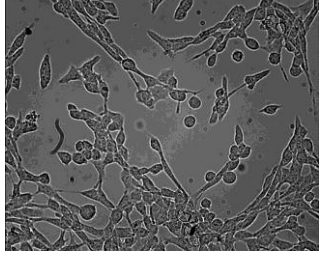
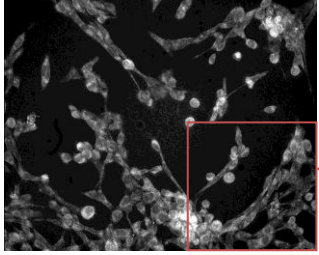
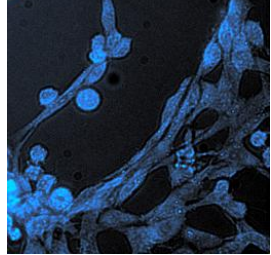
	Brightfield	Fluorescence	Overlay
III.5.6			
III.4.4			
III.5.5			
III.5.3			
III.5.4			

Table 9. Fluorescence of intermediate and new MGBs under Brightfield and DAPI filters in the presence of V79 mammalian cells.

All intermediate MGBs and new MGBs seen under microscopy accumulate in V79 cells but without reaching the nucleus. However different patterns of accumulation can be seen.

Molecules **III.5.6** and **III.4.4** permeate the cell membrane but sit outside the nucleus, while **III.5.4** accumulates around the nucleus without penetrating inside. MGB **III.5.5** accumulates everywhere except in the nucleus; it is anti-nuclear as shown by the pictures below (Figure 42) taken at a higher magnification; the molecule accumulates everywhere opposite the nucleus:

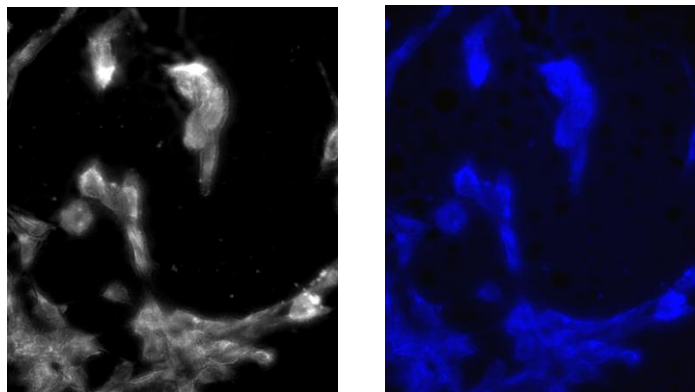


Figure 42. MGB **III.5.5** fluorescent everywhere but in the nucleus of V79 mammalian cells
Magnification X40.

These molecules are not toxic below a concentration of 50 $\mu\text{g}/\text{ml}$.

In comparison, molecule **III.5.3** permeates the cell and reaches the nucleus of V79 mammalian cells, without showing any toxicity below 50 $\mu\text{g}/\text{ml}$. **III.5.3** carries the same head group, the (*E*)-4-(3-methoxystyryl)benzamide, as other new MGBs and intermediates, only the tail group differs. This (*E*)-4-(3-methoxystyryl)benzamide head group seems to give **III.5.3** the right chemical properties to permeate the cell to the nucleus.

3. Conclusion

These pictures show important results regarding MGBs tested. It seems that they could act as potential anti-cancer drugs since several appeared to reach the cell nucleus and could then bind to DNA. The molecules that could have anti-cancer effect are molecules **IV.7**, **IV.6**, both having a morpholine tail group and, respectively, the (*E*)-4-(2-(quinolin-3-yl)vinyl)benzamide and (*E*)-3-(3-methoxystyryl)benzamide feature, and **III.5.3**, which bears the (*E*)-4-(3-methoxystyryl)benzamide and cyano alkene tail group. These molecules do not show any toxicity against V79 fibroblast hamster cells. To demonstrate this possibility would require assays against specific cancer cell lines of interest.

MGBs **IV.7** and **IV.6**, which have the morpholine tail group feature but different head groups, permeated Gram positive bacteria and appeared toxic towards them. However, they

did not accumulate in Gram negative bacteria and showed no toxicity to V79 cells. Hence those two molecules have a selective anti-bacterial effect and are also potential anti-cancer drugs since they penetrate into the nucleus and bind hypothetically to DNA.

In comparison, **III.5.3** (cyano alkene structural feature) accumulated into the nucleus without showing toxicity against V79 mammalian cells. On the other hand it also accumulated in both types of Gram bacteria without being toxic below 20 µg/ml. **III.5.3** could then bind to DNA and act as an anti-cancer molecule without showing any anti-bacterial activity. Structures **III.4.3** (Boc tail group), **III.4.4** (acetate feature), **III.5.4** (guanidine tail group), **III.5.5** (nitro alkene feature) and **III.5.6** (primary alcohol feature) accumulate in cells without reaching the nucleus. Considering the fact that the tail group is the only variable feature in these MGB structures, we could say that the cyano tail group with a pK_a below 0 is the best feature for a potential anti-cancer molecule.

Molecules containing the tertiary alkyl amine feature accumulate in Gram positive bacteria and are toxic towards them but do not reach the V79 cell nucleus. However **IV.3**, bearing the (*E*)-4-(2-(quinolin-3-yl)vinyl)benzamide head group, is the only molecule which is toxic towards V79 mammalian cells, *E. coli* (Gram negative bacteria) and *Staph. aureus* (Gram positive bacteria). This molecule has anti-bacterial properties.

The intermediate MGBs **III.4.4** (which has the acetate protected feature) and **III.5.6** (bearing the primary alcohol tail group) permeate V79 cell membranes and accumulate in Gram positive bacteria without being significantly toxic below 20µg/ml. They do not enter into Gram negative bacteria; hence the lack of toxicity. In comparison, **III.4.3** (Boc protected tail group) penetrates into Gram negative bacteria as well but does not have toxic activity. These three intermediate MGBs do not have any anti-bacterial properties.

MGB **IV.1** ((*E*)-4-(2-(quinolin-3-yl)vinyl)benzamide and guanidine) does not have any anti-bacterial properties, justified by a lack of permeation into either bacterial strains studied. Though microscopy pictures have not been taken, **IV.1** is not toxic against the V79 mammalian cell line.

Molecule **III.5.4**, bearing the guanidine feature, has no anti-bacterial effect and is not cytotoxic. It accumulates both in Gram positive bacteria and V79 mammalian cells. However, it sits outside the nucleus, whereas **III.5.5** (which has the nitro alkene tail group) is anti nuclear and penetrates into *E. coli* without being toxic. Molecules **III.5.4** and **III.5.5** cannot act as potential anti-cancer compounds by the same mechanism as the other MGBs since they do not reach the nucleus and cannot bind to DNA. Furthermore they do not have anti-bacteria activity.

D. Discussion

This discussion should allow to understand the relationship between tail group structure, cell penetration, and biological activity and selectivity. Table 10 below sums up the structural features and biological results.

	Structural features			<i>E. coli</i> (Gram -)	<i>Staph. aureus</i> (Gram +)	V79 fibroblast hamster cells
	Head group	Tail group	pKa tail group	Permeation and toxicity	Permeation and toxicity	Permeation and toxicity
IV.2	(<i>E</i>)-4-(3-methoxystyryl)benzamide	<i>t</i> -amine	9.99	no none	yes 5-7 µg/mL	not nuclear > 20 µg/mL
IV.3	(<i>E</i>)-4-(2-(quinolin-3-yl)vinyl)benzamide	<i>t</i> -amine	9.99	yes ≥ 20 µg/ml	yes 1-2 µg/mL	not nuclear > 5 µg/mL
IV.4	(<i>E</i>)-3-(3-methoxystyryl)benzamide	<i>t</i> -amine	9.99	no none	yes ≥ 20 µg/mL	not nuclear none
IV.5	(<i>E</i>)-4-(3-methoxystyryl)benzamide	morpholine	7.41	no none	no 0.5 µg/mL	not done > 20 µg/mL
IV.7	(<i>E</i>)-4-(2-(quinolin-3-yl)vinyl)benzamide	morpholine	7.41	no none	yes 7-10 µg/mL	nuclear only none
IV.6	(<i>E</i>)-3-(3-methoxystyryl)benzamide	morpholine	7.41	no none	yes ≥ 20 µg/mL	throughout the cell, nucleus included > 20 µg/mL
III.5.3	(<i>E</i>)-4-(3-methoxystyryl)benzamide	cyano <i>N</i> -alkene	<-5	yes none	yes none	nuclear none
III.5.4	(<i>E</i>)-4-(3-methoxystyryl)benzamide	guanidine	12	no none	yes none	around nucleus only none
...

	Structural features			<i>E. coli</i> (Gram -)	<i>Staph. aureus</i> (Gram +)	V79 fibroblast hamster cells
	Head group	Tail group	pKa tail group	Permeation and toxicity	Permeation and toxicity	Permeation and toxicity
III.5.5	(<i>E</i>)-4-(3-methoxystyryl)benzamide	nitro alkene	<1	yes none	yes none	anti-nuclear none
III.4.3	(<i>E</i>)-4-(3-methoxystyryl)benzamide	<i>N</i> -boc	15	yes none	yes none	not done none
III.4.4	(<i>E</i>)-4-(3-methoxystyryl)benzamide	<i>O</i> -acetate	3	no none	yes none	not nuclear none
III.5.6	(<i>E</i>)-4-(3-methoxystyryl)benzamide	OH	15	no none	≥ 20 µg/mL	not nuclear none
IV.1	(<i>E</i>)-4-(3-methoxystyryl)benzamide	guanidine	12	no none	no none	not done none

Table 10. Structural features and biological results.

Looking at the molecules containing the same head group but different tail group, the compounds tested can be arranged in three families.

The members of the (*E*)-4-(3-methoxystyryl)benzamide head group family (**IV.2**, **IV.5**, **III.4.3**, **III.4.4**, **III.5.3**, **III.5.4**, **III.5.5**, **III.5.6**) have different permeability into *E. coli* but are not toxic even if they permeate the cells (**III.4.3**, **III.5.3**, **III.5.5**). All of these compounds accumulate in *Staph. aureus* cells but only **IV.5** shows significant toxicity, while **IV.2** has low antibacterial activity. Furthermore all the compounds except **III.5.3** permeate the V79 wall without reaching the nucleus and without being significantly toxic. The permeation into both V79 cells and bacteria can then be linked to the tail group in the case of Gram negative bacteria and V79 mammalian cells. The pK_as of the tail groups in this series of compounds vary from -5 to 15, allowing a hypothesis to be proposed on the range of tail group pK_a needed for a molecule to reach DNA without being toxic. The cyano *N*-alkene tail group (**III.5.3**), with the lowest pK_a (<-5), seems to have the best structural features as a potential anti-cancer activity. However, it has no anti-bacterial activity. Structure **III.5.4** contains a guanidine tail group and is the only member of this family which does not

accumulate in Gram negative bacteria, probably because it is highly charged at physiological pH. In comparison with other tail groups, the tertiary amine (**IV.2**, $pK_a = 9.99$) and the morpholine (**IV.5**, $pK_a = 7.41$) bring the highest toxicity towards both Gram negative and V79 mammalian cells.

If molecules are ranked according to their tail group, Table 10 suggests that those with a tertiary amine tail group ($pK_a = 9.99$, **IV.2**, **IV.3**, **IV.4**) are more toxic towards both *Staph. aureus* and V79 hamster cells, than those with a morpholine tail group (**IV.5**, **IV.7**, **IV.6**), pK_a of 7.41, which is much less basic. This could be explained by the predominant species of these compounds at physiological pH. The guanidine tail group is more basic ($pK_a = 12$), and does not show any cytotoxicity or anti-bacterial activity. This can be explained biologically by the fact that at physiological pH (7), the predominant chemical form of these three tail groups is the protonated one. Only the morpholine tail group is likely to be present in both the protonated and unprotonated form since its pK_a is close to the physiological pH. Nevertheless no range of pK_a can be determined for toxicity against V79 mammalian cells since both the morpholine and the guanidine tail groups - having respectively a lower pK_a and higher pK_a than the tertiary amine tail group - do not show any cytotoxicity towards such cells.

The molecules with the (*E*)-4-(2-(quinolin-3-yl)vinyl)benzamide head group (**IV.3**, **IV.7** and **IV.1**) show more toxicity than those with (*E*)-4-(3-methoxystyryl)benzamide head group. They have different permeability into bacterial and V79 cells. The molecule bearing the tertiary amine tail group (**IV.3**, $pK_a = 9.99$) has the highest toxicity. Molecule **IV.7**, carrying the morpholine tail group, with a pK_a of 7.41, is the only molecule in this family that could show potential anti-cancer activity. Furthermore it is also selective towards Gram positive bacteria, although its antibacterial activity was found to be weaker than that of **IV.5**.

Structures with the (*E*)-3-(3-methoxystyryl)benzamide head group (**IV.4** and **IV.6**) have the same penetration behaviour into bacteria, and show poor antibacterial activity against *Staph. aureus*. However **IV.6** bearing the morpholine tail group permeated V79 mammalian cells up to the nucleus without significant cytotoxicity, whereas **IV.4** does not reach the nucleus, hence the lack of toxicity. This implies that **IV.6** contains the best features for permeation, probably due to the pK_a of the morpholine tail group, which should appear in two different forms at physiological pH.

Molecules bearing of the tertiary alkyl amine tail group differ from each other in their head groups. All those molecules penetrated into *Staph. aureus* and into V79 hamster cells, however they did not reach the nucleus. Since only the head group differs, the only structural

feature that could explain the cell permeation into the cytosol is the tertiary amine tail group, which is protonated at physiological pH, and would prevent the molecule from entering into the nucleus. These data also suggest that the molecule carrying the (*E*)-4-(2-(quinolin-3-yl)vinyl)benzamide head group (**IV.3**), accumulates into both V79 cells and Gram bacteria, has the most anti-bacterial activity against both Gram positive and negative bacteria and is the more cytotoxic towards V79 cells. In comparison, the molecules (*E*)-1-methoxy-3-styrylbenzene head groups (**IV.2**, **IV.4**) attached at different position to the pyrrole-pyrrole core show similar permeation and similar toxicity for all types of cells and bacteria. However the (*E*)-1-methoxy-3-styrylbenzene, at the para position to the rest of the molecule (**IV.2**), shows higher toxicity towards both *Staph. aureus* and V79 cells, in comparison with the one attached at the meta position (**IV.4**). While the tertiary amine tail group is connected with the toxicity, as proved earlier, the head group enables the permeation and is associated with selective anti-bacterial activity.

Molecules with the morpholine tail group are less toxic than molecules bearing a tertiary amine, and accumulate similarly into both types of bacteria and V79 mammalian cells, except **IV.5** which does not seem to penetrate into Gram positive bacteria yet shows the highest anti-bacterial activity against this type of bacteria (*Staph. aureus*). These results are not confusing, the high toxicity suggests the penetration of **IV.5** into Gram positive bacteria, but no accumulation was seen. A handling error during the antibacterial assay probably occurred. An excess of DMSO added to the bacteria could have been responsible for their death. The high toxicity observed during the assays is then probably related to this excess of DMSO and not to the anti-bacterial effect of **IV.5**. Moreover, according to the results, **IV.5** is the only molecule bearing the (*E*)-4-(3-methoxystyryl)benzamide head group and the morpholine tail group which does not permeate into Gram positive bacteria. So it can be assumed that the results from the microscopy assay were not reliable in this case, and accumulation should have been seen. Molecules containing the morpholine tail group are selective antibacterial agents showing different levels of toxicity.

Molecules with the guanidine tail group (**III.5.4**, **IV.1**) did not show any cytotoxicity or any anti-bacterial activity. They did not penetrate Gram negative cells, and a comparison with V79 cell permeation cannot be made. However, the fact that **III.5.4** did not penetrate the nucleus and that the tail group is responsible for better cell permeability, suggests that **IV.1** is unlikely to reach the nucleus either. Furthermore, looking at the permeation of other MGBs containing the same head groups, no hypothesis can be put forward. Regarding the lack of toxicity, it is interesting to notice that **III.5.4** and **IV.1** contained respectively the (*E*)-4-(3-methoxystyryl)benzamide and the (*E*)-4-(2-(quinolin-3-yl)vinyl)benzamide head

groups, which are the most likely to show toxicity according to the data for structures containing the tertiary alkyl amine tail group. However, it was stated earlier that this toxicity is more probably associated with the tertiary amine tail group. The guanidine tail group is fully protonated at physiological pH, so it can be assumed that an active transport mechanism is required, allowing the corresponding molecules to be taken up into V79 mammalian cells.

E. Conclusion and Future work

The results obtained from the synthetic work and biological assays do not allow us to make any conclusions on whether any particular range of pK_a of tail group is beneficial for anti-cancer activity. The anti-bacterial activity or cytotoxicity of a MGB depends on many structural factors and not just one structural feature. However, the results obtained confirm that the tertiary amine tail group is connected with the highest toxicity whichever head group is carried. The only molecule synthesized that could have anti-cancer activity if binding with DNA is structure **III.5.3**; however, it has no anti-bacterial activity. MGBs containing an *E*-alkene head group is known to have the most significant anti-bacterial activity ^[52], nevertheless the new MGBs synthesized in this project containing this head group were poor anti-bacterial molecules, a result that could possibly be associated with their novel, non-basic tail groups.

The permeation of MGBs into *E. coli* has never been seen before; however no significant toxicity was shown. Permeation into Gram positive cells seemed to be easier for almost all of the MGBs tested than permeation into Gram negative cells. This can be simply due to the different structure of the bacterial cell wall in Gram positive and Gram negative bacteria and the difference in thickness of the peptidoglycan layer.

Different transport mechanisms are probably implied in cell permeation: an active transport for a highly protonated and hydrophilic molecule like **III.5.4** or a passive transport for molecules that are hydrophobic enough to permeate cell membranes.

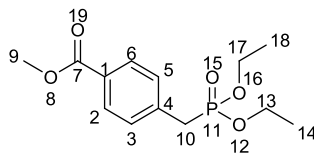
Further work requires to be done in order to understand exactly the chemical properties needed at the head group and the tail group of MBG molecules in order to get potential anti-cancer or selective anti-bacterial molecules. If penetration into the nucleus and eventual binding with DNA occurs, the strength of the bond with DNA could be investigated by measuring the melting temperature (T_m). In the short term, MGBs with oxetane tail groups could be synthesized and tested since the molecular modeling did not show any incompatibility with DNA.

F. Experimental

I. Chemistry Procedures

1. Preparation of (E)-4-(3-methoxystyryl)benzoic acid

a) First step: formation of methyl 4-[(diethoxyphosphoryl)methyl]benzoate **I.2.2**

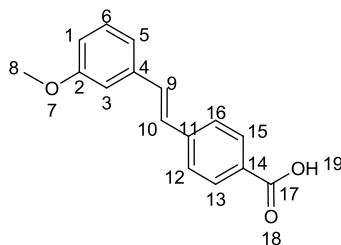


A mixture of methyl 4-(bromomethyl)benzoate (2.515 g, 11.00 mmol) and triethylphosphite (3.80 mL, 22.16 mmol) was heated under reflux under N₂ (g) for 2 h. The excess of triethylphosphite was removed under high vacuum to give a pale yellow oil (3.168 g, 11.07 mmol, not totally dry).

¹H NMR (DMSO-d₆): δ^H ppm

7.90 (2H, d, *J* = 8.0 Hz, 2 x aromatic CH² ⁶); 7.43 (2H, dd, *J* = 2.5 Hz and 8.5 Hz, 2x aromatic CH³ ⁵); 3.94 (4H, m, 2 x CH₂ ¹³ ¹⁷); 3.8 (3H, s, CH₃ ⁹); 3.36 and 3.31 (2H, 2s, CH₂ ¹⁰); 1.16 (6H, t, *J* = 7.00 Hz, 2 x CH₃ ¹⁸ ¹⁴).

b) Second step: formation of (E)-4-(3-methoxystyryl)benzoic acid **I.3**



To a solution of methyl 4-[(diethoxyphosphoryl)methyl]benzoate (3.106 g, 10.85 mmol) in THF (10 mL) under N₂ (g) was added NaH (0.711 g, 19.72 mmol, 60%). After cooling the reaction mixture to 0°C, m-anisaldehyde (1.5 mL, 12.3 mmol) in 16 mL of dry THF was added dropwise while stirring. The reaction mixture was stirred for 1 h 30 min and then quenched with water and neutralized with dilute HCl (1:3) until the pH became acidic. The organic layer was separated with ethyl acetate and the solvent was evaporated under vacuum to give an orange oil.

This oil (0.834 g, 3.10 mmol) was directly mixed with ethanol (10 mL). NaOH (0.872 g, 21.8 mmol) in water (20 mL) was added, and the solution was heated to reflux for 3 h. Dilute

HCl (1:3) was added dropwise, at 0°C, until the pH became acidic and gave a white solid. The solid was filtered on Büchner funnel and washed with water (0.461 g, 1.81 mmol).

Yield: 92%

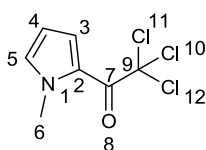
LCMS: found 253.07 g.mol⁻¹ (M-H) calculated for C₁₆H₁₄O₃, 254.29.

¹H NMR (DMSO-d₆): δ^H ppm

12.80 (1H, broad s, OH), 7.93 (2H, d, *J* = 8.40 Hz, CH^{13 15}), 7.71 (2H, d, *J* = 8.40 Hz, CH^{12 16}), 7.38 (1H, d, *J* = 16.5 Hz, H⁹), 7.33 (1H, d, *J* = 16.5 Hz, H¹⁰), 7.28 (1H, m, H³), 7.21 (2H, m, H^{1 5}), 6.87 (1H, m, H⁶), 3.80 (1H, s, CH₃⁸).

IR (KBr): 3065 to 2566; 1673 (C=O); 1598; 1432, 1318; 1281; 1244; 1185; 1040; 947; 851; 773 cm⁻¹.

2. Preparation of 2-trichloroacetyl-N-methylpyrrole III.1.2 ^[70]



Trichloroacetyl chloride (20 mL, 178.2 mmol) and DCM (86 mL) were mixed in a round bottomed flask under nitrogen, to exclude H₂O and prevent the formation of the carboxylic acid. A solution of *N*-methylpyrrole (16 mL, 180.3 mmol) in DCM (50 mL) was added drop wise over 1.50 hour to the mixture. The solution turned from yellow to orange then dark brown. The solution was stirred overnight. The compound was filtered on a silica gel column. The red colour impurities stuck to the silica gel while a yellow compound was eluted slowly with DCM. Once the yellow product was filtered, the DCM was evaporated under vacuum to recover orange-yellowish crystals (33.30 mg, 147.04 mmol).

Yield: 83 %

¹H NMR (DMSO-d₆): δ^H ppm

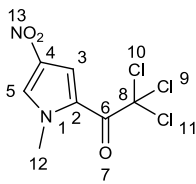
7.43 (1H, m, *J* = 2.0 & 4.4 Hz, H^{5 3}), 6.29 (1H, dd, *J* = 2.4 and 4.0 Hz, H⁴), 3.91 (3H, s, N-CH₃).

¹³C NMR (DMSO-d₆): δ^C ppm

38.44 (C⁶); 98.12 (C⁹), 109.61 (C³); 121.18 (C²); 124.19 (C⁴); 135.81 (C⁵); 172.35 (C⁷).

Melting Point: 63-66 °C (Lit. = 64-65 °C) ^[70]

3. Preparation of 2,2,2-trichloro-1-(1-methyl-4-nitro-1H-pyrrol-2-yl)ethanone
III.1.3^[71]



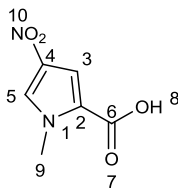
To acetic anhydride (35.00 mL) was added dropwise 70% nitric acid (6.00 mL) at -25°C (carbon dioxide dry ice dropped into acetone). The solution was stirred for 30 min. This solution was then added drop wise to 2-trichloroacetyl-*N*-methylpyrrole (5.098 g, 22.81 mmol) dissolved in acetic anhydride (24.7 mL) at -27 °C. The solution became thick so a further portion of acetic anhydride (3.0 mL) was added. A yellowish white solid precipitated and the mixture was allowed to return to RT while stirring over 40 min. The precipitate dissolved to give a bright yellow solution, which was then cooled down at -40 °C. At this temperature, water (30 mL) was added to allow the precipitation of a white solid. The temperature of the solution was allowed to rise to 0 °C. The precipitate was filtered on a Büchner funnel, washed with water (2 x 5 mL) and hexane (15 mL). A bright yellow powder was recovered (4.535 g, 16.70 mmol).

Yield: 73%

¹H NMR (DMSO-*d*₆): δ^H ppm
8.55 (1H, d, *J* = 1.6 Hz, H⁵); 7.79 (1H, d, *J* = 1.6 Hz, H³); 3.99 (3H, s, N-CH₃).

Melting Point: 135-139 °C (Lit. = 135-140 °C)^[71]

4. Preparation of 1-methyl-4-nitro-1H-pyrrole-2-carboxylic acid **III.1.4**^[70]



To a solution of 2,2,2-trichloro-1-(1-methyl-4-nitro-1H-pyrrol-2-yl)ethanone (**III.1.3**, 1.07 g, 3.94 mmol) dissolved in EtOH (6 mL) was added NaOH (0.320 g) in water. The solution was heated to reflux for 1 h 15 min and then cooled to 0°C in an ice bath and water (10 mL) was added. The solution was acidified by diluted hydrochloric acid (1:3). The product was

filtered and washed with water and hexane. An off-white product was recovered (0.561 g, 3.32 mmol).

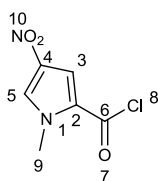
Yield: 89%

¹H NMR (DMSO-*d*₆): δ^H ppm
8.04 (1H, d, $J = 2.0$ Hz, H⁵), 7.08 (1H, d, $J = 2.0$ Hz, H³), 3.91 (3H, s, N-CH₃).

IR (KBr): 3551 to 2549 (pyrrole ring); 3141; 1698 (C=O); 1421; 1313 (NO₂), 1256; 756 cm⁻¹.

Melting point: 209-210 °C (Lit. = 199-199.5 °C) ^[70]

5. Preparation of 1-methyl-4-nitro-1H-pyrrole-2-carbonyl chloride III.1.5 ^[70]



Method 1. To 1-methyl-4-nitro-1H-pyrrole-2-carboxylic acid (1.408 g, 8.27 mmol) was added thionyl chloride (20 mL). The solution was heated to reflux under N₂ for 2 h 20 min. The solvent was evaporated under vacuum to give a brown solid (0.617 g, 3.27 mmol).

Yield: 88 %

Method 2. 1-Methyl-4-nitro-1H-pyrrole-2-carboxylic acid (0.240 g, 1.41 mmol) was dissolved in anhydrous DMF (2 mL) under N₂, and 1-chloro-*N,N*,2-trimethylpropenylamine (Ghosez's reagent, 245 μ L, 1.85 mmol, 1.31 eq) was added. The solution was stirred at RT for 5 h 20 min. The solvent was evaporated under high vacuum to give an off-white solid (0.226 g, 1.20 mmol). The NMR showed that the Ghosez's reagent was totally removed.

Yield: 85 %

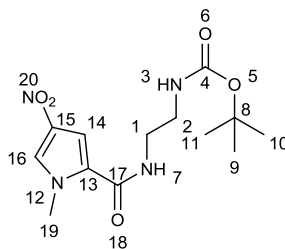
¹H NMR (DMSO-*d*₆): δ^H ppm
8.21 (1H, d, $J = 2.0$ Hz, H⁵), 7.25 (1H, d, $J = 2.0$ Hz, H³), 3.91 (3H, s, N-CH₃).

¹³C NMR (DMSO-*d*₆): δ^C ppm
37.95 (C⁹); 111.87 (C³); 124.23 (C⁵); 129.66 (C⁴); 134.49 (C²); 161.37 (C⁶).

IR (KBr): 3425; 3127; 1743 (C=O); 1493; 1403, 1333 (NO₂); 844 cm⁻¹.

Melting Point: 92-93 °C (Lit. = 91-92 °C) ^[70]

6. Preparation of *t*-butyl 2{[(1-methyl-4-nitro-1*H*-pyrrol-2-yl)carbonyl]amine}ethylcarbamate III.2.1 ^[72]



To a solution of 2,2,2-trichloro-1-(1-methyl-4-nitro-1*H*-pyrrol-2-yl)ethanone (0.600 g, 2.21 mmol) dissolved in DCM (15 mL) was added a solution of *N*-*boc*-ethylenediamine (354 μ L, 2.24 mmol) in DCM (5 mL). 1 h 17 min later the TLC showed that the reaction was not yet completed, but there was no more *N*-*boc*-ethylenediamine to add. Some white solid precipitated, so the solution was filtered on a Büchner funnel, and a white bright solid was recovered (0.333 g, 1.07 mmol).

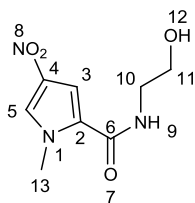
Yield: 48%

¹H NMR (DMSO-*d*₆): δ^H ppm

8.36 (1H, t, $J = 5.3$ Hz, NH⁷); 8.10 (1H, d, $J = 1.5$ Hz, Ar-H¹⁶); 7.39 (1H, d, $J = 1.5$ Hz, Ar-H¹⁴), 6.87 (1H, t, $J = 5.5$ Hz, NH³), 3.88 (3H, s, NCH₃, H¹⁹), 3.22 (2H, q, $J = 6.2$ Hz, CH₂²), 3.07 (2H, q, $J = 6.2$ Hz, CH₂¹), 1.36 (9H, s, 3(CH₃)^{9 10 11}).

Melting Point: 185-187 °C (Lit. = 158-164 °C) ^[72]

7. Preparation of the *N*-(2-hydroxyethyl)-1-methyl-4-nitro-1*H*-pyrrole-2-carboxamide III.2.2 ^[73]



To a solution of 2,2,2-trichloro-1-(1-methyl-4-nitro-1*H*-pyrrol-2-yl)ethanone (2.181 g, 8.03 mmol) dissolved in DCM (20 mL) was added a solution of ethanolamine (490 μ L, 8.12 mmol) in DCM (6 mL). The solution was stirred for 3 hours and the solution was then filtered to recover a yellow solid (1.542 g, 7.23 mmol) which was recrystallised from ethanol to give the required product (1.042 g, 4.89 mmol).

Yield: 72%

¹H NMR (DMSO-*d*₆): δ^H ppm

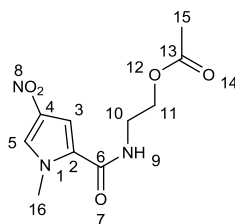
8.37 (1H, t, *J* = 5.5 Hz, NH⁹); 8.10 (1H, d, *J* = 1.5 Hz, H⁵); 7.44 (1H, d, *J* = 1.45 Hz, H³), 4.68 (1H, s, O-H¹²); 3.89 (3H, s, N-CH₃¹³), 3.47 (2H, q, *J* = 6.0 Hz, CH₂¹¹); 3.25 (2H, q, *J* = 6.0 Hz, CH₂¹⁰).

¹³C NMR (DMSO-*d*₆): δ^C ppm

37.81 (C¹³); 42.05 (C¹⁰); 60.09 (C¹¹); 107.82 (C³); 126.97 (C²); 128.23 (C⁵); 134.22 (C⁴); 160.40 (C⁶).

Melting Point: 152-155 °C (Lit. = 158-160 °C) ^[73]

8. Preparation of 2-[[[1-methyl-4-nitro-1H-pyrrol-2-yl)carbonyl]amino]ethyl acetate III.2.3 ^[73]



To a solution of *N*-(2-hydroxyethyl)-1-methyl-4-nitro-1*H*-pyrrole-2-carboxamide (1.698 g, 7.97 mmol) dissolved in dry DCM (16 mL) cooled to 0 °C, acetyl chloride (570 μL, 8.01 mmol), followed by distilled triethylamine (1.7 mL 11.94 mmol) were added. The solution was heated to reflux for 2 h 30 min then allowed to return to RT. The product (2.617 g) was first worked up using DCM and the organic layer was washed with water (3 x 20 mL) to remove the salt, then it was dried over MgSO₄. The solvent was evaporated under vacuum to give a pale yellow solid which was recrystallised from methanol and then purified by flash chromatography EtOAc/Hexane (1:2).

Yield: 81%

¹H NMR (DMSO-*d*₆): δ^H ppm

8.51 (1H, t, *J* = 5.6 Hz, NH⁹); 8.12 (1H, d, *J* = 2.00 Hz, H⁵); 7.41 (1H, d, *J* = 2.05 Hz, H³); 4.09 (2H, t, *J* = 5.7 Hz, CH₂¹¹); 3.89 (3H, s, NCH₃¹⁶); 3.42 (2H, q, *J* = 5.6 Hz, CH₂¹⁰); 2.00 (3H, s, CH₃¹⁵).

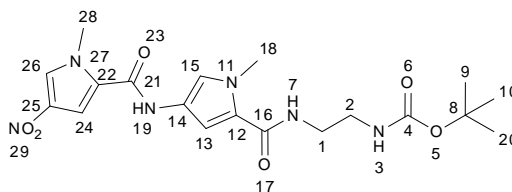
¹³C NMR (DMSO-*d*₆): δ^C ppm

21.15 (C¹⁵); 37.82 (C¹⁶); 38.25 (C¹⁰); 62.77 (C¹¹); 107.95 (C³); 126.65 (C²); 128.41 (C⁵); 134.25 (C⁴); 158.02 (C⁶); 160.53 (C¹³).

IR (KBR): 3401 (O=C-(N-H)); 3110 (aromatic CH); 2950 (CH₃); 1723 (O-(C=O)); 1659 (NH-(C=O)); 1524 (NO₂); 1308 cm⁻¹ (aromatic C-N).

Melting Point: 119-123°C (Lit. = 127-129 °C) ^[73]

9. Preparation of t-Butyl 2{[(1-methyl-4-[(1-methyl-4-nitro-1H-pyrrol-2-yl)carbonyl]amine)-1H-pyrrol-2-yl]carbonyl}amino}ethylcarbamate **III.3.3**
[74]



To a solution of t-butyl 2{[(1-methyl-4-nitro-1H-pyrrol-2-yl)carbonyl]amine}ethylcarbamate (0.672 g, 2.15 mmol) dissolved in MeOH (10 mL) was added slowly in an ice bath and under N₂, Pd/C (10%) (0.336 g). The solution was stirred under H₂ for 6 hours, then filtered on Kieselguhr (round bottom flask wrapped with aluminium foil) and the solvent removed under reduced pressure. A yellowish white solid is obtained **III.3.1**.

The residue **III.3.1** was dissolved in dry DMF (1.3 mL), and added to a stirred solution of 1-methyl-4-nitro-1H-pyrrole-2-carbonyl chloride (0.430 g, 2.28 mmol) and NEt₃ (390 μL, 2.81 mmol) in dry DCM (10 mL). The solution was stirred overnight. The mixture was then evaporated under vacuum to give a yellow oil which was taken up in DCM and washed with water (3 x 20 mL). The solvent was then evaporated under reduced pressure, and the residue was recrystallised from EtOAc to give the product **III.3.3** (0.235 g, 0.54 mmol).

Yield: 25%

¹H NMR (DMSO-d₆): δ^H ppm

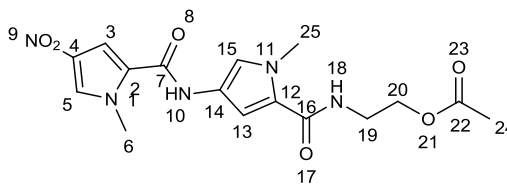
10.22 (1H, s, NH¹⁹); 8.16 (1H, d, *J* = 1.5 Hz, Ar-H¹⁵), 8.01 (1H, t, *J* = 5.0 Hz, NH⁷); 7.56 (1H, d, *J* = 1.5 Hz, Ar-H¹³); 7.19 (1H, s, *J* = 1.5 Hz, Ar-H²⁶); 6.84 (2H, s, NH³ and Ar-H²⁴); 3.94 ppm (3H, s, NCH₃²⁸); 3.80 (3H, s, NCH₃¹⁸); 3.20 (2H, q, *J* = 6.5 Hz, CH₂²); 3.05 (2H, q, *J* = 6.0 Hz, CH₂¹); 1.37 (9H, s, 3(CH₃)^{9 10 20}).

¹³C NMR (DMSO-d₆): δ^C ppm

28.71 (C^{9 10 20}); 36.50 (C^{28 18}); 37.92 (C^{1 2}); 78.12 (C⁸); 104.55 (C²⁴); 108.0 (C¹³); 118.52 (C¹⁴); 121.83 (C²⁶); 123.56 (C¹²); 126.78 (C²²); 128.66 (C¹⁵); 134.25 (C²⁵); 156.16 (C⁴); 157.33 (C¹⁶); 161.73 (C²¹).

IR (KBr): 3397 (O=C-(N-H)); 3132 (aromatic CH); 2976 (CH₃); 1712 (O-(C=O)); 1631 (NH-(C=O)); 1538 (NO₂); 1307 cm⁻¹ (aromatic C-N).

10. Preparation of 2{[(1-methyl-4-[[[(1-methyl-4-nitro-1H-pyrrol-2-yl)carbonyl]]-1H-pyrrol-2-yl)carbonyl]amino}ethyl acetate **III.3.4**



To a solution of 2{[(1-methyl-4-nitro-1H-pyrrol-2-yl)carbonyl]amino}ethyl acetate **III.2.3** (0.914 g, 3.58 mmol) dissolved in MeOH (25 mL), was added Pd/C (10%) (0.454 g) under nitrogen. Because the addition did not take place at 0 °C, a small flame occurred while adding the Pd/C. The solution was stirred for 7 h under H₂. It was then filtered on Kieselguhr and the solvent was removed under reduced pressure (round-bottom flask wrapped with aluminium foil). The residue **III.3.2** was dissolved in dry DMF (2 mL) and a stirred solution of NEt₃ (700 μL, 5.04 mmol) and 1-methyl-4-nitro-1H-pyrrole-2-carbonyl chloride (0.676 g, 3.58 mmol) dissolved in dry DCM (10 mL) was added. The solution was stirred overnight. The recrystallisation was undertaken with EtOAc to give the dimer as a yellow solid **III.3.4**, which was filtered and washed with hexane (0.932 g, 2.47 mmol).

Yield: 69%

LCMS: found 376 g.mol⁻¹ (M-1) calculated for C₁₆H₁₉N₅O₆, 377.35.

¹H NMR (DMSO-d₆): δ^H ppm

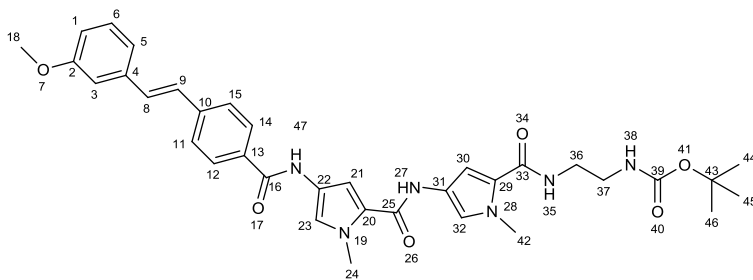
10.3 (1H, s, NH¹⁰); 8.17 (2H, d, *J* = 2.0 Hz, Ar-H¹⁵ and NH¹⁸); 7.61 (1H, d, *J* = 2.0 Hz, Ar-H¹³); 7.22 (1H, d, *J* = 2.0 Hz, Ar-H⁵); 6.87 (1H, d, *J* = 2.0 Hz, Ar-H³); 4.08 (2H, t, *J* = 5.8 Hz, CH₂²⁰); 3.95 (3H, s, NCH₃⁶); 3.80 (3H, s, NCH₃²⁵); 3.41 (2H, q, *J* = 5.8 Hz, CH₂¹⁹); 2.00 (3H, s, CH₃²⁴).

¹³C NMR (DMSO-d₆): δ^C ppm

36.51 (C²⁴); 37.93 (C⁶); 38.03 (C²⁵); 45.83 (C¹⁹); 63.04 (C²⁰); 104.75 (C⁵); 108.09 (C¹³); 118.70 (C¹⁴); 121.87 (C⁵); 123.36 (C¹²); 126.76 (C²); 128.66 (C¹⁵); 134.25 (C⁴); 157.35 (C¹⁶); 161.81 (C⁷); 170.83 (C²²).

IR (KBr): 3414 (O=C-(N-H)); 3132 (aromatic CH); 2925 (N-CH₃); 1735 (O-(C=O)); 1642 (NH-(C=O)); 1537 (NO₂); 1311 cm⁻¹ (aromatic C-N).

11. (E)-*t*-Butyl 2-(4-(4-(4-(3-methoxystyryl)benzamido)-1-methyl-1H-pyrrole-2-carboxamido)-1-methyl-1H-pyrrole-2-carboxamido)ethylcarbamate III.4.3



Method 1. *t*-Butyl 2{[(1-methyl-4-[(1-methyl-4-nitro-1*H*-pyrrol-2-yl)carbonyl]amine)-1*H*-pyrrol-2-yl)carbonyl]amino}ethylcarbamate **III.3.3** (0.030 g, 0.07 mmol) was dissolved in MeOH (2.0 mL) and Pd/C (10%, 0.028 g) was added slowly at 0°C, under N₂ (g). The solution was stirred 3 h 25 min under H₂ (g) at RT at atmospheric pressure, and then filtered on Kieselguhr. The solvent was evaporated under reduced pressure. The residue **III.4.1** was dissolved in dry DMF (1 mL) and a solution of (*E*)-4-(3-methoxystyryl)benzoic acid (0.019 g, 0.07 mmol) in dry DMF (2 mL) and dry NEt₃ (30 μL, 0.22 mmol). Then HBTU (0.057 g, 0.15 mmol) was then added. The solution was stirred overnight at RT, and the solvent evaporated under high vacuum to give a dark orange solid, which was purified by HPLC to yield a brown solid **III.4.3** (33 mg, 0.05 mmol).

Yield: 71%

Method 2. Butyl 2{[(1-methyl-4-[(1-methyl-4-nitro-1*H*-pyrrol-2-yl)carbonyl]amine)-1*H*-pyrrol-2-yl)carbonyl]amino}ethylcarbamate **III.3.3** (0.354 g, 0.81 mmol) was dissolved in MeOH (10.0 mL), and Pd/C (10%, 0.115 g) was added slowly at 0°C, under N₂ (g). The solution was stirred 3 h under H₂ (g) at RT and under atmospheric pressure, and then filtered on Kieselguhr. The solvent was evaporated under reduced pressure. A solution of (*E*)-4-(3-methoxystyryl)benzoic acid (0.248 g, 0.97 mmol) in dry DMF (3.0 mL) and *N,N*-diisopropylethylamine (430 μL, 2.47 mmol) was added to the residue **III.4.1**, then 2-Propanephosphonic acid anhydride (T₃P, 50% in DMF, 620 μL) was added at 0°C. The solution was allowed to return to room temperature while stirring overnight and the volatiles were evaporated under vacuum. The solution was then poured into a solution of saturated sodium bicarbonate (30 mL). The product precipitated, and was stirred overnight before being filtered to give a pale brown solid **III.4.3** (0.422 g, 0.66 mmol).

Yield: 81%

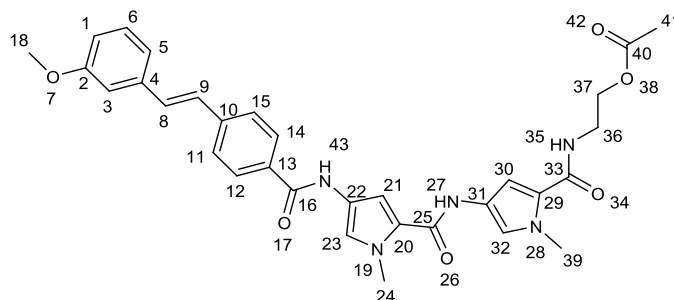
LCMS: found 663 g.mol⁻¹ (M+H+Na) calculated for C₃₅H₄₀N₆O₆, 640.73.

¹H NMR (DMSO-d₆): δ^H ppm

10.3 (1H, s, NH²⁷); 9.94 (1H, s, NH⁴⁷); 7.97 (3H, m, NH³⁵ & H^{12 14}); 7.73 (2H, m, H^{11 15}); 7.35 (1H, d, *J* = 16.05 Hz, H⁸), 7.31 (1H, d, *J* = 16.05 Hz, H⁹), 7.29 (2H, m, NH³⁸ & H²¹); 7.21 (3H, m, H^{3 23 32}); 7.08 (1H, d, *J* = 1.5 Hz, H³⁰); 6.87 (3H, m, H^{1 5 6}); 3.86 (2H, s, NCH₃²⁴); 3.80 (6H, 2 s, NCH₃⁴² and OCH₃¹⁸); 3.19 (2H, t, *J* = 6.3 Hz, CH₂³⁷); 3.06 (2H, t, *J* = 6.2 Hz, CH₂³⁶); 1.37 (9H, s, C(CH₃)₃^{44 45 46}).

12. Preparation of (E)-2-(4-(4-(4-(3-methoxystyryl)benzamido)-1-methyl-1H-pyrrole-2-carboxamido)-1-methyl-1H-pyrrole-2-carboxamido)ethyl acetate

III.4.4



Method 1. 2{[(1-methyl-4{[(1-methyl-4-nitro-1H-pyrrol-2-yl)carbonyl]}-1H-pyrrol-2-yl)carbonyl]amino}ethyl acetate **III.3.4** (0.050 g, 0.13 mmol) was dissolved in MeOH (3.0 mL) and Pd/C (10%, 0.044 g) was added slowly at 0°C, under N₂ (g). The solution was stirred for 4 h 30 min under H₂ (g) at RT and under atmospheric pressure, and then filtered on Kieselguhr. The solvent was evaporated under reduced pressure. The residue **III.4.2** was dissolved in dry DMF (2 mL) and a solution of (*E*)-4-(3-methoxystyryl)benzoic acid (0.034 g, 0.13 mmol) in dry DMF (2 mL) and HBTU (0.104 g, 0.27 mmol) was added. The solution was stirred overnight at RT, and the solvent evaporated under high vacuum to yield a dark orange solid, which was purified by HPLC to give a pale brown solid **III.4.4** (24 mg, 0.04 mmol).

Yield: 31%

Method 2 2{[(1-methyl-4{[(1-methyl-4-nitro-1H-pyrrol-2-yl)carbonyl]}-1H-pyrrol-2-yl)carbonyl]amino}ethyl acetate **III.3.4** (0.050 g, 0.13 mmol) was dissolved in MeOH (1.0 mL) and Pd/C (10%, 0.022 g) was added slowly at 0 °C, under N₂ (g). The solution was stirred for 3 h under H₂ (g) at RT and under atmospheric pressure, and then filtered on Kieselguhr. The solvent was evaporated under reduced pressure. The residue **III.4.2** was dissolved in dry DMF (1 mL) and a solution of (*E*)-4-(3-methoxystyryl)benzoic acid (0.039 g, 0.15 mmol) in dry DMF (1 mL), *N,N*-diisopropylethylamine (450 μL, 2.58 mmol) and then 2-Propanephosphonic acid anhydride (T₃P, 50% in DMF, 101 μL) was added at 0 °C. The solution was allowed to return to RT and stirred overnight. The volatiles were

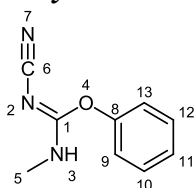
with MgSO₄, and the solvent was evaporated under vacuum to recover the amine **III.5.1** as an oil (0.011 g, 0.02 mmol). The LC/MS spectrum showed that the amine was recovered.

Yield : 100 %

LC/MS: found 541 g.mol⁻¹ (M+H) and 563 g.mol⁻¹ (M+H+Na) calculated for C₃₀H₃₂N₆O₄, 540.61.

b) *Preparation of N-((Z)-4-cyano-3-(methylamino)but-3-en-1-yl)-4-(4-(4-((E)-3-methoxystyryl)benzamido)-1-methyl-1H-pyrrole-2-carboxamido)-1-methyl-1H-pyrrole-2-carboxamide III.5.3*

i. *Preparation of (Z)-phenyl N'-cyano-N-methylcarbamide III.5.2*



A mixture of methylamine (33% in absolute ethanol, 47 µL, 1.15 mmol, 1 eq) and commercially available diphenyl cyanocarbodinimide (301 mg, 1.25 mmol, 1.1 eq) in dichloromethane (25 mL) was heated to reflux for 8h 25min. The reaction was then cooled down and the solvent was evaporated under reduced pressure. The residue was purified by flash chromatography using a hexane/ethyl acetate (gradient 20% to 50% ethyl acetate) to yield a white powder (85 mg, 0.485 mmol).

Yield : 38%

LC/MS: found 176.20 g.mol⁻¹ (M+H) calculated for C₉H₉N₃O, 175.19.

¹H NMR (CDCl₃): δ^H ppm

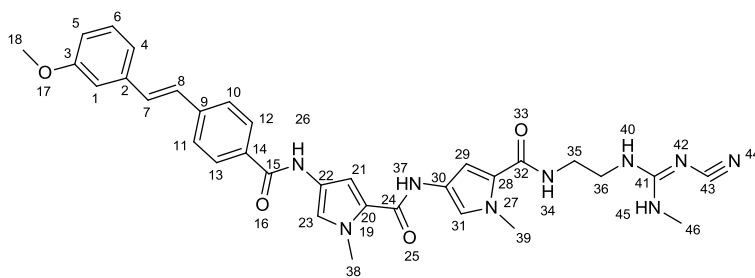
7.41 (2H, m, H¹² & H¹⁰), 7.31 (1H, m, H¹¹), 7.11 (2H, m, H⁹ & H¹³), 3.14 (3H, d, J=4.5 Hz, CH₃⁵), 2.97 (1H, broad s, NH³).

ELEMENTAL ANALYSIS:

Found: C, 61.61; H, 5.20; N, 23.90 %

Expected: C, 61.70; H, 5.18; N, 23.99 %

ii. *Preparation of N-((Z)-4-cyano-3-(methylamino)but-3-en-1-yl)-4-(4-(4-((E)-3-methoxystyryl)benzamido)-1-methyl-1H-pyrrole-2-carboxamido)-1-methyl-1H-pyrrole-2-carboxamide III.5.3*



(*E*)-*N*-(2-aminoethyl)-4-(4-(4-(3-methoxystyryl)benzamido)-1-methyl-1H-pyrrole-2-carboxamido)-1-methyl-1H-pyrrole-2-carboxamide **III.5.1** (18.0 mg, 0.03 mmol, 1 eq) in propan-1-ol (2 mL) and (*Z*)-phenyl *N'*-cyano-*N*-methylcarbamimidate **III.5.2** (5.25 mg, 0.03 mmol, 1 eq) in propan-1-ol (1 mL) was refluxed for 5h 30 min. The residue recovered after evaporation of solvent was purified on silica gel chromatography using hexane/ethyl acetate to yield a pale yellow solid (9.0 mg, 0.01 mmol)

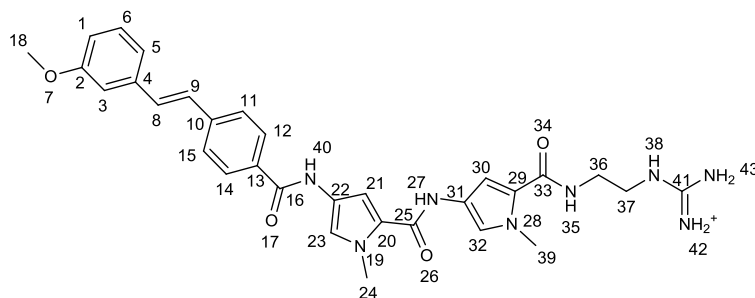
Yield: 33%

LRMS: found 644.60 g.mol⁻¹ (M+Na+H) and 620.20 g.mol⁻¹ (M-H) calculated for C₃₃H₃₅N₉O₄, 621.69.

¹H NMR (CDCl₃): δ^H ppm

7.86 (2H, m, H¹² & H¹³), 7.61 (2H, m, H¹⁰ & H¹¹), 7.34 (1H, m, H⁷), 7.31 (1H, m, H⁸), 7.29 (2H, m, H²³ & H³¹), 7.19 (2H, m, H⁴ & H²¹), 7.07 (1H, d, *J* = 2.0 Hz, H²⁹), 6.78 (2H, m, H¹⁵), 6.62 (1H, d, *J* = 8.0 Hz, H⁶), 3.87 (9H, s, CH₃³⁸ & CH₃³⁹ & CH₃¹⁸), 3.11 (2H, m, CH₂³⁵), 2.96 (2H, m, CH₂³⁶), 2.67 (3H, s, CH₃⁴⁶).

c) *Preparation of (E)-amino((2-(4-(4-(4-(3-methoxystyryl)benzamido)-1-methyl-1H-pyrrole-2-carboxamido)-1-methyl-1H-pyrrole-2-carboxamido)ethyl)amino)methaniminium III.5.4*



(*E*)-*N*-(2-aminoethyl)-4-(4-(4-(4-(3-methoxystyryl)benzamido)-1-methyl-1H-pyrrole-2-carboxamido)-1-methyl-1H-pyrrole-2-carboxamide **III.5.1** (0.031 g, 0.057 mmol) was dissolved in distilled EtOAc (2.5 mL). Then potassium carbonate (0.017 g, 0.13 mmol) and

2-methyl-2-thiopseudourea sulfate (0.033 g, 0.12 mmol) in distilled EtOH (0.5 mL) were added and the solution was heated to reflux in a sealed tube under N₂ (g) overnight (17 h) at 80°C. A white product precipitated. The yellow solution was filtered to remove a yellow impurities. The yellow solution was evaporated under reduced pressure, and the product **III.5.4** (0.030g, 0.051 mmol) was recovered. The purification was undertaken with reverse phase flash chromatography using MeOH and water + 0.1% TFA as eluents.

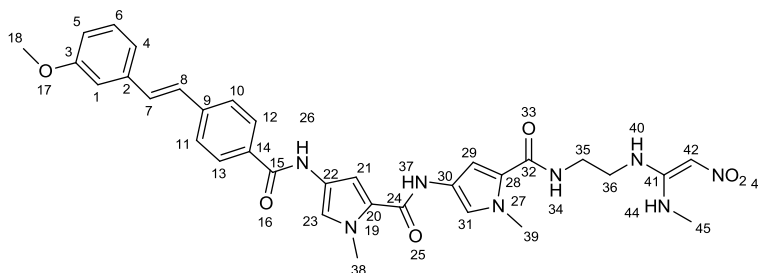
Yield: 51%

LCMS: found 584.40 g.mol⁻¹ (M+H), calculated for C₃₁H₃₅N₈O₄⁺, 583.66

¹H NMR (CDCl₃): δ^H ppm

8.07 (2H, d, *J* = 8.5 Hz, H¹² & H¹⁴), 7.71 (2H, m, NH₂⁴³); 7.61 (2H, d, *J* = 8.0 Hz, H¹¹ & H¹⁵); 7.54 (1H, m, H⁸), 7.31 (1H, d, *J* = 16.0 Hz, H⁹); 7.20 (2H, m, H^{5,21}); 7.14 (3H, m, H^{23,30,32}); 6.88 (3H, m, H^{1,3,6}); 3.87 (9H, s, CH₃²⁴ & CH₃³⁹ & CH₃¹⁸); 2.97 (2H, s, CH₂³⁶), 2.90 (2H, s, CH₂³⁷).

d) *Preparation of 4-(4-((E)-3-methoxystyryl)benzamido)-1-methyl-N-(1-methyl-5-((2-(((E)-1-(methylamino)-2-nitrovinyl)amino)ethyl)carbonyl)-1H-pyrrol-3-yl)-1H-pyrrole-2-carboxamide III.5.5*



(*E*)-*N*-(2-aminoethyl)-4-(4-(4-(3-methoxystyryl)benzamido)-1-methyl-1H-pyrrole-2-carboxamido)-1-methyl-1H-pyrrole-2-carboxamide **III.5.1** (0.039 g, 0.072 mmol) was dissolved in distilled EtOAc (1.5 mL). Potassium carbonate (0.020 g, 0.14 mmol) and *N*-methyl-1-(methylthio)-2-nitroethenamine (0.022 g, 0.14 mmol) in distilled EtOH (0.5 mL) were added and the solution was heated to reflux in a sealed tube under N₂ (g) overnight at 90°C under nitrogen. The solvents were evaporated under reduced pressure to yield a pale yellow residue corresponding to impure **III.5.5**. The purification was undertaken with reverse phase flash chromatography using MeOH and water + 0.1% TFA as eluents to yield **III.5.5** (0.007 g, 0.011 mmol).

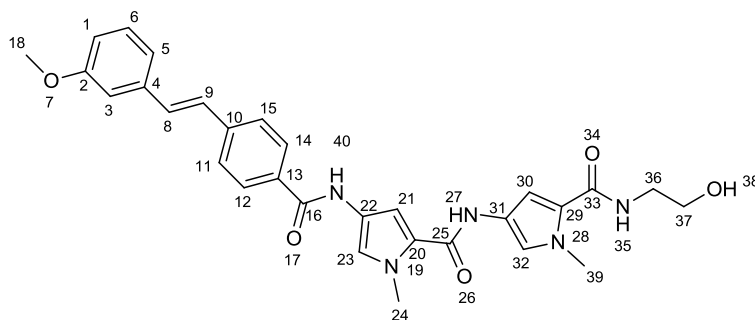
Yield: 15%

LCMS: found 641.53 g.mol⁻¹ (M+H) and 663.60 g.mol⁻¹ (M+H+Na) , calculated for C₃₃H₃₆N₈O₆, 640.69.

¹H NMR (CDCl₃): δ^H ppm

8.07 (2H, d, *J* = 8.5 Hz, H¹² & H¹³), 7.61 (2H, d, *J* = 8.5 Hz, H¹⁰ & H¹¹), 7.31 (1H, d, *J* = 16.3 Hz, H⁷), 7.22 (1H, d, *J* = 16.3 Hz, H⁸), 7.19 (3H, m, H⁴ ²³ ³¹), 7.14 (2H, m, H¹⁵), 7.07 (2H, m, H²¹ ²⁹), 6.86 (1H, m, *J* = 7.5 Hz, H⁶), 4.56 (1H, s, H⁴²), 3.86 (9H, d, CH₃¹⁸ & CH₃³⁸ & CH₃³⁹), 3.12 (2H, m, H³⁵), 3.05 (2H, m, H³⁶), 2.86 (3H, d, *J* = 3.5 Hz, CH₃⁴⁵).

14. Preparation of (E)-N-(2-hydroxyethyl)-4-(4-(4-(3-methoxystyryl)benzamido)-1-methyl-1H-pyrrole-2-carboxamido)-1-methyl-1H-pyrrole-2-carboxamide
III.5.6



(E)-2-(4-(4-(4-(3-methoxystyryl)benzamido)-1-methyl-1H-pyrrole-2-carboxamido)-1-methyl-1H-pyrrole-2-carboxamido)ethyl acetate **III.4.4** (0.298 g, 0.511 mmol) was dissolved in ethanol (4 mL), and a solution of sodium hydroxide (0.067 mg, 1.68 mmol) in water (5 mL) was added. The solution was heated to reflux for 2 h. The solution was freeze dried and the residue was recrystallised from EtOAc then filtered to give an off white solid **III.5.6** (0.274 mg, 0.506 mmol).

Yield: 99%

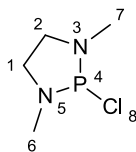
LCMS: found 540.27 g.mol⁻¹ (M-H) and 1081.73 g.mol⁻¹ (M+M+H), calculated for C₃₀H₃₁N₅O₅, 541.60.

¹H NMR (DMSO-d₆): δ^H ppm

10.31 (1H, s, NH²⁷); 9.92 (1H, s, NH⁴⁰); 7.96 (2H, d, *J* = 8.0 Hz, Ar-H¹² ¹⁴); 7.90 (1H, t, *J* = 5.5 Hz, NH³⁵); 7.73 (2H, d, *J* = 8.5 Hz, H¹¹ ¹⁵); 7.36 (1H, d, *J* = 16.5 Hz, H⁸); 7.32 (1H, d, *J* = 16.5 Hz, H⁹); 7.29 (2H, m, H²³ ³²); 7.21 (3H, m, H¹³ ⁵); 7.19 (1H, d, *J* = 1.5 Hz, H²¹), 7.08 (1H, d, *J* = 1.5 Hz, H³⁰); 6.88 (1H, m, H⁶); 3.86 (3H, s, NCH₃²⁴); 3.80 (6H, s, NCH₃³⁹ and OCH₃¹⁸); 3.47 (2H, q, *J* = 6.0 Hz, CH₂³⁷); 3.24 (2H, q, *J* = 6.0 Hz, CH₂³⁶).

15. Preparation of (E)-4-(4-(3-methoxystyryl)benzamido)-1-methyl-N-(1-methyl-5-(2-(pyrrolidin-1-yl)ethylcarbamoyl)-1H-pyrrol-3-yl)-1H-pyrrole-2-carboxamide III.5.9

a) Preparation of 2-chloro-1,3-dimethyl-1,3,2-diazaphospholidine III.5.7 ^[75]



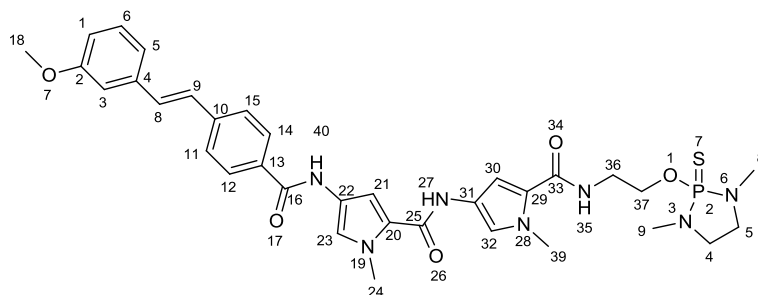
A solution of *N,N'*-dimethylethylenediamine (7 mL, 65.00 mmol) and distilled triethylamine (5 mL, 36 mmol) in dry DCM (10 mL), and a solution of PCl_3 (5 mL, 57.3 mmol) in 10 mL of dry DCM, were added simultaneously to dry DCM (30 mL) at $-40\text{ }^\circ\text{C}$, under $\text{N}_2(\text{g})$. After the addition, the solution was allowed to warm to $-30\text{ }^\circ\text{C}$, and another solution of dry triethylamine (5.5 mL, 63.03 mmol) in dry DCM (10 mL) was added. The solution was then allowed to return to RT for 2 h. The solvent was removed under reduced pressure to give a white yellow solid. This solid was decanted with dry ether (3 x 100 mL). Ether washings were combined and concentrated to give a yellow oil as a crude product. This oil was distilled at $150\text{ }^\circ\text{C}$ to give a white solid (1.147 g, 7.52 mmol).

Yield: 13%

$^1\text{H NMR}$ ($\text{DMSO-}d_6$): δ^{H} ppm

2.53 (3H, s, CH_3); 2.56 (3H, s, CH_3); 2.96 (2H, q, $J = 5.0\text{ Hz}$, CH_2); 3.29 (2H, m, $J = 5.5\text{ Hz}$, CH_2).

b) Preparation of (E)-*N*-(2-(1,3-dimethyl-1,3,2-diazaphospholidin-2-yloxy)ethyl)-4-(4-(4-(3-methoxystyryl)benzamido)-1-methyl-1H-pyrrole-2-carboxamido)-1-methyl-1H-pyrrole-2-carboxamide III.5.8



To a solution of 2-chloro-1,3-dimethyl-1,3,2-diazaphospholidine (31 mg, 0.238 mmol) in anhydrous DCM (6 mL) under N_2 (g), was added dropwise, at $-60\text{ }^\circ\text{C}$, a solution of (E)-*N*-(2-hydroxyethyl)-4-(4-(4-(3-methoxystyryl)benzamido)-1-methyl-1H-pyrrole-2-carboxamido)-1-methyl-1H-pyrrole-2-carboxamide (0.080 g, 0.148 mmol) in dry DCM (6 mL) and dry

NEt₃ (0.180 mmol, 25 μ L). The solution was allowed to reach RT for 1 h 40 min and a solution of sulfur flowers (15 mg, 0.475 mmol) dissolved in dry DCM (2 mL) was added. The solution was stirred for 40 min. The solvent was evaporated under reduced pressure to give a crude product.

The crude product was dissolved in MeOH to precipitate impurities which were filtered. The yellow filtrate was concentrated under reduced pressure to give a yellow solid (0.139 g, 0.20 mmol, yield: 136%).

The product was purified by flash chromatography using a gradient of hexane/EtOAc to recover several fractions (0.016 g, 0.02 mmol, yield: 16%).

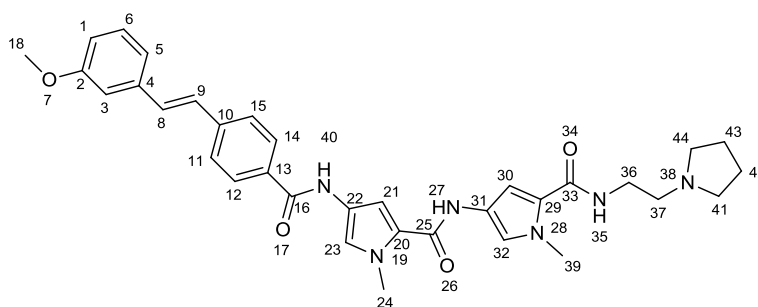
LCMS: found 690 g.mol⁻¹ (M+H) and 712 g.mol⁻¹ (M+H+Na), calculated for C₃₄H₄₀N₇O₅PS, 689.76.

³¹P NMR (MeOD): 81.63 ppm .

¹H NMR (MeOD): δ^H ppm

7.93 (2H, d, $J = 8.3$ Hz, H¹² & H¹⁴), 7.70 (2H, d, $J = 8.3$ Hz, H¹¹ & H¹⁵), 7.29 (2H, m, H³ & H⁵), 7.18 (1H, m, H⁶), 6.85 (2H, m, H⁸ & H⁹), 6.28 (1H, m, H¹), 3.94 (3H, s, CH₃¹⁸), 3.84 (6H, s, CH₃²⁴ & CH₃³⁹), 3.45-3.69 (4H, m, CH₂³⁶ & CH₂³⁷), 2.74-2.55 (10H, m, CH₃⁸ & CH₃⁹ & H⁴ & H⁵).

c) Attempted preparation of (*E*)-4-(4-(3-methoxystyryl)benzamido)-1-methyl-N-(1-methyl-5-(2-(pyrrolidin-1-yl)ethyl)carbamoyl)-1*H*-pyrrol-3-yl)-1*H*-pyrrole-2-carboxamide **III.5.9** [73]



(*E*)-*N*-(2-(1,3-Dimethyl-1,3,2-diazaphospholidin-2-yloxy)ethyl)-4-(4-(4-(3-methoxystyryl)benzamido)-1-methyl-1*H*-pyrrole-2-carboxamido)-1-methyl-1*H*-pyrrole-2-carboxamide (0.030 g, 0.043 mmol) in anhydrous pyrrolidine (4 mL) was heated to reflux overnight, at 80 °C, in a thick walled sealed tube. The excess of pyrrolidine was distilled under reduced pressure to leave an orange oil. The mass spectrum showed that the product **III.5.9** was not formed.

II. Biological assays

1. Anti-bacterial assays

Colonies of *Staphylococcus aureus* RN4220 and *E. coli* NM522 were inoculated respectively into sterile Muller Hinton broth and Luria Betani broth, and then incubated overnight in a stirring incubator at 140 rpm at 37 °C. The broth was then centrifuged at 4000 rpm for 5 minutes and the cells resuspended in sterile normal saline (20 mL). The solution was spun again at 4000 rpm for 5 minutes. The procedure was repeated until a clear supernatant was obtained. The pellets were then resuspended in sterile normal saline (20 mL) and several dilutions were made until an O.D₆₀₀ of 0.5 was obtained. Then each medium containing bacteria was plated in 96 well plates: column 1 had only the broth medium and helped prevent an edging effect. Column 2 was the control (media containing bacteria only). Column 3 had DMSO, column 4 had ampicillin, and finally column 5 to 12 had varying concentration of MGB: 0.5, 1, 2, 3, 4, 5, 10, 20 µg/mL. Resazurin (10 µL) was added to the wells. The plates were wrapped and placed in an incubator at 37 °C. Plates were incubated for 24 hours and absorbances were measured at different times to give the curves. Two different graphs were plotted: the first one plotted the absorbance against the concentration at a fixed time, and the other the absorbance against the time.

2. Cytotoxicity assays

Cell viability was determined using Dulbecco Modified Eagle Media (DMEM) with 5% L-glutamine and 10% Foetal Bovine Serum (FBS) and 5% Penicillin/Streptomycin (cf APPENDIX FILE n°2, p42) in humidified atmosphere of 5% CO₂. The cells were grown on a 75 cm² flask which was incubated at 37°C for 18-24 hrs to obtain a confluent monolayer. After removing the supernatant medium, the serum was removed with FBS and the cells were collected by adding trypsin/EDTA) and left 5 min in humidified atmosphere of 5% CO₂ at 37°C. Then fresh medium was added and poured in a centrifuge tube. The cells were centrifuged at 1000 rpm for 5 mins and then resuspended in growth medium to count using a hemacytometer. After dilution, 100 µL of the suspension was added to the central 8 or 10 columns in the 96 well plates to be incubated at 37°C, 5% CO₂ for 24 hours to allow the population to grow until each well was 70% occupied. Several dilutions of MGBs in fresh DMEM were made to obtain 7 different concentrations (1, 2, 5, 7, 10, 20 µg/mL) from which 100 µL were inserted in each well, and the plates were incubated at 37°C, 5% CO₂ for 24hrs. At the end of the exposure period of cells to drugs, 20 µL of MTT was added to each well and incubated to 37°C, 5% CO₂ for 2 hrs. DMEM and MTT were then removed from the

wells and 100 μ L of DMSO (cf APPENDIX FILE n°2, p41) was added to each well. The plates were then incubated 10 minutes during which the MTT crystals were dissolved to give a purple color. The absorbance was recorded at 540 nm to give the curves below.

3. Microscopy assays

Bacteria were grown overnight in respective media. Slides were prepared by spreading 1 drop of a mixture made of 100 μ l of bacteria and 1 μ L MGB or DAPI , and 1 drop of V79 cells with 1 drop of MGB or DAPI. A cover slip was then placed over the slide.

REFERENCES

- [1]. nobelprize.org.
This website provides a background of Nobel Prize winner since 1901 with biographies, interviews, photos, articles and information about the Nobel Laureates and their work.
- [2]. Suckling C. J., *J. Phys. Org. Chem.*, **2008**, *21*, 575-583.
- [3]. <http://chemistry.umeche.maine.edu/CHY431/Nucleic3.jpg>.
- [4]. www.dnafb.org.
This website provides information on the basics of DNA, genes and heredity
- [5]. www.chemheritage.org.
This website informs on the chemistry's impact on society.
- [6]. Neidle S., *Nat. Prod. Rep.*, **2001**, *18*, 291-309.
- [7]. Suckling C. J., *Expert Opin. Ther. Patents*, **2004**, *14*, 12.
- [8]. Yang Y. H., Wang Q. H., Nie H., Chen H., Cheng M. S., *Molecules*, **2008**, *13*, 1179-1188.
- [9]. Lukhtanov E. A., Lokhov S. G., Vermeulen N. M. J., *WO 03/078450*.
- [10]. Dervan P. B., *Bioorg. Med. Chem*, **2001**, *9*, 2215-2235.
- [11]. <http://journals.prous.com>.
This website provides journals about drugs.
- [12]. Anthony N. G., Breen D., Clarke J., Donoghue G., Drummond A. J., Ellis E., Gemmell C., J-Hellexbeux J., Hunter I. S., Khalaf A. I., MacKay S. P., Parkinson J. A., Suckling C. J., Waigh R. D., *J. Med. Chem.*, **2007**, *50*, 6116-6125.
- [13]. www.mun.ca.
This university website provides information on research.
- [14]. www.cgl.ucsf.edu.
This website is a resource for biocomputing, visualization and informatics and research and development in biomedical research in Hampshire.
- [15]. Hampshire A. J., Khairallah H., Khalaf A. I., Ebrahimabadi A. H., Waigh R. D., Suckling C. J., Brown T., Fox K. R., *Bioorg. Med. Chem. Lett.*, **2006**, *16*, 3469-3474.
- [16]. biop.ox.ac.uk.
This website describes the structures of complex biological macromolecules and macromolecular assemblies.
- [17]. Walker W.L., Landaw E.M., Dickerson R.E., Goodsel D.S., *Proc Natl Acad Sci USA*, **1998**, *14*, 95(8), 4315-4320.
- [18]. Karin M., Ben-Neriah Y., *Annu. Rev. Immunol.*, **2000**, *18*, 621.

- [19]. Wurtz N. R., Pomerantz J. L., Baltimore D., Dervan P. B., *Biochemistry*, **2002**, *41*, 7604.
- [20]. Carter C. A., Waud W. R., Li L. H. and al., *Clin. Cancer Res.*, **1996**, *2*, 1143.
- [21]. Schwartz G. H., Patnaik A., Hammond L. A. and al., *Ann. Oncol.*, **2003**, *14*, 775.
- [22]. Pahl H. L., *Oncogene*, **1999**, *18*, 621.
- [23]. Arnt H., Hauschild K.E., Sullivan D.P., Lake K., Dervan P.B., Ansari A.Z., *J. Am. Chem. Soc.*, **2003**, *125*, 13322.
- [24]. Manak J.R., Scott, M.P., *Dev. Suppl*, **1994**, *61*.
- [25]. Scott M.P., Carroll, S.B., *Cell*, **1987**, *51*, 689.
- [26]. Lewis E.B., *Nature*, **1978**, *276*, 565.
- [27]. Weatherbee S.D., Halder G., Kim J., Hudson A., Carroll S.B., *Genes Dev.*, **1998**, *12*, 1474.
- [28]. Van Dijk M.A., Murre C., *Cell*, **1994**, *78*, 617.
- [29]. Passner J.M., Ryoo H.D., Shen L., Mann R.S., Aggarwal A.K., *Nature*, **1999**, *397*, 714.
- [30]. Galant R., Walsh C.M., Carroll S.B., *Development*, **2002**, *129*, 3115.
- [31]. Brezinski M., Warren C.L., Ansari A.Z., Unpublished work.
- [32]. Stafford R.L., Dervan P.B., *J. Am. Chem. Soc.*, **2007**, *129*, 14026.
- [33]. Laughton C., Luisi B., *J. Mol. Bio.*, **1998**, *288*, 953-963.
- [34]. Fishleigh R. V., Fox K. R., Khalaf A. I., Pitt A. R., Scobie M., Suckling C. J., Urwin J., Waigh R. D., Young S. C., *J. Med. Chem.*, **2000**, *43*, 3257-3266.
- [35]. Anthony N. G., Fox K. R., Johnston B. F., Khalaf A. I., Mackay S. P., McGroarty I. S., Parkinson J. A., Skellern G. G., Suckling C. J., Waigh R. D., *Bioorg. Med. Chem. Lett.*, **2004**, *14*, 1353-1356.
- [36]. Genesoft, Inc., *WO0174898*, **2000**.
- [37]. Univ. Geneva, *WO02095022*, **2002**.
- [38]. Cozzi P., *Il Farmaco*, **2003**, *58*, 213-220.
- [39]. Scripps Res. Inst., *US6060608*, **2000**.
- [40]. Taiho Pharm. Co. Ltd, *US6660742*, **2003**.
- [41]. Gregson S.J., Howard P.W., Barcella S., *Bioorg. Med. Chem. Lett.*, **2000**, *10*, 1845-1847.
- [42]. Gregson S.J., Howard P.W., Barcella S., *Bioorg. Med. Chem. Lett.*, **2000**, *10*, 1849-1851.
- [43]. Gregson S.J., Howard P.W., Hartley J.A., *J. Med. Chem.*, **2001**, *44*, 737-748.
- [44]. Queens Univ. Belfast, Cancer Res. UK, Univ. Reading, *US6589871*, **2003**.

- [45]. Scripps Res. Inst., *WO0196313*, **2001**.
- [46]. Univ. North Carolina at Chapel Hill, *US6172104*, **2001**.
- [47]. Univ. North Carolina at Chapel Hill, Georgia State Univ., *US6008247*, **1999**.
- [48]. Univ. North Carolina at Chapel Hill, Georgia State Univ., *US6127554*, **2000**.
- [49]. American Chem. Society, 10/26/ 2007.
- [50]. Bürli R.W., Ge Y., White S., Touami S. M., Taylor M., Kaizerman J.A., Moser H.E., *Bioorg. Med. Chem. Lett.*, **2002**, *12*, 2591-2594.
- [51]. Bürli R.W., Kaizerman J.A., Duan J.-X., Jones P., Johnson K.W., Iwamoto M., Truong K., Hu W., Stanton T., Chen A., Touami S., Gross M., Jiang V., Ge Y., Moser H.E., *Bioorg. Med. Chem. Lett.*, **2004**, *14*, 2067-2072.
- [52]. Anthony N. G., Breen D., Donoghue G., Khalaf A. I., Mackay S. P., Parkinson J. A., Suckling C.J., *Org. & Biomol. Chem.*, **2009**, *7*, 1843-1850.
- [53]. Freydank A.C, Humphrey M.G., Friedrich R.W., Luther-Davies B., *Tetrahedron*, **2002**, *58*, 1425-1432.
- [54]. Graham L. Patrick, *An Introduction to Medicinal Chemistry, Third Edition*, **2005**.
- [55]. Gillies E. R., Dolain C., Léger J. M., Huc I., *J. Org. Chem.*, **2006**, *71*, 7931-7939.
- [56]. Archimica, T3P brochure.
- [57]. Matsuno K., Nakajima T., Ichimura M., Giese N. A., Yu J.-C., Lokker N. A., Ushiki J., Ide S.-I., Oda S., Nomoto Y., *J. Med. Chem.*, **2002**, *45*, 4513-4523.
- [58]. Berthelot M., Besseau F., Laurence C., *Eur. J. Org. Chem.*, **1998**, 925.
- [59]. Besseau F., Luçon M., Laurence C., Berthelot M., *J. Chem. Soc. Perkin Trans. 2*, **1998**, 101.
- [60]. Wuitschik G., Rogers-Evans M., Buckl A., Bernasconi M., Märki M., Godel T., Fiischer H., Wagner B., Parilla I., Schuler F., Schneider J., Alker A., Bernd Schweizer W., Müller K., Carreira A. M., *Angew. Chem. Int. Ed.*, **2008**, *47*, 4512-4515.
- [61]. Wuitschik G., Rogers-Evans M., Müller K., Fischer H., Wagner B., Schuler F., Polonschuk L., Carreira E. M., *Angew. Chem. Int. Ed.*, **2006**, *45*, 7736.
- [62]. Wang H., Loughton C. A., *Methods*, **2007**, *42*, 196-203.
- [63]. http://gsbs.utmb.edu/microbook/images/fig2_6.jpg.
This website provides information about Gram bacteria.
- [64]. www.desmech.com/?p=26.
This website explains what cell disruption is and gives diagrams of Gram positive and Gram negative bacteria.
- [65]. Sarker S. D., Nahar L., Kumarasamy Y., *Methods*, **2007**, *42*, 4, 321-324.

- [66]. <http://en.wikipedia.org/wiki/Ampicillin>.
This website defines ampicillin, its structure, its use and its properties.
- [67]. AHFS DRUG INFORMATION 2006, *American Society of Health-System Pharmacists*, **2006**.
- [68]. <http://en.wikipedia.org/wiki/DAPI>.
This website defines dapi, its structure, its use and its properties.
- [69]. Du H., Fuh R.A., Li J., Corkan A., Lindsey J.S., *Photochemistry and Photobiology*, **1998**, *68*, 141-142.
- [70]. Suckling C. J., Khalaf A.I., Pitt A.R., Scobie M., *Tetrahedron*, **2000**, *56*, 5225.
- [71]. Hotzel. C., Marotto. A., Pindur. U., *Eur. J. Med. Chem.*, **2003**, *38*, 189.
- [72]. Beria I., Baraldi P.G., Cozzi P., Calderelli M., Geroni C., Marchini S., Mongelli N., *J. Med. Chem.*, **2004**, *47*, 2611.
- [73]. Hermans R. J. M., Buck H. M., *J. Org. Chem.*, **1987**, *23*, 5150.
- [74]. Jaramillo D., Wheate N.J., Ralph S.F., Howard W.A., Tor Y., Aldrich-Wright J.R., *Inorganic Chemistry*, **2006**, *45*, 6004.
- [75]. McGuigan C., Anson M.S., *J. Chem. Soc. Perkin Trans.*, **1989**, *1*, 715.

APPENDIX

FILE n°1: EXPERIMENTAL EQUIPMENT / CHEMISTRY

i. NMR

Bruker DPX-400 MHz spectrometer was used to carry out ^1H , ^{13}C , and ^{31}P -NMR spectra.

The chemical shifts are given in ppm (δ values).

ii. IR

Spectra were recorded on a Perkin Elmer One, FT-IR spectrometer.

iii. UV

Spectra were recorded on a Thermo Spectronic Unicam UV300

iv. LC/MS

Mass spectra were obtained on Finnigan LC Q Duo Thermo Quest, with a PDA detector and MS pump surveyor Thermo Quest.

High resolution mass spectrometry was recorded by Glasgow University.

v. MELTING POINT

Melting points were recorded on a Reichert heater and Reichert 284395 Shandon microscope.

vi. THIN LAYER CHROMATOGRAPHY

Thin Layer Chromatography was carried out using silica gel 60 F₂₅₄ plates or pre-coated C18-silica plates on glass (RP-18W/UV254).

vii. COLUMN CHROMATOGRAPHY

Normal phase flash chromatographies were carried out on silica gel Zeoprep SI24001 with particles size between 40 μm to 63 μm from Appollo Scientific Limited.

Lichroprep RP-18 with particlex size between 40 μm to 63 μm , from Merck, was used for reverse phase flash chromatographies.

viii. HPLC

Time	A	B	Flow rate (ml/min)
0	70	30	6
25	50	50	6
30	30	70	6
35	70	30	6

39	70	30	6
40	70	30	0
40.10	70	30	0

Waters 1525 Binary HPLC pump, and a Waters 2487 dual λ absorbance detector at 254 nm using a C18 Luna column (60 x 21,20 mm, 5 microns) with the following gradient were used for reverse phase HPLC.

Mobile phase

A = Water + 0.1% TFA

B = MeOH + 0.1% TFA

ix. FREEZE DRYER

The samples were dried with an EDWARDS freeze-dryer where the pump was an EDWARDS model RV5.

FILE n°2 : EXPERIMENTAL EQUIPMENT/BIOLOGY

i. Bacteria and cells

Activity tests of MGBs against bacteria required the use of both Gram positive bacteria *Staphylococcus aureus RN4220* and Gram negative bacteria *E. Coli NM522*.

The mammalian cell line used for tissue culture was V 79 Hamster Lung cells.

ii. Media

Depending on the type of bacteria used for testing, different media were prepared. They include:

- Luria Betani (LB) media

Broth: To prepare 1 litre of LB, tryptone (10g), sodium chloride (NaCl, 10g) and yeast extract (5g) was measured and distilled water (1L) was added, mixed and autoclaved at 121°C for 15 minutes.

Agar: To prepare the agar, agar (20g) was added to tryptone (10g), sodium chloride (NaCl, 10g) and yeast extract (5g) dissolved in distilled water (1L), mixed and autoclaved at 121°C for 15 minutes.

- Mueller Hinton (MH) media (Oxoid®, UK)

Broth: To prepare 1L of Mueller Hinton broth, powder (21g) is measured into distilled water (1L) and autoclaved at 121°C for 15 minutes.

Agar: To prepare 1L of Mueller Hinton agar, powder (38g) is dissolved into distilled water (1L) and autoclaved at 121°C for 15 minutes.

iii. Chemicals

- DMSO

DMSO was used as a control during bacterial experiments, and as a solvent to dissolve the MGBs before introducing them to bacterial or mammalian cells.

- Ampicillin hydrochloride

The solution at 50 µg/mL was prepared as follows: a stock solution of ampicillin hydrochloride 10 mg/mL was prepared. 10 µL of the stock solution was dissolved up to 2ml to obtain the final solution.

- Glutamine

It is one of the 20 amino acids encoded by the standard genetic code. Its side chain is an amide formed by replacing the side-chain hydroxyl of glutamic acid with an amine functional group.

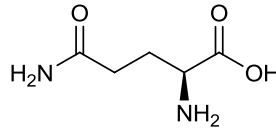


Figure 43. Structure of glutamine

- Fetal bovine serum (FBS)

It is the portion of plasma remaining after coagulation of blood, during which process the plasma protein fibrinogen is converted to fibrin and remains behind in the clot. Fetal Bovine serum comes from the blood drawn from the unborn bovine fetus and is the most widely used serum due to being low in antibodies and containing more growth factors, allowing for versatility in many different applications. FBS is used in the culturing of eukaryotic cells.

- Penicillin/Streptomycin

Penicillin inhibits bacterial growth by inhibiting peptidoglycan synthesis. Streptomycin belongs to the aminoglycoside antibiotics and inhibits bacterial growth by inhibiting protein synthesis. Penicillin-Streptomycin is used for the prevention and elimination of bacterial contaminants in cell culture.

- Trypsin/EDTA

Trypsin is a serine protease found in the digestive system of many vertebrates, where it hydrolyses proteins. Trypsin is produced in the pancreas as the inactive proenzyme trypsinogen. Trypsin predominantly cleaves peptide chains at the carboxyl side of the amino acids lysine or arginine, except when either is followed by proline. It is used for numerous biotechnological processes.

EDTA is a widely used acronym for the chemical compound ethylenediaminetetraacetic acid, which is a polyamino carboxylic acid. Its usefulness arises because of its role as a chelating agent, i.e. its ability to "sequester" metal ions such as Ca²⁺ and Fe³⁺. After being bound by EDTA, metal ions remain in solution but exhibit diminished reactivity.

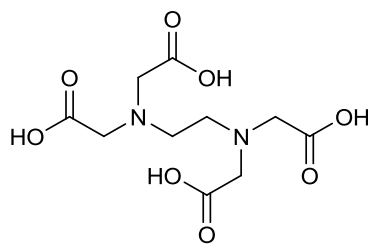


Figure 44. Structure of EDTA

The solution was used to detach adherent cells from the flask.

- MTT

Also known as 3-(4,5-methylthiazol-2-yl)-2,5-diphenyltetrazolium bromide, a tetrazole. It is yellow and is reduced to purple formazan in living cells. These reductions take place only when reductase enzymes are active, and therefore conversion is often used as a measure of living cells.

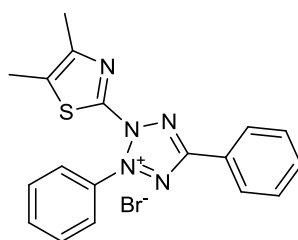


Figure 45. Structure of MTT

MTT (1.2 mg) was dissolved in DMSO (1 mL) before being introduced to the DMEM.

- Resazurin

Also known as 7-hydroxy-3*H*-phenoxazin-3-one 10-oxide, resazurin is a blue dye used mainly as an oxidation-reduction indicator in the resazurin test for bacteria.

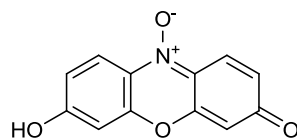


Figure 46. Structure of resazurin

Resazurin (blue) is reduced by living cells in resorufin, which results in a pink color. Resorufin is then reduced in hydroresorufin (colorless).

255 mg tablets were dissolved in 38 mL of sterile distilled water.

- Sterile Normal Saline

0.9 g of NaCl was dissolved in 100 mL sterile distilled water.

iv. SHAKING INCUBATOR

The flasks containing the bacteria in media were placed in an Unitron INFORS shaking incubator at 37°C at 140 rpm.

v. CENTRIFUGES

Cells : MSE MISTRAL 2000

Bacteria : Beckman Centrifuge & Rotors Avanti J-30 I

vi. OVENS

The flasks or plates containing growing cells were left in Hera cell oven at 37°C with 5% CO₂.

The plates containing the bacteria were stored in an oven at 37°C.

vii. O.D.

The growing curves were obtained using a Beckman DU650 spectrophotometer.

viii. ABSORBANCE

The final absorbance of microplate-based assays was measured by Labsystems iEMS Reader MF with filter 6 at 540 nm.

ix. MICROSCOPE

The microscopy was realised on a NIKON Eclipse TE 2000-5 microscope.

The pictures were taken by a Hamamatsu digital camera C4742-95 linked to a computer containing IP Lab software.